THE PULSARS IN 47 TUCANAE

September 2000

By

Paulo César Carvalho Freire

Department of Physics and Astronomy

Jodrell Bank Observatory

Contents

List of Tables

List of Figures

Abstract

Radio observations of the globular cluster 47 Tucanae have been performed over the last 11 years. These observations have resulted in the discovery of 20 millisecond pulsars, nine of which are presented in this work. We find that thirteen of the pulsars are members of binary systems, including all the nine new discoveries. Prior to this work only three binary systems had their orbital parameters determined; we now know the orbital parameters for twelve binary systems.

Three of the new discoveries are eclipsing binary pulsars. One of these (47 Tuc R) has the shortest orbital period measured for a radio pulsar (96 minutes). For two of the new binary pulsars (47 Tuc S and T), the orbital parameters were determined using a new procedure, described in this work, that uses the detected pulsar accelerations to determine the orbital parameters of the binary system.

We also present improved pulse profiles and luminosities for these pulsars, and find that their pulsewidth and flux density distributions are typical of galactic millisecond pulsars.

Prior to this work, only two of the pulsars in 47 Tuc had published timing solutions. Here we improve upon these two and present 13 new solutions. This new database is used to determine a variety of physical properties of the pulsars and of the cluster as a whole.

We find that all 15 pulsars with timing solutions are located within $1\rlap{.}'2$ of the cluster core. Their spatial density within that distance is consistent with a distribution of the type $n(r) \propto 1/r^2$ with a cutoff distance of four core radii.

Two pulsars (J0024−7204G and J0024−7204I) have a projected separation of only 0$.\!\!''$12, and could be part of a triple system containing these two observable pulsars.

We have measured the proper motions of four of the pulsars. The weighted mean of these motions is found to be a good approximation of the proper motion motion of 47 Tuc, and it is $\mu_\alpha = (5.9 \pm 0.6)\,\mathrm{mas\,yr^{-1}}$ and $\mu_\delta = (-4.1 \pm 0.6)\,\mathrm{mas\,yr^{-1}}$. This value is more precise than the value for the proper motion of 47 Tuc measured by Hipparcos, which still is in good agreement with the value we derived.

The measured period derivatives of the pulsars are used to estimate limits for the surface mass density of the cluster. We verified that the average of the pulsar accelerations and their distribution are well described by a King model of 47 Tuc with nominal parameters for the distance and the stellar line-of-sight velocity dispersion at the centre of the cluster. All pulsars have characteristic ages greater than $170\,\mathrm{Myr}$ and have magnetic fields smaller than $2.3 \times 10^5\,\mathrm{T}$; their average characteristic age is larger than $1\,\mathrm{Gyr}$. We also find an apparent relation between the DM of the pulsars and $\dot{P}$, suggesting that the observed variations in DM are due to plasma in the cluster, with a total column density of $\sim 0.5\ \mathrm{cm^{-3}\ pc}$.

We have also measured the rate of advance of periastron for the binary pulsar J0024−7204H, $\dot{\omega} = (0.073 \pm 0.005)^\circ\,\mathrm{yr^{-1}}$. This implies that the binary system has a total mass of $(1.9 \pm 0.2)\,\mathrm{M_\odot}$, at the 95% confidence level. We also discovered a modulation of DM with orbital phase for PSR J0023−7203J, this information is used to study the plasma envelope of the companion object and to improve the coherent timing solutions for this pulsar.

Declaration

No portion of the work referred to in this thesis has been submitted in support of an application for another degree or qualification of this or any other university or other institution of learning.

Copyright

Preface

Acknowledgements

There were many people that contributed for the success of my stay here at Jodrell Bank and for the success of the 47 Tuc project. I thank Andrew Lyne for all the many things he taught me, and for giving me the opportunity of working here at Jodrell Bank - not the best place in the world if you are too concerned with food, or the weather, but in my opinion one of the best places in the world to do pulsar astronomy. I must also thank him for assigning me, a "rookie" in observational astronomy, such an interesting and motivating project, for which he and Dick Manchester deserve much credit - indeed, I found the software and machinery ready to start in the beginning of the project, and lots of data waiting to be analysed. I also have to thank António A. da Costa, for giving me the opportunity to start my involvement in science, back in the distant days of 1994, and for being a constant and supportive friend.

I must also thank my parents and brother back in Portugal for their steady and warm support for my endeavours, no matter how strange they might seem to them. This support made me go forth, mainly in times of self-doubt and uncertainty about the future.

I must, off course, have to thank my fellow students here in Jodrell Bank, for

observations.

Last, but not the least, I am grateful for the generous support of Fundação para a Ciência e a Tecnologia, provided through grant BD/11446/97; without which this work would not have started.

The Author

The author graduated from Instituto Superior Técnico, Universidade Técnica de Lisboa, in July 1994 in Physics. He obtained his Grau de Mestre em Física (Physics MSc Degree) from that same institution in July 1997.

He registered as a PhD student at Jodrell Bank in October 1997. His research work at Jodrell Bank has culminated in the publication of this thesis.

Publications

Freire, P. C. & Da Costa, A. A. (1999), 'Behaviour of centrifugal forces in neutron stars', *MNRAS*, **304**, 235.

Freire, P. C. & Da Costa, A. A. (2000), 'Centrifugal forces and optical geometry in neutron stars', *Astrophysics and Space Science* **272**, p. 275.

Camilo, F. , Lorimer, D. R., Freire, P. C., Lyne, A. G. & Manchester, R. N. (2000), 'Observations of 20 millisecond pulsars in 47 Tucanae at 20 cm', *ApJ,* **535**, 975.

Freire, P. C., Camilo, F. C., Lorimer, D. R., Lyne, A. G. & Manchester, R. N. (2000a), 'Millisecond pulsars in 47 Tucanae' in 'Pulsar Astronomy − 2000 and Beyond', ASP Conference Series, Vol. 202, 2000; M. Kramer, N. Wex and R. Wielebinski, eds., p. 87.

Freire, P. C., Kramer, M. & Lyne, A. G. (2000), 'Determination of the orbital parameters of binary pulsars', *MNRAS, .* in press

Freire, P. C., Camilo, F. C., Lorimer, D. R., Lyne, A. G., Manchester, R. N. & D'Amico, N. (2000b) 'Timing the millisecond pulsars in 47 Tucanae', *MNRAS,* submitted

Related publications, planned or in preparation

Freire, P. C., Lyne, A. G., Manchester, R. N. & D'Amico, N. (2000c) 'A plasma cloud in 47 Tucanae', in preparation.

Freire, P. C., Stappers, B., Lyne, A. G., Manchester, R. N. & D'Amico, N. (2000d) 'The eclipsing binaries in 47 Tucanae', in preparation.

Freire, P. C., Lyne, A. G., D'Amico, N. & Manchester, R. N. (2000f) 'Emission properties and population studies of the pulsars in 47 Tucanae' (planned).

Freire, P. C., Camilo, F., Lyne, A. G., Manchester, R. N. & D'Amico, N. (2000e) 'High precision timing of the millisecond pulsars in 47 Tucanae' (planned).

List of Abbreviations

The following abbreviations are used:

47 Tuc – The globular cluster 47 Tucanae.

AS23 – Search in acceleration - period space for pulsars in 47 Tuc using 2^{23} time samples.

AS25 – Search in acceleration - period space for pulsars in 47 Tuc using 2^{25} time samples.

DM – Dispersion Measure.

CM – Reference frame of the centre of mass of a binary pulsar or the reference frame of an isolated pulsar.

Jy – Jansky flux unit (1 Jy = 10^{-26} W m^{-2} Hz^{-1}).

LMXB – Low Mass X-ray Binary.

IMXB – Intermediate Mass X-ray Binary.

M$_\odot$ – Solar mass unit (1.99×10^{30} kg).

m_p – Mass of a pulsar.

m_c – Mass of the companion to a pulsar (in a binary system).

(S/N) – Signal-to-noise ratio.

SSB – The barycentre of the Solar System.

TOA – Time of arrival of a pulse at the location of a radio telescope.

Chapter 1

Introduction

In this chapter, we will briefly review the present knowledge of pulsars and millisecond pulsars in general and of pulsars in globular clusters in particular, with a focus on the pulsars in 47 Tucanae, the subject of the remainder of this work.

1.1 Normal and millisecond pulsars

1.1.1 Introduction to pulsars

The first works describing the fundamental properties of neutron stars were produced soon after Chadwick discovered the neutron in 1932. Baade & Zwicky (1934) proposed that the new particle might form compact stars, and even predicted they might form in supernovae, extremely violent episodes of stellar collapse; suggesting therefore that neutron stars should be found near supernova remnants. Landau (1938) suggested that neutron stars could be a source of stellar energy, and made a first estimate of their sizes and densities, and one year later Oppenheimer & Volkoff (1939) calculated the structure of such a star. Because of their extremely small predicted radius (about 10 km), these stars were thought to be essentially unobservable. For this reason, theoretical interest in neutron stars

faded until the discovery of extrassolar X-ray sources (Giaconni et al. 1962). This reawakened theoretical investigation of these objects, now as a possible source of the observed X-ray emission (for a review, see Pacini, 1998).

The discovery of the "pulsating radio stars" (soon called "pulsars"), made in November 1967 by Jocelyn Bell and Anthony Hewish at Cambridge (Hewish et al. 1968) defied, for some time, any explanation. These were periodic radio signals, which have very well-determined pulsation periods between 0.3 and 3 seconds. The early explanations attributed the cause of the radio pulsations to vibrating white dwarfs. However, no optical counterparts were observed near the pulsars. Gold (1969) realized that it was difficult for a white dwarf to vibrate with periods of 0.3 seconds, he attributed the cause of the radio signals to rotating neutron stars. Based on this idea, he predicted that the pulse period should increase with time, for the pulsar loses rotational energy as it radiates. This essential prediction would soon be confirmed: normally pulsars slow down with rotational period derivatives ($\dot{P}$) of the order of $\sim 10^{-15}$ s s^{-1}.

Pacini (1967) studied the Crab nebula, and reached the conclusion that it was probably powered by the fast rotation of a strongly magnetized neutron star. This was later confirmed by the discovery of a 33-ms pulsar in the nebula (Staelin & Reifenstein 1968), PSR B0531+21. The fast pulsation of this source could only be explained as a rotating neutron star. The supernova that formed this nebula was witnessed in the year 1054 BC by Chinese astronomers, and the discovery of the pulsar cemented the link predicted by Baade and Zwicky between pulsars and supernovae.

After this discovery, the idea that pulsars are rotating neutron stars became universally accepted. Pulsars emit radio waves continuously in a collimated beam co-rotating with the neutron star, when this beam sweeps past the Earth we can detect a pulse. Their slowdown is due to their large magnetic dipoles, and the

fact that these are not aligned with their rotation axis (the basic electrodynamics of pulsars was established by Goldreich & Julian, in 1969). The star therefore radiates electromagnetic energy at the spin frequency and its low harmonics. This loss of energy acts as a braking torque on the star, given by

$$N = I\dot{\omega} = -\frac{2}{3c^3}\frac{B_0^2}{R_0^6}\omega^3 \qquad (1.1)$$

where I is the moment of inertia of the star, $\omega \equiv 2\pi/P$ is the angular velocity of the rotation and $\dot{\omega} = 2\pi\dot{P}/P^2$ is its first time derivative (Manchester 1992), B_0 is the magnetic flux density at the surface of the neutron star and R_0 is the neutron star radius. For a constant magnetic flux density, and assuming that the spin rate at birth was much greater than its present value, the characteristic age of the pulsar is given by

$$\tau = \frac{P}{2\dot{P}} \qquad (1.2)$$

and the surface magnetic flux density is given by

$$B \simeq 3.2 \times 10^{15} T\sqrt{P\dot{P}} \qquad (1.3)$$

Therefore, the period and period derivative are essential diagnostics for every pulsar, their knowledge allows a determination of age and magnetic flux density of a pulsar (see Fig. 1.1). Normal pulsars last no longer than about 10^8 years, after this time their rotation is so slow that the induced electric field becomes much weaker, therefore no electron-positron pair production occurs, and the neutron star ceases to function as a radio pulsar (Chen & Ruderman 1993).

In 1974, Hulse and Taylor discovered the first binary pulsar, PSR B1913+16. (Hulse & Taylor 1974). Measurements of the motion of the observable pulsar yielded masses of approximately 1.4 $M_\odot$ for both objects (e.g., Taylor and Weisberg, 1989). Because these masses could be measured in a variety of ways, the consistency between all measured values for the mass provided a test of general relativity and a confirmation of the existence of gravitational radiation.
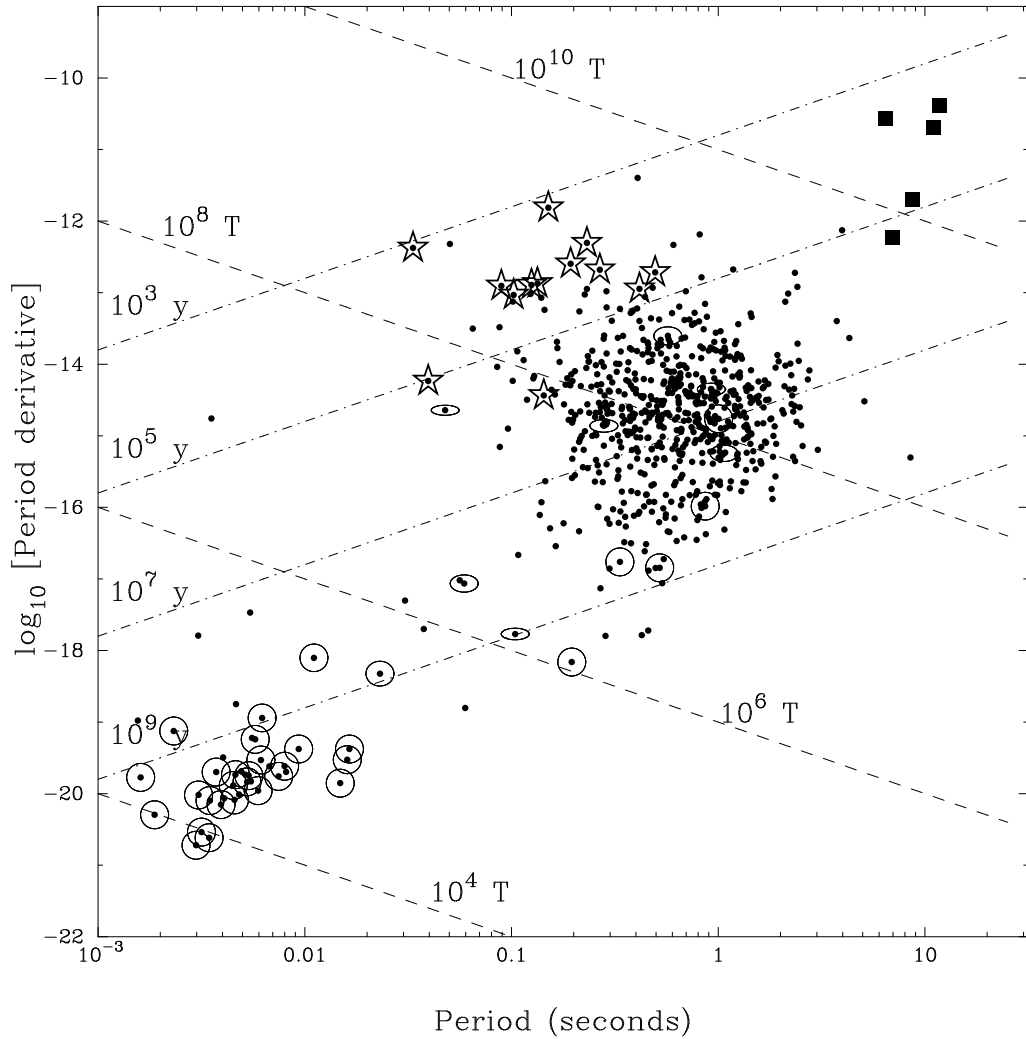
Figure 1.1: Observed periods and period derivatives for 706 pulsars. The normal radio pulsars are seen at the centre of the plot, with typical periods of 1 second and typical period derivatives of $\sim 10^{-15}$. The youngest of such pulsars have shorter periods and higher $\dot{P}$, and are normally associated with supernova remnants (stars), according to Baade and Zwicky's prediction. The millisecond pulsars cluster on the lower left of the plot, with very weak magnetic flux densities at the surface. These pulsars are predominantly found in binary systems (ellipses), while the normal pulsars are normally isolated. The flattening of the ellipse measures the eccentricity of the pulsar, true millisecond pulsars are normally found in binary systems with very circular orbits. The filled squares indicate Anomalous X-ray Pulsars, or AXPs, which have extremely high magnetic flux densities at their surfaces. Data from the Jodrell Bank pulsar catalogue.

The measured neutron star masses have astrophysical meaning too. Their values confirmed a prediction made by Chandrasekhar in 1931 : the maximum mass allowed for a white dwarf is 1.4 $M_\odot$, if the star exceeds this limit (e.g. during a supernova explosion) it collapses by recombination of its protons and electrons, forming neutrons and neutrinos (Baade & Zwicky 1934). One percent of the predicted energy of the neutrinos is sufficient to power the explosion as detected in the electromagnetic domain (Colgate & White 1966). Recently, a large flux of neutrinos was seen emanating from the 1987A supernova (Bionta et al. 1987, Hirata et al. 1987), thus lending further support to the theory that neutron stars are formed in supernova explosions. So far, no pulsar has been detected in the nebula associated with Supernova 1987A (Manchester & Peterson 1996).

Therefore, all predictions made in the 1930's regarding neutron stars were eventually confirmed, this is certainly one of the biggest triumphs of 20th century astrophysics. It is, however, ironic that the property that makes radio pulsars detectable, their radio pulsation, was never predicted; and remains to this day enigmatic.

1.1.2   Millisecond pulsars

The first true millisecond pulsar (henceforth MSP), PSR B1937+21, was discovered by Backer et al. (1982) in a radio source called 4C21.53, in the constellation Vulpecula (The Fox). This pulsar was (and still is) the fastest rotating star known, with a period of only 1.57 ms. Such a short rotational period implied that the radius of the object must be smaller than 75 km, otherwise the equator would be rotating at the speed of light, and probably a much smaller radius, for the object to hold together under the force of its gravitation (e.g. Glendenning 1992).

Apart from their very small rotation period, MSPs have some other peculiar

features: their period derivative is extremely small (about 10^{-19}, compared to 10^{-15} for normal pulsars) and most of them are members of binary systems (see Fig. 1.1). From these observational features and equations 1.2 and 1.3 comparatively weak dipole fields can be deduced (about 10^{4-5} T, compared to 10^{7-9} T for normal pulsars) as well as slowdown ages of about 10^9 years (compared to an average of 10^6 for normal pulsars). For this reason, MSPs are thought to be active radio sources for periods hundreds or thousands of times longer than normal pulsars. Taking active lifetimes into account, it appears that there may be comparable numbers of active young "normal" pulsars and active MSPs in the Galaxy (Lyne et al. 1985), although the birthrate of MSPs is thought to be $\approx 10^4$ smaller. Pulse smearing due to the Interstellar Medium (ISM) and to orbital motion also works against the detection of these pulsars (e.g. Bhattacharya 1998), the first effect reduces effectively the volume on which they might be detected. There is still another important difference: the velocities of MSPs in space are lower than those of normal pulsars by a factor of 5 (Cordes & Chernoff 1997).

Alpar et al. (1982) suggested that low-mass X-ray binaries are the progenitors of millisecond pulsars. According to this scenario, these binaries are composed by a light main-sequence star and a neutron star, itself formed in a previous supernova. The main sequence star fills its Roche lobe, and matter falls onto the neutron star, and this process can go on for hundreds of millions of years. The falling gas slowly transfers its angular momentum to the star, this process also releases large amounts of energy in the form of the X-rays that make LMXBs detectable (Lewin & Joss 1983). It is not clear if magnetic field decay occurs spontaneously or as a result of the accretion process in LMXBs, however the observation of pulsars with long periods and strong magnetic fields in globular clusters (§ 1.2), where all stars capable of generating pulsars in supernovas exploded about ten billion years ago, suggests that magnetic fields decay as a result

of prolonged accretion. Stripped of most of its mass, the main-sequence star eventually becomes a white dwarf, while the neutron star re-starts emitting radio waves, for it now spins very fast[1]. This became the "standard model" of millisecond pulsar formation, for a review see Bhattacharya & van den Heuvel (1991) and references therein.

Other scenarios have also been proposed, mainly for pulsars in globular clusters. The Accretion Induced Collapse model (Michel 1987, Romani 1990, Bailyn & Grindlay 1990) suggests that the accreting object was originally a white dwarf that eventually reached its Chandrasekhar mass limit and imploded as a consequence. Whatever the case, it seems quite clear that MSPs are formed by accretion of mass from a companion object. This idea is supported by the aforementioned fact that most millisecond pulsars are members of binary systems. Also, the orbits of these systems are quite circular (Camilo 1995a); orbit circularization is very likely to happen when the companion star is in the giant phase and near the compact star, because then the tidal forces on the companion are very strong. These forces dissipate large amounts of heat and tend to circularize orbits (Zahn 1977). Further support for this theory comes from the observed relation between binary period and companion mass (Refsdal & Weigert 1971, Joss et al. 1987). Heavier white dwarf companions were formed by heavier stars, which filled their Roche lobes at larger distances from the accreting neutron star, thus generating systems with longer orbital periods.

The fact that some millisecond pulsars are isolated is still not completely understood. Generally, it is thought that the pulsar can in some cases destroy its companion by ablation. This seems to be happening today in some binary systems (see chapter 7).

---

[1]One of the apparent conditions for radio emission is a strong induced electric field, dB/dt. Millisecond pulsars have magnetic flux densities one thousand times weaker than normal pulsars, but they rotate one thousand times faster, therefore the induced electric fields are similar to those of normal radio pulsars.

1.2 Globular clusters

Globular clusters have this name because they look like a giant and spherical swarm of stars [2]. Normally they contain from 10^4 to 5×10^6 stars (van den Bergh 1993). Near the centre of this cluster, the star density is normally over 1000 times larger than the star density near the Sun. The core radius of the cluster, r_c, is where the light surface density (in a CCD detector, or as seen from Earth) is half the central density. This can vary from 0.3 to 10 pc. The tidal radius of the cluster (its "outer end", when stars are tidally pulled by the Milky Way), r_t, varies from 10 to 100 times r_c. The central brightness can vary from cluster to cluster by a factor of 300. This means some globular clusters have cores much more compact than others.

About 200 globular clusters are known in our galaxy (Djorgovski & Meylan 1993). They lie in a sphere with a radius of 60 kpc concentric with the Milky Way, and the number of globular clusters increases as we approach the centre of the galaxy. All the stars in a given globular cluster are thought to have formed at about the same time, which makes possible an accurate determination of the age of the globular cluster, provided convenient knowledge of its distance. All globular clusters in the Milky Way seem to be more than 10^{10} years old (Carreta et al. 2000); and they cannot form new stars, because they have a very low gas content. This was probably swept away at the beginning of the life of the cluster by large numbers of supernova explosions. The stars in the cluster have almost no metals (about 1 percent of the solar system abundance, see, e.g., Reid 1998), which makes us believe their constituent gas is primordial.

To describe stellar motions in a globular cluster newtonian gravity is perfectly adequate. Several equilibrium models have been built, and these normally rest on three assumptions (Spitzer 1987):

---

[2]Not all globular clusters are spherical. ω Centauri is slightly elliptical, being the shorter axis 4/5 the size of the larger axis. This is, however, an exception among globular clusters.

- The potential is a slowly varying function of position, and the stars can be thought of as a continuum gas.

- All globular cluster properties are independent of time.

- The cluster has complete spherical symmetry. The gravitational potential is a function of the distance to the centre only.

Among the most useful of all such cluster models are those called King models, which assume that all stars have the same mass (King 1966). We use one such model for the globular cluster 47 Tuc in chapter 6 to constrain some properties of the cluster and its pulsars.

1.3   Pulsars in globular clusters

1.3.1   Searches

According to Lewin & Joss (1983) , LMXBs are among the brightest X-ray sources in the sky. This implies that the 11 known sources in globular clusters represent the complete sample. An additional 31 weak X-ray sources have been found in globular clusters (Johnston & Verbunt 1995), but these cannot be readily interpreted as LMXBs. These numbers suggest that globular clusters contain far more LMXBs per unit mass than the disk of the Milky Way (Verbunt 1987). This fact led Hamilton et al. (1985) to search for MSPs in globular clusters. They surveyed 12 globular clusters with the VLA seeking for unresolved continuum sources which might be millisecond pulsars. Their only good pulsar candidate was a weak source inside the core of M28. This object was seen later to have a high degree of linear polarisation and a very red spectrum, both common pulsar characteristics. In that same year, with the aid of the Lovell radio telescope at Jodrell Bank and a Cray X-MP supercomputer, the source was found to be a 3.05

ms pulsar (Lyne et al. 1987). This object, PSR 1821−24, is an isolated MSP, which was considered surprising, having in mind the fact that the formation mechanisms for these objects invariably postulate their formation in a binary system.

Six months later, the second MSP (PSR 1620−26) was found on the core of the globular cluster M4, with a period of 11 ms (Lyne et al. 1988, McKenna & Lyne 1988). This pulsar was in a 191-day binary system, its large second period derivative later showed it to be a member of a triple stellar system (Backer 1993, Thorsett, Arzoumanian & Taylor 1993, Backer et al. 1993, Backer & Thorsett 1995), being the third member a possible planet (Rasio 1994, Sigurdsson 1995, Arzoumanian et al. 1996, Joshi & Rasio 1997), with a mass of about 0.01 $M_\odot$ and an orbital period of $\sim$ 62 years (Thorsett et al. 1999).

Some subsequent surveys have been conducted at Arecibo, Jodrell Bank and Parkes, they discovered 32 more pulsars (Kulkarni & Anderson 1996). The fact that many of these are MSPs is an important confirmation of the evolutionary scenario proposed in subsection 1.1, however some of these are *not* MSPs.

At Arecibo, six millisecond pulsars were found in the globular clusters M5 (Wolszczan, Anderson, Kulkarni & Prince 1989), M13 and M53 (Kulkarni et al. 1991) and NGC 6760 (Anderson et al. 1990). Eight pulsars were found in M15 (Wolszczan, Kulkarni, Middleditch, Backer, Fruchter & Dewey 1989, Anderson et al. 1990, Anderson 1992). The first six discoveries were surprising, since these globular clusters have low density cores, their MSPs have very low or undetected period derivatives, which again suggest low density cores.

The first pulsar found in M15 had a period of 111 ms and, most surprisingly, a negative period derivative, something that at the time was unique (Wolszczan, Kulkarni, Middleditch, Backer, Fruchter & Dewey 1989). Acceleration by accretion seems quite unlikely, since no companion can be seen in the timing data,

so it seemed clear that this pulsar is accelerating in the gravitational field of the cluster. This idea has been confirmed by the fact that all non-accreting pulsars with negative period derivative found since lie in globular clusters. This feature can be used to study the matter distribution in the globular cluster (see chapter 6). One of the pulsars in M15, PSR B2127+11C, is a 30 ms pulsar in an eccentric orbit around another neutron star (Prince et al. 1991, Anderson 1992). This system is rather like PSR 1913+16, but unfortunately it cannot be used to test general relativity, because of perturbations from the globular cluster field. From accurate timing, we know that this object lies at about 50 arc-seconds from the centre of the cluster, so it must have suffered a large kick at birth.

Before 1997, the Jodrell Bank/Parkes surveys discovered a total of 9 pulsars in the globular clusters M4 and M28 (mentioned above), NGC 6342 (Lyne et al. 1993), NGC 6440 (Manchester et al. 1989), Terzan 5 (Lyne, Johnston, Manchester, Staveley-Smith, D'Amico, Lim, Fruchter & Goss 1990), NGC 6539 (D'Amico et al. 1990, D'Amico et al. 1993) and NGC 6624 (Biggs et al. 1990). A total of 11 pulsars were found in the globular cluster 47 Tucanae (§ 1.3.2).

Of all the Jodrell Bank/Parkes pulsars, three show eclipses caused by the companion object, these are PSR B0021−72J, PSR B1718−19 and PSR B1744−24A (see § 7.4). Pulsars B1820−30A and 2127+11D show quite large period derivatives, which are not typical of millisecond pulsars. These are probably due to the fact that they are very close to the core of the cluster and so accelerating strongly towards it, and away from the Earth.

Table 1.1 lists all the aforementioned pulsars. The present total number of known pulsars in globular clusters is 44, although there are doubts that PSR B1718−19 and PSR J1748−2444 are associated with the globular clusters NGC 6342 and Terzan 5 respectively. This population is different from that in the Galactic disk.

Globular clusters have, compared to their masses, a larger number of pulsars than the disk of the Galaxy (Kulkarni & Anderson 1996). This happens because in globular clusters the stellar density is remarkably high compared to that of the Milky Way; thus old invisible neutron stars have a far larger probability of interacting with the large number of binaries in the cluster (Hut et al. 1992), normally main-sequence/main-sequence binaries. In such interactions, the most likely outcome is the ejection of the lightest component of the binary and its replacement by the neutron star (Phinney & Sigurdsson 1991). After this stage, the neutron star might be recycled just like in a normal LMXB system.

Thus the pulsar populations in globular clusters are clearly recycled. Another important difference between the globular cluster and the galactic pulsar populations is that the former has far less long period pulsars, while in the Milky Way we expect to find millisecond pulsars and normal pulsars in nearly equal numbers (Lyne et al. 1998). This is to be expected, because globular clusters no longer contain massive stars capable of generating normal, young pulsars in supernovae.

It is therefore surprising that some "normal" pulsars are to be found at all in globular clusters, like PSR B1718$-$19, in NGC 6342, or PSR J1745$-$20, in NGC 6440, with characteristic ages of 10^7 years. This is one of the reasons why some of these associations with globular clusters are doubtful. Those that are indeed associated with globular clusters are probably recycled as well, but to a lesser extent than the remaining millisecond pulsars. Considering the comparatively low lifetime of of these pulsars, their formation mechanism must be rather efficient in order to make any of them detectable at the present time. It is interesting to note that these "young" globular cluster pulsars are always found in massive globular clusters with very dense cores. For a concise discussion of the formation mechanisms of these objects, see Lyne, Manchester & D'Amico (1996) .

Cluster Pulsar	Period (ms)	$\dot{P}$ (10^{-18})	DM (cm^{-3} pc)	P_{orb} (days)	e	Reference
47 Tuc						
J0023−7204C	5.757	−0.049842(4)	24.6	-	-	(This work)
J0024−7204D	5.358	−0.003381(6)	24.7	-	-	(This work)
J0025−7205E	3.536	+0.098520(4)	24.2	2.257	0.000319	(This work)
J0024−7204F	2.624	+0.064520(2)	24.4	-	-	(This work)
J0024−7204G	4.040	−0.042172(8)	24.4	-	-	(This work)
J0024−7204H	3.210	−0.00158(1)	24.4	2.358	0.070550	(This work)
J0024−7204I	3.485	−0.04589(5)	24.4	0.230	0.000	(This work)
J0023−7203J	2.101	−0.0097843(6)	24.6	0.121	0.0000	(This work)
J0024−7204L	4.346	−0.1220(1)	24.4	-	-	(This work)
J0023−7205M	3.677	−0.03843(1)	24.4	-	-	(This work)
J0024−7204N	3.053	−0.02177(3)	24.6	-	-	(This work)
J0024−7204O	2.643	+0.03037(2)	24.4	0.136	0.0000	(This work)
B0021−72P	3.643	*	24.3	0.147	0.000	(This work)
J0024−7204Q	4.033	+0.03419(7)	24.3	1.189	0.00007	(This work)
B0021−72R	3.480	*	24.4	0.066	0.000	(This work)
B0021−72S	2.830	*	24.4	1.202	0.00	(This work)
J0024−7204T	7.588	+0.2944(3)	24.4	1.126	0.0004	(This work)
J0024−7203U	4.343	+0.095239(7)	24.3	0.429	0.00016	(This work)
B0021−72V	4.810	*	24.1	*	*	(This work)
B0021−72W	2.352	*	24.3	0.133	0.00	(This work)
M53						
B1310+18	33.163	*	24.0	255.8	0.002	(Kulkarni et al. 1991)
M5						
B1516+02A	5.553	−0.04122(6)	30.1	-	-	(Anderson et al. 1997)
B1516+02B	7.947	−0.00333(26)	29.5	6.858	0.13784	(Anderson et al. 1997)
M4						
B1620−26	11.076	+0.671	62.9	191	0.02531545(12)	(Thorsett et al. 1999)
M13						
B1639+36A	10.378	*	30.4	-	-	(Kulkarni et al. 1991)
B1639+36B	3.528	*	29.5	1.259	< 0.001	(Anderson 1992)
NGC 6342						
B1718−19	1004.037	+1590(20)	75.9	0.258	0.000	(Lyne et al. 1993)
NGC 6440						
B1745−20	288.603	+400(1)	220	-	-	(Lyne et al. 1996)
Terzan 5						
J1748−2446A	11.563	−0.0340(4)	242.1	0.0756	0.0	(Lyne et al. 2000)
J1748−2446C	8.436	−0.606(4)	237	-	-	(Lyne et al. 2000)
J1748−2444	442.839	+110.7(4)	207.3	-	-	(Lyne et al. 2000)
NGC 6539						
B1802−07	23.101	+0.475(9)	186.4	2.617	0.2120	(Thorsett et al. 1993a)
NGC 6624						
B1820−30A	5.440	+3.385(1)	86.8	-	-	(Biggs et al. 1994)
B1820−30B	378.596	+31.5(3)	87.0	-	-	(Biggs et al. 1994)
M28						
B1821−24	3.054	+1.61845(5)	120	-	-	(Foster et al. 1988)
NGC 6760						
B1908+00	3.62	< 0.1	200	0.14	< 0.01	(Deich et al. 1993)
M15						
B2127+11A	110.665	−21.07(3)	67.25	-	-	(Anderson 1992)
B2127+11B	56.133	+9.56(6)	67.3	-	-	(Anderson 1992)
B2127+11C	30.529	+4.991(25)	67.1	0.33	0.6814	(Anderson 1992)
B2127+11D	4.803	−1.075(12)	67.3	-	-	(Anderson 1992)
B2127+11E	4.651	+0.178(7)	67.3	-	-	(Anderson 1992)
B2127+11F	4.027	+0.032(8)	67.3	-	-	(Anderson 1992)
B2127+11G	37.660	+2.0(5)	67.3	-	-	(Anderson 1992)
B2127+11H	6.743	+0.024(13)	67.3	-	-	(Anderson 1992)

Table 1.1: The 44 known globular cluster pulsars. The asterisk means an ill determined parameter. The reference contains the latest and most precise data for the timing or orbital parameters of the pulsar.

1.3.2 Pulsars in 47 Tuc

Among the globular clusters in the Galactic system, 47 Tucanae (henceforth 47 Tuc) holds the record for the number of pulsars found, 20 so far. The first of these pulsars, PSR B0021-72C[3], was discovered in 640 MHz observations of 47 Tuc made in 1989 (Manchester et al. 1990), these observations also determined that the pulsars PSR B0021-72A and B, reported earlier, do not exist. Ten new millisecond pulsars (B0021-72D-M) were reported one year later (Manchester et al. 1991) after processing of further 640 and 660 MHz observations. Six of these (E, H, I, J, K, L) were suspected binaries, but their detection rate was so low that it was difficult to know for sure. In 1994 and 1995, Robinson (1994) and Robinson et al. (1995) determined that PSR B0021-72K does not exist, but discovered the eleventh pulsar, B0021-72N, in observations made after 1991 at 430 MHz. The latest works also included phase-coherent timing solutions for 47 Tuc C and D, the two brightest isolated pulsars in the cluster. Recently, nine new binary millisecond pulsars have been discovered in 1400 MHz observations of the cluster (Camilo et al. 2000, this work).

The known pulsar population of 47 Tuc is very different from the population in the Galactic disk: all of the pulsars have periods of less than 8 ms, and 13 are members of binary systems. Radio maps of the cluster (Fruchter & Goss 2000, McConnell & Ables 2000) show three scintillating point sources, the positions of which coincide with the brightest pulsars in the cluster: 47 Tuc C, D and J. It is therefore improbable that any bright pulsars remain to be discovered, even with the severe selection effects against the detection of binaries with very short orbital periods and pulsars with very short rotational periods discussed in § 2.2 and § 2.5. No definite identifications have been made for the two isolated pulsars with previously known timing solutions (47 Tuc C and D) in gamma-rays

---

[3]Because all pulsars in this cluster are detected in the same telescope beam pattern, and precise positions were not available originally, the pulsars were named B0021−72C, D, etc.

Parameter	Value	Reference
Center R.A., $\alpha_{47\ \mathrm{Tuc}}$ (J2000)	$00^{\mathrm{h}}24^{\mathrm{m}}05\overset{\mathrm{s}}{.}29 \pm 0\overset{\mathrm{s}}{.}28$	(De Marchi et al. 1996)
Center Decl., $\delta_{47\ \mathrm{Tuc}}$ (J2000)	$-72°04'52\overset{''}{.}3 \pm 1\overset{''}{.}3$	(De Marchi et al. 1996)
Distance, D	$5.0 \pm 0.4\,\mathrm{kpc}$	(Reid 1998)
Age	$10.0 \pm 0.4\,\mathrm{Gyr}$	(Gratton et al. 1997)
Total mass	$(1.07 \pm 0.04) \times 10^6\,\mathrm{M_\odot}$	(Meylan 1989)
Tidal radius	$40'$ ($54\,\mathrm{pc}$)	(Da Costa 1979)
Core radius, θ_c (r_c)	$23\overset{''}{.}1 \pm 1\overset{''}{.}7$ ($0.6\,\mathrm{pc}$)	(Howell et al. 2000)
Escape velocity	$58\,\mathrm{km\,s^{-1}}$	(Webbink 1985)
Central density	$\sim 1.3 \times 10^5 \mathrm{M_\odot pc^{-3}}$	(Pryor & Meylan 1993)
Radial velocity dispersion at centre, $v_z(R_\perp = 0)$	$11.6 \pm 1.4\,\mathrm{km\,s^{-1}}$	(Meylan & Mayor 1986)
Proper motion in R.A., μ_α	$5.9 \pm 0.6\,\mathrm{mas\,yr^{-1}}$	this paper (sect. 6.2)
Proper motion in Decl., μ_δ	$-4.1 \pm 0.6\,\mathrm{mas\,yr^{-1}}$	this paper (sect. 6.2)

Table 1.2: Parameters of the globular cluster 47 Tuc.

(Ferguson et al. 1999) or X-rays (Verbunt & Hasinger 1998).

In addition to this unusual set of pulsars, there is a collection of other exotic objects in the core of 47 Tuc: at least 15 X-ray sources (Hasinger, Johnston & Verbunt 1994; Verbunt & Hasinger 1998) and more than 20 blue stragglers (Guhathakurta et al. 1992). Evidence has also been found for the existence of cataclysmic variables in the core (Edmonds et al. 1996). The high stellar density necessary for the formation of these objects may increase the rate of exchange of stars in binaries (Hut et al. 1991), leading to the formation of LMXBs and millisecond pulsars, a process described in detail by Rasio, Pfahl and Rappaport (2000) for the specific case of 47 Tuc.

Table 1.2 summarises the basic parameters of 47 Tuc which we use to interpret our results.The position of the centre of 47 Tuc is taken to be point "D" of plate 1 of De Marchi et al. (1996). We derive the absolute position of "D" by comparing its position with that of point "G" on the same plate, whose absolute position was obtained by Guhathakurta et al. (1992). Recent Hipparcos data (Reid 1998) implies that the distance to 47 Tuc is $(5.0 \pm 0.4)\,\mathrm{kpc}$, 10% larger than previously thought (Webbink 1985). The stellar line-of-sight velocity dispersion at the centre (Meylan & Mayor 1986) is smaller than the previously accepted value of $13.2\,\mathrm{km\ s^{-1}}$ (Webbink 1985), and according to Howell, Guhathakurta &

Time span	N_{obs}	F_c (MHz)	ΔF (MHz)	N_{chan}	τ (min)	t_{samp} (μs)	t_{res} (μs)	S_{eq} (Jy)
7/89–5/92	47	640/660	32	128	74	300	350	90
5/91–11/93	42	436	32	256/16	90/60	300	430	90
1/98–4/98	18	660	32	256	105	125	155	90
8/97–8/99	108	1374	288	96	280	125	270	35
8/99–6/00	72	1390	256	512	280	80	88	35

Table 1.3: Summary of 11 years of radio observations of 47 Tuc. N_{obs} is the number of observing days, F_c is the central radio frequency used, ΔF is the total bandwidth recorded, N_{chan} is the number of frequency channels per polarization, τ is the most common integration time, t_{samp} is the sampling time and t_{res} is the time resolution for each set of observations at the central frequency. With $\delta F_{\text{chan}} \equiv \Delta F / N_{\text{chan}}$, the time resolution was obtained using equations 2.4 and 2.5. S_{eq} is the equivalent flux density in the direction of 47 Tuc.

Gilliland (2000), the core radius is double the value used previously (De Marchi et al. 1996). The value for the proper motion was obtained from Hipparcos data: $\mu_\alpha = (7.0 \pm 1.0)\,\text{mas}\,\text{yr}^{-1}$ and $\mu_\delta = (-5.3 \pm 1.0)\,\text{mas}\,\text{yr}^{-1}$ (Odenkirchen et al. 1997). The value in Table 1.2 is derived in § 6.2 from a weighted average of the pulsar proper motions measured in this work.

1.4 Observations of 47 Tuc

Most of the early observations of 47 Tuc were made at 660 MHz using the 64-m radio telescope at Parkes, Australia, between 1989 and 1991 , with a bandwidth of 32 MHz. Starting in May 1991, regular 436 MHz observations were also made, also using a bandwidth of 32 MHz, this observing program continued until the end of 1993 (see Table 1.3). In August 1997, observations of 47 Tuc were resumed at Parkes, after a four-year gap, and continue to date. The majority of these observations were made using the central beam of a multi-beam system (Lyne et al. 2000) at a central radio frequency of 1374 MHz. The system consists of a cooled, dual linear polarization, 13-beam receiver package (Staveley-Smith et al. 1996), and new filter banks, single-bit digitizer, and data-acquisition computer.

This data is the main source of new information reported in this work.

Each of the 13 beams has a half-power diameter of about 14′ on the sky. Since a single beam encompasses the great majority of the cluster stars (cf. Table 1.2), we record data from the central beam only (but see discussion in § 2.5.2), while pointing the telescope at 47 Tuc C, the first pulsar discovered in this cluster.

From August 1997 to August 1999, the incoming signals from two orthogonal polarisations were down-converted and filtered in a $2 \times 96 \times 3$-MHz filterbank used by the multi-beam system for the central beam. After summing the polarisation pairs, the resulting voltages were one-bit sampled every $125 \, \mu$s. After August 1999, a new $2 \times 512 \times 0.5$ MHz filterbank started operating, and we have been using it since, sampling the data every $80 \, \mu$s. The sampled noise intensity levels, together with accurate time referencing and relevant telescope information, are written to magnetic tape for off-line processing. Data are usually collected on days when a pulsar survey of the Galactic plane is also underway (Lyne et al. 2000). There is a 7-hour interval every sidereal day when the parts of the galaxy being surveyed by this multi-beam survey are below the horizon of the Parkes telescope, it is a fortunate coincidence that 47 Tuc can be observed during this time.

1.5 Aims and structure of the thesis

1.5.1 Searching for millisecond pulsars in 47 Tuc

In chapter 2, we describe the first accelerated searches for pulsars in 47 Tuc. These searches used mainly the 20 cm data obtained since 1997 until August 1999 (see Table 1.3). Nine new binary millisecond pulsars have been found, increasing the number of known pulsars in 47 Tuc from 11 to 20. We also estimate the sensitivities of the surveys for isolated and binary pulsars, compare them to that

of past surveys of 47 Tuc and summarize the results, including parameters for the newly discovered pulsars and updated parameters for some previously known systems. We discuss some limitations, and implications, of our surveys and their results.

These searches proceed to date, now in the more recent 1400-MHz data, which has 3 times higher time resolution. New pulsars are still being found because scintillation makes their flux densities vary by orders of magnitude. Therefore, very weak pulsars can occasionally be amplified above the sensitivity threshold of the Parkes radio telescope, making them detectable for periods up to a few hours.

In chapter 3, we present the pulse profiles for the 20 pulsars at the three bandwidths at which they have been observed and an estimate of their flux densities at 1400-MHz.

Apart from detecting new pulsars, searching for pulsars in a globular cluster also produces more detections of known pulsars, because all pulsars can be observed in the same beam. These re-detections are very important to determine or refine the orbital characteristics of the binary pulsars. In chapter 4, we describe a novel procedure for estimating the orbits of poorly sampled pulsars. We use this procedure to estimate the orbital parameters of 47 Tuc S and T. In this chapter, we also review the well known method for determining the orbital parameters of a binary system from variations in the apparent rotational period of the pulsar ("period analysis").

1.5.2 Timing the millisecond pulsars in 47 Tuc

Although all pulsars in M15 have had positions and period derivatives determined using pulsar timing techniques, this has been possible, before this work, for only two of the pulsars in 47 Tuc. This is due mainly to the different telescopes used

and different interstellar scintillation characteristics: at Arecibo, Puerto Rico, the majority of the distant pulsars in M15, whose apparent fluxes vary little, are detectable on most days, while at Parkes, Australia, most pulsars in 47 Tuc are visible only when the interstellar weather is propitious and the pulsar signals are amplified in the observing radio band by scintillation. Unfortunately this has meant that many of the scientific objectives suggested by the wealth of pulsars known in 47 Tuc remained, before this work, unfulfilled.

The increase of the detection rates for these pulsars in the 1400 MHz observations made since 1997 permitted the determination of thirteen new coherent timing solutions, bringing the number of pulsars with coherent timing solutions in 47 Tuc to 15. With these coherent timing solutions, we have reprocessed the data from the early nineties as well, in most cases extending the solutions back to 1991. We have essentially processed all data listed in Table 1.3 for the purpose of timing.

We present the basics of pulsar timing in chapter 5. In that chapter, we also discuss the data reduction and analysis techniques used to obtain these new timing solutions, and the solutions themselves. These contain a wealth of astrophysical information which we discuss in the rest of this work.

In chapter 6, we investigate the pulsar distribution in 47 Tuc and the proper motion of the cluster. We also use the period derivatives of the pulsars to constrain the accelerations produced upon them by the gravitational field of 47 Tuc. From that, we derive some constraints for the surface mass density of the cluster, and verify that the accepted models of the cluster can explain the distribution of $\dot{P}$s observed among the pulsars in 47 Tuc. We also derive limits on the characteristic ages and magnetic flux densities for the pulsars. We also investigate an interesting observation: the pulsars in 47 Tuc with negative period derivatives have higher DMs than the remaining. This suggests the presence of a cloud

of plasma in the cluster; the properties of this cloud will be investigated more thoroughly in the near future.

In chapter 7, we discuss some characteristics of the binary systems, their formation mechanisms and the effect the globular cluster had on their orbital characteristics, with particular emphasis on the orbital eccentricities. We discuss the implications of the rate of advance of periastron measured for PSR J0024−7204H, and present a short study of the eclipsing pulsar 47 Tuc J, which is observed to change its DM with orbital phase. Finally, in chapter 8, we summarise our results and briefly discuss the prospects for future observations of the pulsars in 47 Tuc.

Chapter 2

Searching for pulsars in 47 Tuc

We now present the searches for new pulsars in 47 Tuc made since August 1997. § 2.1.1 explains the basics of pulsar searching, which was based on Camilo (1995a), to which we refer the reader for more detailed information on searches for pulsars in the galactic disk. The subsequent material related to the findings of AS23 has been published in the Astrophysical Journal (Camilo et al. 2000). We also present here for the first time the 2^{25}-point search (AS25) and some of its early results.

2.1 Data analysis

2.1.1 General pulsar search techniques

For most pulsars, the individual pulses are too weak for detection. For this reason, the signals must be averaged over minutes, if not hours. Therefore, the simplest implementation of a search strategy is to sample the total intensity from some part of the sky fast enough and then do a Fourier transform of the time series to search for periodic signals. In practice, pulsar duty cycles tend to be short (for the pulsars in 47 Tuc, the intensity is above half the maximum for only a

few percent of the rotational cycle of the pulsar). Therefore, the pulsars have their power spread over many harmonics, thus searching for a single harmonic is not very efficient. Furthermore, the broadband signals arriving from the pulsar are dispersed. This effect is caused by the fact that the group velocity v_g in the interstellar plasma is slower for lower frequencies. The exact relation is

$$v_g = c \left(1 - \frac{\nu_p^2}{F^2}\right)^{1/2} = c \left(1 - \frac{\nu_p^2}{2F^2}\right) + \mathcal{O}\left(\frac{c\nu_p^4}{F^4}\right) \qquad (2.1)$$

where

$$\nu_p = (n_e e^2/\pi m_e)^{1/2} = 8.97 \times 10^3 . \sqrt{n_e} \qquad (2.2)$$

is the plasma frequency and e, m_e and n_e are the electron charge, mass and local number density and F is the observing frequency. For the interstellar medium, $n_e \sim 0.03$ cm^{-3}, this yields $\nu_p \sim 1.6$ kHz. Therefore, for frequencies above ~ 100 MHz, like those used in this work, the higher order terms in equation 2.1 can be ignored.

This difference in group velocities causes the dispersive effect itself, which is a delay in arrival times of the pulses compared to a signal with infinite frequency. This delay is given, for a radio frequency F, by

$$dt(F) = \frac{e^2}{2\pi m_e c} \frac{1}{F^2} \int_0^D n_e dl \, \text{s} = 4.14 \times 10^{15} F^{-2} \text{DM} \, \text{s} \qquad (2.3)$$

where D is the distance of the pulsar to the Earth, and dl is an element of length along the line-of-sight. The integral defines the Dispersion Measure (henceforth DM), and it is conventionally measured in units of cm^{-3} pc.

Therefore, in a wide band receiver the signal from the pulsar is smeared, which in some cases prevents its detection. This effect can be largely removed by sampling the power levels separately in several narrow frequency channels spanning a bandwidth as large as possible. Then, for each channel a delay of the form of equation 2.3 is subtracted, according to the frequency F of each channel

and a given DM. After this, the signal from all channels is added, creating a de-dispersed time series.

Even in this situation, there will still be dispersive smearing of the signal from the pulsar across each channel, because each of these channels detects a finite range of frequencies δF. This smearing is given by

$$\delta t = \frac{e^2}{\pi m_e c}\frac{1}{F^3}\mathrm{DM}\delta F\,\mathrm{s} = 8.3\left(\frac{\mathrm{DM}}{\mathrm{cm}^{-3}\,\mathrm{pc}}\right)\times\left(\frac{\delta F}{\mathrm{MHz}}\right)\times\left(\frac{F}{\mathrm{GHz}}\right)^{-3}\mu\mathrm{s}, \qquad (2.4)$$

provided that δF is much smaller than F. In the low radio frequencies (i.e, less than tens of GHz) normally used to observe pulsars, narrow filters are always used to reduce dispersive smearing, therefore this condition is normally satisfied.

Further smearing occurs because of the finite sampling interval t_{samp}. For a known pulsar with a known DM, the timing resolution t_{res} is defined as the observed width of a very narrow feature in the pulse profile. t_{res} is given by

$$t_{\mathrm{res}}^2 = \delta t^2 + t_{\mathrm{samp}}^2 \qquad (2.5)$$

t_{samp} should be smaller, but of the same order, of δt, and therefore depends on the DM of the source. A low sampling rate will be the main cause of deterioration of the signal, while a very high sampling rate generates a cumbersome amount of data without improving the time resolution.

By removing the dispersive delay typical of each channel frequency F and adding the time series from each channel, we generate a de-dispersed time series. This will be different according to the particular DM used in the de-dispersion. To search for unknown pulsars, we make a Fourier transform of this de-dispersed series. Any signal with a frequency higher than half of the sampling frequency is by definition meaningless (this is the Nyquist criterion). Generally, these spectra cover frequencies from ~ 0.1 Hz to a few kHz.

Even at this stage, any new pulsars are probably too weak to produce observable peaks in the Fourier spectrum. We know, however, that if there are any

new pulsars, they should present signals with some unknown frequency and then harmonics with twice, three, four... times the basic frequency. Therefore, the Fourier spectrum is normally shrank in frequency by a factor of two, three, four, eight and sixteen, and for each of these factors it is added to itself. This process strengthens the fundamental harmonic, making it detectable.

It is at this stage that the software looks for significant peaks in the composite spectrum. A database of known interference frequencies is used to exclude interference (e.g., signals with frequencies of 50 Hz are probably caused by the mains). After this, follow-up work is aimed at confirming that the signal is indeed dispersed and at improving the rotational period and, in the case of a binary, determining the orbital parameters (see chapter 4).

When searching for pulsars in the galaxy many DMs have to be tried, for there is no *a priori* knowledge of periods and DMs in which to find new pulsars. Therefore, such searches represent a large computational effort. In the case of searches for pulsars in globular clusters, mainly for those with a known pulsar, only a narrow range of DMs around the DM of the known pulsar must be searched in order to find new pulsars, for generally all pulsars in a cluster have very similar DMs (see Table 1.1). We will now discuss these searches in more detail.

2.1.2 Searches for pulsars in globular clusters

Searches for millisecond pulsars in globular clusters encounter two main difficulties. Firstly, since globular clusters are on average more distant than the $\sim 2\,\mathrm{kpc}$ within which most large-area surveys have been sensitive to millisecond pulsars (see, e.g., Camilo et al. 1996), much longer observation times are typically required than for Galactic searches. This in turn increases the complexity of the data-reduction task. Such observation times are feasible only because of the small number of search targets; and searching for pulsars in these large data

sets is feasible because of the small range of DMs in which new pulsars are to be found. Secondly, for binary pulsars there is the added difficulty that the apparent pulse period may change significantly as the pulsar experiences orbital accelerations during the longer integration. If this issue is not addressed at the data reduction stage — and with significant exceptions (Anderson et al. 1990) it rarely is, because of the massive computational requirements — many relatively bright binary pulsars may remain undetected.

Despite these difficulties, the rewards of a thorough search can be significant. Because of the high probability of close stellar interactions, unusual binary systems not otherwise expected in the Galactic disk may form in clusters. The fact that 47 Tuc is a relatively nearby cluster with a high stellar density makes it an attractive target for pulsar searches. This cluster, together with M15, have been by far the most prolific cluster targets for pulsar searches to date, with surveys previous to this work revealing 11 and eight pulsars respectively (Manchester et al. 1991, Robinson et al. 1995, Anderson 1992), all of which can be observed in a single telescope beam. The observed population of pulsars in these two clusters is very different (see Table 1.1): while those in 47 Tuc are all millisecond pulsars, the pulsars in M15 are more varied in their properties, including slowly-spinning pulsars and a rare double neutron-star binary (Prince et al. 1991).

As we mentioned before (§ 1.4), a new, sensitive system for observing pulsars at a wavelength of 20 cm became available at the Parkes radio telescope in mid-1997. Pulsars are in general steep-spectrum sources (Lorimer et al. 1995), and all pulsars in 47 Tuc known until 1997 were discovered at a wavelength of 50 or 70 cm (Manchester et al. 1990, 1991; Robinson et al. 1995). However, the new system provided such performance improvements that observations to study the known pulsars and to find previously undetected pulsars seemed desirable. These observations were so successful in the rate of detection of previously known pulsars

and discovery of new ones that we have moved to observing the cluster almost exclusively with the new system. In this chapter we report on the discovery of nine binary millisecond pulsars in 47 Tuc and give improved parameters for some of the previously known pulsars.

With the computing resources presently at our disposal, it is impracticable to reduce such data sets in single, coherent, Fourier analyses. Furthermore, since about one third of the pulsars already known in 47 Tuc are in binary systems, some with orbital periods of under 3 h (Robinson et al. 1995), we would select against such systems if we analyzed each large data set as a whole. As a compromise between computational feasibility and sensitivity (both to weak radio sources and relatively short-period binaries), we restrict the data analysis reported in this chapter to contiguous blocks of 2^{23} time samples (17.5 min) or, alternatively, 2^{25} time samples (70 min).

The data were de-dispersed to a reference DM of $24.6\,\mathrm{cm^{-3}\,pc}$, the DM of 47 Tuc C. This was done by anticipating samples from the lower-frequency channels to account for the slower propagation through the ionized interstellar medium, before summing data from all channels into a one-dimensional time series. For the present analysis, where we are particularly interested in looking for binary pulsars with short orbital periods, this choice was made largely to keep the total computational effort manageable. The pulsars presently known in 47 Tuc exhibit a range of DMs between 24.1 and $24.7\,\mathrm{cm^{-3}\,pc}$ (Table 2.1). In the current analysis, any pulsar with a true DM that is within one unit of $24.6\,\mathrm{cm^{-3}\,pc}$ will have its pulse smeared by at most 1 ms as a result of this single-DM approximation.

As noted by a number of authors (Middleditch & Priedhorsky 1986, Johnston & Kulkarni 1991), standard pulsar search analyses, which look for significant harmonics in the power spectrum of a de-dispersed time series, suffer reductions in sensitivity to pulsars in short-period binary systems. The effect of the binary

Pulsar	Period (ms)	DM $(\mathrm{cm}^{-3}\,\mathrm{pc})$	w_{50} (%)	Flux density (mJy)
		Previously Known		
47 Tuc C	5.756780	24.6	11	0.38(4)
47 Tuc D	5.357573	24.7	4	0.23(3)
47 Tuc E	3.536329	24.2	17	0.22(3)
47 Tuc F	2.623579	24.4	12	0.16(2)
47 Tuc G	4.040379	24.4	9	0.06(1)
47 Tuc H	3.210341	24.4	8	0.09(1)
47 Tuc I	3.484992	24.4	8	0.10(1)
47 Tuc J	2.100634	24.6	10	0.58(6)
47 Tuc L	4.346168	24.4	47	0.04(1)
47 Tuc M	3.676643	24.4	25	0.08(2)
47 Tuc N	3.053954	24.6	6	0.03(1)
		Newly Discovered		
47 Tuc O	2.643343	24.4	6	0.10(1)
47 Tuc P	3.643021	24.3	15	-
47 Tuc Q	4.033181	24.3	9	0.05(1)
47 Tuc R	3.480463	24.4	15	-
47 Tuc S	2.830406	24.4	9	-
47 Tuc T	7.588480	24.4	11	0.08(1)
47 Tuc U	4.342827	24.3	5	0.07(1)
47 Tuc V	4.810	24.1	7	-
47 Tuc W	2.352344	24.3	47	-

Table 2.1: Periods, DMs, duty cycles and flux densities for the known pulsars in 47 Tuc. The duty cycles and flux densities are estimated in chapter 3.

motion is to cause a change in the apparent pulse frequency during the integration, spreading the emitted signal power over a number of spectral bins, thereby reducing the apparent signal-to-noise ratio. In order to recover the signal, it is necessary to transform the time series to the rest frame of an inertial observer with respect to the pulsar before carrying out the periodicity search. This transformation is readily achieved by applying the Doppler formula to relate a time interval in the pulsar frame, τ, to the corresponding interval in the observed frame, t:

$$\tau(t) = \tau_0(1 + v(t)/c), \qquad (2.6)$$

where $v(t)$ is the observed radial velocity of the pulsar along the line-of-sight, c is the speed of light, and we have neglected terms in (v/c) of order higher than the first. Ideally, if the orbital parameters of the binary system are known, $v(t)$ can be calculated from Kepler's laws. For the purposes of a blind search, where the orbital parameters are a priori unknown, assuming a Keplerian model for $v(t)$ would require a five-dimensional search of all the parameter space —

a computationally non-trivial task! The search can, however, be considerably simplified by assuming that the orbital acceleration a is constant during the observation, i.e., $v(t) = at$. This assumption is commonly used in searches of this kind (Anderson 1992) and turns out to be reasonable over a wide range of orbital parameters, phases, and observation lengths. We investigate this in more detail in § 2.5.1.

Given a prescription for $v(t)$, the re-sampling process is straightforward. The time intervals in the new frame are calculated from equation 2.6. New sample values are then created based on a linear interpolation running over the original time series (see also Middleditch & Kristian 1984). We choose to define the value of τ_0 such that τ is equal to the original sampling interval, t_{samp}, at the mid-point of the integration. For the condition $v(t) = at$, it follows that

$$\tau_0 = \frac{t_{\mathrm{samp}}}{1 + aT/2c},$$

(2.7)

where T is the integration time, 17.5 or 70 min in our case. This condition guarantees that, under the approximations made here, the number of samples in the corrected time series is the same as in the original one. The re-sampling process is relatively trivial in terms of computation time and can be readily carried out for a number of trial accelerations for each de-dispersed time series in order to effect a search in "acceleration space".

In the analyses carried out in this work, each de-dispersed time series was re-sampled and analyzed for a number of trial accelerations. For the 2^{23} sample search, the accelerations are in the range $|a| < 30 \, \mathrm{m\,s^{-2}}$, for the 2^{25} sample search the accelerations are in the range $|a| < 5 \, \mathrm{m\,s^{-2}}$. We will therefore refer to these searches as AS23 and AS25 ("AS" stands for "accelerated search"). Most pulsars in presently known binary systems typically undergo accelerations of up to about $5 \, \mathrm{m\,s^{-2}}$. There are however other binary systems, mainly with short orbital periods, which can display extreme accelerations. These include the

double neutron-star binary PSR B2127+11C in M15, originally discovered at a
trial acceleration of $-9.5\,\mathrm{m\,s^{-2}}$ (Anderson et al. 1990), and the eclipsing binary
PSR B1744$-$24A in Terzan 5 (Lyne et al. 1990), where the maximum line-of-sight
acceleration is $33\,\mathrm{m\,s^{-2}}$. This motivated us to use a larger range of acceleration
space in AS23. Doing the same in AS25 is extremely time-consuming, given the
small acceleration step needed for this search. The step size between each trial
acceleration is $0.3\,\mathrm{m\,s^{-2}}$ for AS23 and $0.02\,\mathrm{m\,s^{-2}}$ for AS25. Some care is required
when choosing this interval in order to strike a compromise between unnecessary
processing time incurred by oversampling the parameter space and the loss of
sensitivity caused by under-sampling. Assuming that the constant acceleration
approximation adequately describes the Doppler shifts during the integration, it
follows that the number of spectral bins across which a signal will drift due to
the assumed trial acceleration being different from the true value by an amount
Δa is given by $\Delta a \times T^2/Pc$, where P is the pulse period. Our choices of step
sizes thus guarantee that any pulsar period or harmonic with a period greater
than $2\,\mathrm{ms}$ will not drift by more than one spectral bin during the integration.

Following the de-dispersing and re-sampling procedures outlined above, each
time series is analyzed independently according to standard pulsar search tech-
niques. The analysis procedure is very similar to that described in detail by
Manchester et al. (1996). In brief, we compute discrete Fourier transforms of
each time series, and sum harmonically related spectral components for 1, 2,
4, 8, and 16 harmonics in turn, in order to maintain sensitivity to a variety of
pulse profile relative widths, or duty-cycles. For each harmonic sum, candidates
are ranked in order of spectral signal-to-noise ratios[1]. At this stage, all spectral

---

[1]Spectral signal-to-noise ratios are defined throughout this work to be the height of a feature
in the amplitude spectrum divided by the spectral rms. In general, spectral signal-to-noise ratios
and ratios calculated from reconstructed time-domain pulse profiles are different, although in
practice, for relatively low values — relevant for search sensitivity calculations (§ 2.2; § 2.5.1) —
they are identical, and we use the nomenclature (S/N) in both instances. To estimate average
flux densities (§ 3.2), where some signal-to-noise ratios are large, we carry out all computations

features with $(S/N) \geq 6$ are stored, along with the period of the signal.

Once computations are completed for the time series corresponding to all trial accelerations of AS23 or AS25, we plot (S/N) versus trial acceleration for multiple occurrences of each period, within a suitable tolerance, detected above a pre-defined "significance" threshold. This threshold can be estimated theoretically from the statistics of the phase-space searched, but practical considerations (such as the presence of radio-frequency interference) result in our determining this value empirically. We generate plots such as that in Figure 2.1 for all cases where at least one detection of a multiply detected period has $(S/N) \geq 9$. The software used to do all the previous analysis was developed by Duncan Lorimer in 1996, and is still being used to date.

2.2   Sensitivity

To estimate the sensitivity of our searches we calculate the minimum flux density S_{min} that a pulsar must have in order to be detectable. Following Dewey et al. (1984), this is given by

$$S_{\mathrm{min}} = \frac{(S/N)\eta \, S_{\mathrm{sys}}}{\sqrt{n \, \Delta F \, T}} \left(\frac{w}{P - w} \right)^{1/2} . \tag{2.8}$$

Here (S/N) is the signal-to-noise ratio threshold of the survey (9 in our case); η is a constant that takes account of losses in sensitivity due to digitization of the incoming data and other inefficiencies in the system ($\sim$1.5 for our system); S_{sys} is the system equivalent flux density ($\sim$35 Jy for the present system in the direction of 47 Tuc); n is the number of polarisations summed (two in our case); ΔF is the total observing bandwidth (288 MHz); T is the integration time (1049 s or 4196 s); and w and P are the pulse width and period respectively.

The observed pulse width w in the above expression is in general greater

---

in the time domain.
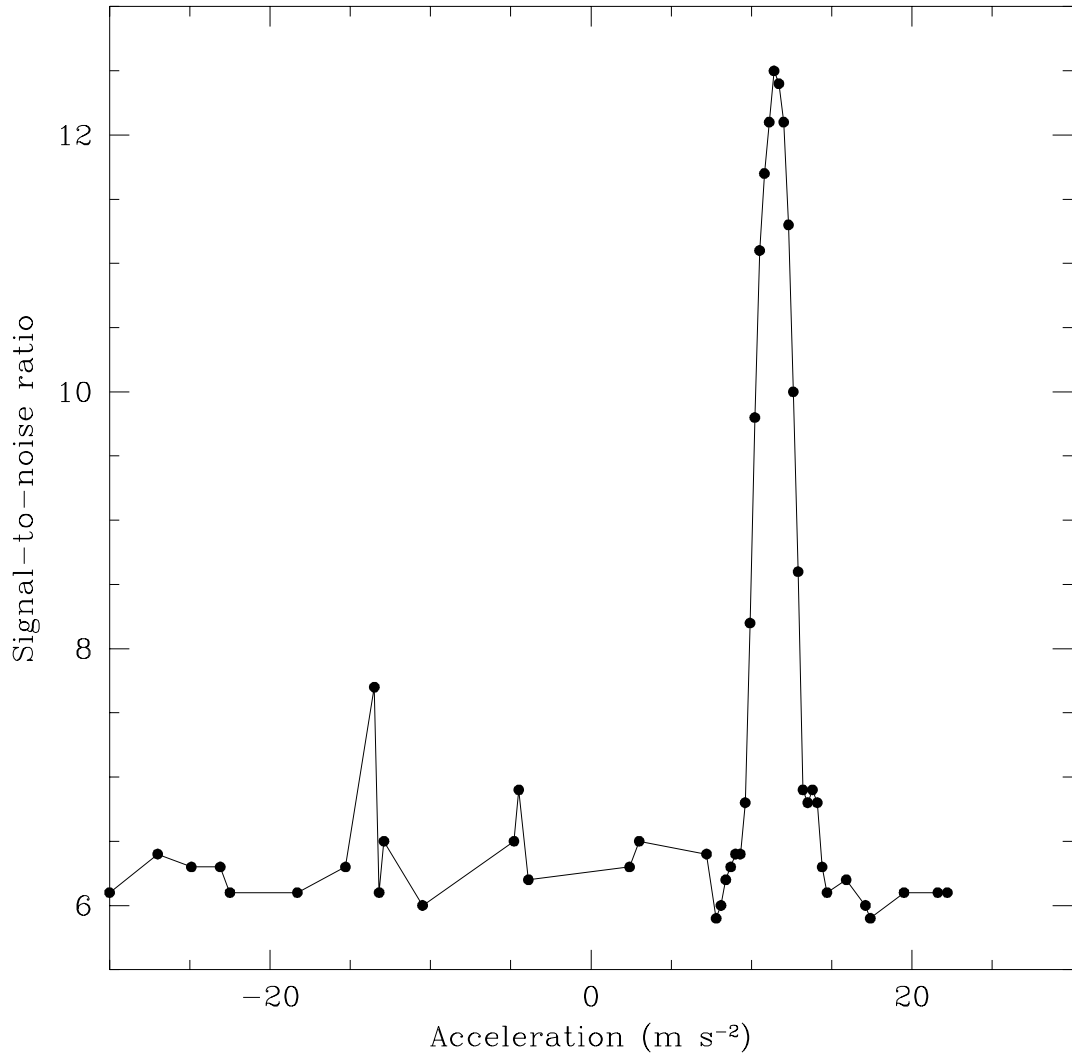
Figure 2.1: Signal-to-noise ratio (S/N) versus trial acceleration for the discovery of 47 Tuc R. This plot corresponds to one of seven AS23 integrations (17.5-min), out of a total of eight on MJD 50742, in which (S/N) in at least one trial acceleration was higher than the threshold of 9. Most points with $(S/N) < 8$ correspond to random noise rather than detection of the pulsar.

than the intrinsic width w_{int} emitted at the pulsar because of the dispersion and scattering of pulses by free electrons in the interstellar medium, and the post-detection integration performed in hardware. Interstellar scattering is negligible for most observations toward 47 Tuc, which is relatively nearby and located well away from the Galactic plane. The observed pulse width for unaccelerated pulsars is therefore the convolution of the intrinsic pulse width and broadening functions due to dispersion and integration, and can be estimated from the quadrature sum

$$w^2 = w_{\text{int}}^2 + t_{\Delta\text{DM}}^2 + t_{\text{res}}^2. \tag{2.9}$$

where t_{res} is given by equation 2.5. $t_{\Delta\text{DM}}$ is the overall pulse broadening due to the difference ΔDM between the single DM at which we de-disperse all data and the true DM of a pulsar; it can be obtained from equation 2.3:

$$t_{\Delta\text{DM}} = 4.14 \times 10^{15} \left(F_1^{-2} - F_2^{-2} \right) \Delta\text{DM s} \tag{2.10}$$

where F_1 and F_2 are respectively the lowest and highest frequencies being observed.

The effective time resolution for these 47 Tuc observations, calculated from equation 2.5, the data in Table 1.3 and a DM of $25\,\text{cm}^{-3}\,\text{pc}$, is approximately $0.3\,\text{ms}$ at the center frequency of observations for the data obtained from August 1997 to August 1999, although it falls to $0.4\,\text{ms}$ at the low-frequency end. In the more recent data, it is of the order of $0.1\,\text{ms}$. However in many cases (particularly, in the data with high time resolution), the effective time resolution is limited by the $t_{\Delta\text{DM}}$ term in equation 2.9, which amounts to $0.9\,(\frac{\Delta\text{DM}}{\text{cm}^{-3}\,\text{pc}})\,\text{ms}$ at $1374\,\text{MHz}$.

Figure 2.2 shows the search sensitivity as a function of period for a $17.5\,\text{min}$ integration and a 70-min integration based on equations 2.8–2.9. Here we have assumed a box-car pulse shape and an intrinsic duty-cycle of 15%, typical of many among the pulsars known in 47 Tuc. The only two pulsars with flux densities above the minimum limit of AS23 are 47 Tuc C and J. AS25 is twice as sensitive,

and pulsars 47 Tuc D, E and F are above its sensitivity limit. All remaining pulsars are clearly below the sensitivity threshold of AS25, being occasionally detectable because of the effect of interstellar scintillation.

The improvement in sensitivity provided by the new 20 cm system is apparent when comparing its sensitivity curve to that based on a 42 min observation assuming the parameters of the 50 cm system used by Manchester et al. (1990, 1991) to discover pulsars 47 Tuc C–M; that sensitivity curve is also shown in Figure 2.2. For flat spectrum sources one may compare the 20 and 50 cm curves directly. A more realistic comparison between the two searches is shown by the scaled version of the present 20 cm curve assuming the typical pulsar spectral index of -1.6. With this assumption we see that the present system represents a twofold improvement in sensitivity for a ~ 2 ms pulsar such as 47 Tuc J.

The sensitivity calculations described in this section take no account of the effects of the degradation in (S/N) of any binary pulsar whose apparent period may change significantly during each integration. We investigate this issue in detail in § 2.5.1.

2.3 Results of AS23

We have reduced all data listed in Table 2.6 in the manner described in § 2.1.2. In this table we list the number of AS23 integrations analyzed on each day, giving both the number of daily integrations in which the search code detected the pulsar — i.e., in which $(S/N)_{\text{search}} \geq 9$ — and the average daily (S/N), scaled to a 17.5 min integration, obtained from summing all data for that day using the pulsar's ephemeris (the coherent timing solutions described in chapter 5). We detected some 50 distinct periods for which the (S/N) vs. trial acceleration plots are broadly similar to that of Figure 2.1, i.e., have a clearly defined and significant maximum in trial acceleration. Eleven of these we identified with
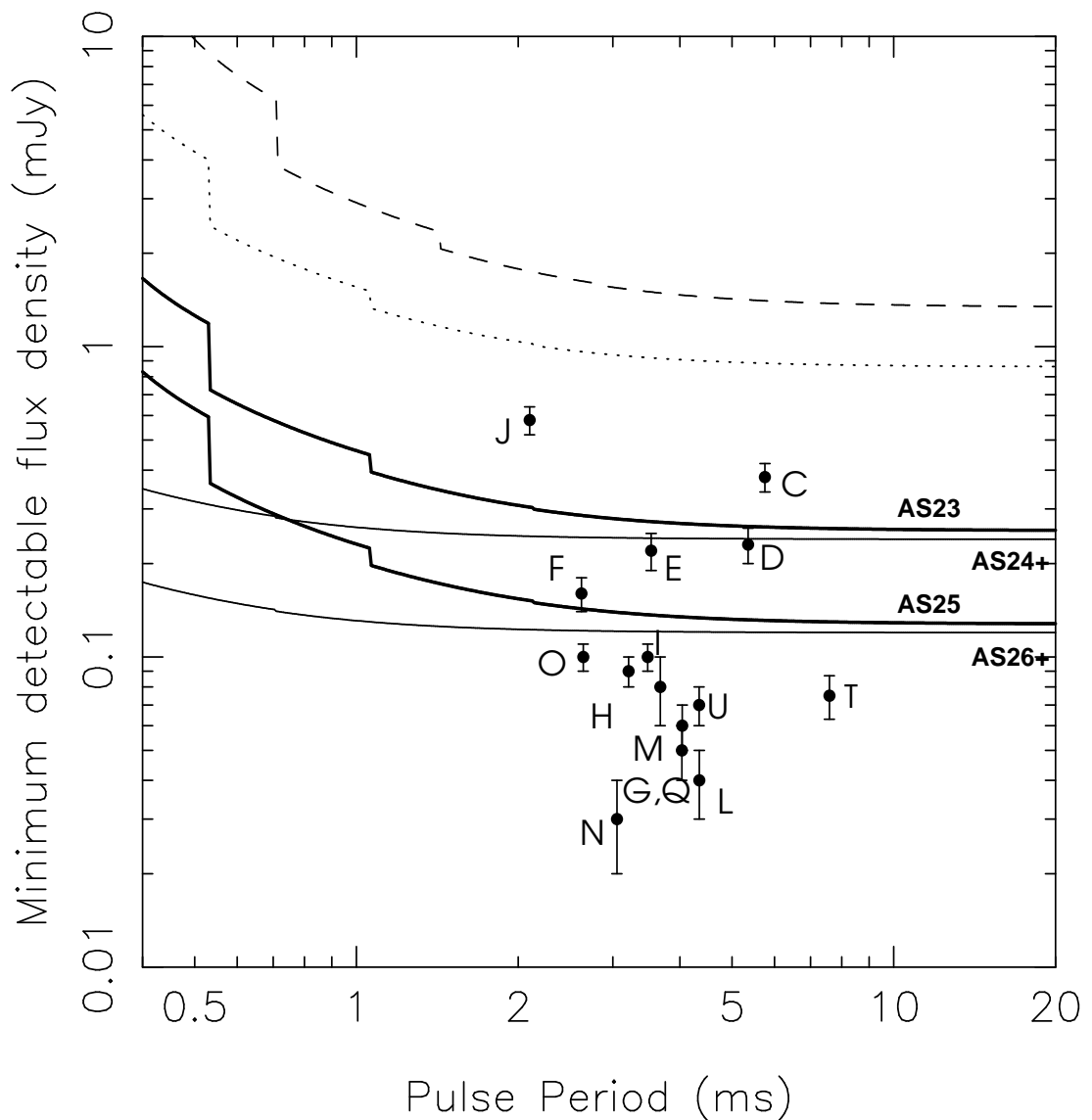
Figure 2.2: Sensitivity as a function of pulse period. Indicated are the sensitivities for an assumed pulsar duty-cycle of 15% of AS23 and AS25. The steps in the curves going from right to left reflect loss of power in the frequency domain as higher-order harmonics drop out of the spectrum. The pulsars in 47 Tuc with an estimate of flux density are presented for comparison (data from Table 2.1). The dashed curve is an estimate of the sensitivity at 50 cm based on data from Table 1.3, for an integration time of 42 min (Manchester et al. 1991). The dotted curve scales the curve of AS23 to a wavelength of 50 cm assuming a pulsar spectral index of −1.6 Also plotted are the sensitivity limits for 2^{24} and 2^{26} sample searches (22-min and 89-min) for the data taken since August 1999 (AS24+ and AS26+). The slightly longer integrations compensate for a slightly smaller bandwidth, but the sensitivity to sub-millisecond pulsars is greatly enhanced.

previously known pulsars in 47 Tuc.

2.3.1 Previously known pulsars

The detection rate for the previously known pulsars ranges from 10% (47 Tuc N),
to 90% (47 Tuc C and J), with all but two of the 11 pulsars detected on at least
25% of the observing days. In contrast, at 50 cm, all but 47 Tuc C are detected
less than 25% of the time, and the same is true at 70 cm for seven of the pulsars
(Robinson 1994). The detection rates with the new observing system are clearly
much higher than with past observations. The mere period analysis, described in
detail in § 4.4, has lead to much improved parameters for all pulsars (see Table
2.2).

47 Tuc L is not a binary pulsar (a possibility according to Robinson et al. 1995).
We have detected this pulsar on 11 separate occasions spanning over 500 days
(Table 2.6), and the barycentric period is constant (see Table 2.1, which lists
the pulse periods, DMs, and observed duty-cycles of all pulsars detected in our
observations).

Finally, we were also able to obtain a binary solution for 47 Tuc H. The very
significant eccentricity for this system (Table 2.2) is unique among this class of
binaries, and it will be discussed in chapter 7.

2.3.2 Newly discovered pulsars

Nine of the remaining periods detected in our data appeared in at least two
17.5 min integrations on one day, with some being detected in most integrations.
For each detection of such a period, we de-dispersed the raw data at several trial
values of DM about the nominal DM. In all nine cases there was a clearly defined
maximum signal-to-noise ratio as a function of DM, ensuring that the periodic
signals were truly dispersed. After viewing the corresponding time-domain pulse

profiles, and judging them suitably "pulsar-like", we felt secure in identifying each of these nine periods with previously unknown pulsars in 47 Tuc. Table 2.3 lists detections for the newly discovered pulsars that are seen only occasionally.

For all nine of the newly detected pulsars, the period changed within an observing day in a manner consistent with the Doppler shifts arising in binary systems (see chapter 4 for how the orbital parameters of these systems are determined from changes in the observed rotational period of the pulsar).

Only three of the nine pulsars (47 Tuc O, Q and U) were detected on many occasions (Table 2.6), which allowed the immediate determination of their orbital parameters. Fortunately, three of the remaining six (47 Tuc P, R, and W) have such short orbital periods that it was possible to cover more than an entire orbit on their discovery days, and hence establish good orbital parameters (see Fig. 2.3). Binary parameters for all pulsars are summarized in Table 2.2.

In this table, we also present the mass function and an estimate of the mass of the companion m_c. The mass function f_1 is given by

$$f_1(m_p, m_c, i)/\mathrm{M}_\odot \equiv \frac{(m_c \sin i)^3}{(m_p + m_c)^2} = x^3 \left(\frac{2\pi}{P_B}\right)^2 \left(\frac{1}{T_\odot}\right) \qquad (2.11)$$

where $T_\odot \equiv \mathrm{GM}_\odot/c^3 = 4.925490947\,\mu\mathrm{s}$, P_B is the orbital period and x is the projected semi-major axis of the orbit described by the pulsar, in time units. The right term of the equality is available to observation. If we assume a given mass for the neutron star (normally $m_p = 1.4\,\mathrm{M}_\odot$) and a given inclination angle i, we can make an estimate of the mass of the companion, m_c. For Table 2.2, we assumed $\cos i = 0.5$. The reason for this is that $\cos i$ has a uniform probability if the binary systems are randomly aligned. Therefore, there is a 50% chance that the companion star is heavier or lighter than what is indicated in the table.

Most of the newly discovered pulsars appear to be similar in their binary characteristics to the previously known pulsars in the cluster. For instance, 47 Tuc O, P, and R have short orbital periods ($P_b \sim 1.5$–$5.5\,\mathrm{h}$) and low companion masses

Pulsar	P_b (d)	x (s)	T_0 (MJD)	ω (deg)	e	f ($M_\odot$)	m_c* ($M_\odot$)
Previously Known							
47 Tuc E	2.2568	1.9818	51004.05	-	0.000	0.00164	0.18
47 Tuc H	2.3577	2.1528	51000.974	110	0.071	0.00193	0.19
47 Tuc I	0.2298	0.0385	50740.579	-	0.0	0.00000116	0.015
47 Tuc J	0.1207	0.0404	51000.766	-	0.0	0.00000487	0.024
Newly Discovered							
47 Tuc O	0.1360	0.0452	51000.021	-	0.0	0.00000535	0.025
47 Tuc P	0.1472	0.0380	50689.679	-	0.0	0.00000271	0.02
47 Tuc Q	1.1891	1.4622	51002.175	-	0.0	0.00237	0.21
47 Tuc R	0.0662	0.0334	50742.637	-	0.0	0.00000909	0.03
47 Tuc S	1.2017	0.7663	51000.965	-	0.0	0.000335	0.10
47 Tuc T	1.1262	1.3385	51000.317	-	0.0	0.00203	0.20
47 Tuc U	0.4291	0.5270	51002.645	-	0.0	0.000853	0.14
47 Tuc V	~ 0.2?	-	-	-	-	-	-
47 Tuc W	0.1330	0.2435	51214.950	-	0.0	0.000876	0.14

Table 2.2: Orbital parameters for the binary pulsars in 47 Tuc. Uncertainties in all fitted parameters are one or less in the last digits quoted, the calculation of T_0 assumes a circular orbit except for 47 Tuc H. The calculation of m_c assumes a pulsar mass of $1.35\,M_\odot$ and inclination angle for the orbit of $i = 60°$. The orbital parameters of 47 Tuc S and T are discussed in chapter 4.

($m_c \sim 0.03\,M_\odot$), similar to the previously known 47 Tuc I and J. Although the period of 47 Tuc R, at 96 min, is considerably shorter than that of 47 Tuc J, there is no reason to suspect that these systems are fundamentally different.

In contrast, 47 Tuc Q, S, T and U are similar to 47 Tuc E and H, with $m_c \sim 0.2\,M_\odot$; the companion stars are presumably low-mass helium white dwarfs much like those found in similar systems in the Galactic disk (e.g., Lundgren et al. 1996). The binary periods for 47 Tuc Q, S, T and U are somewhat shorter than the corresponding ones for 47 Tuc E and H (0.4–1.2 d vs. 2.3 d; see Table 2.2), but we believe this betrays no fundamental difference between the various systems.

It thus appears the vast majority of the binary pulsars known to date in 47 Tuc fall into one of two classes. However, the two pulsars discovered most recently, 47 Tuc V and W, are not so easily categorized.

Pulsar 47 Tuc V has been detected on two different days, at seemingly identical orbital phases (with period increasing as a function of time, hence on the "near-side" of its companion — see Fig. 2.4), and it displays an apparent orbital velocity
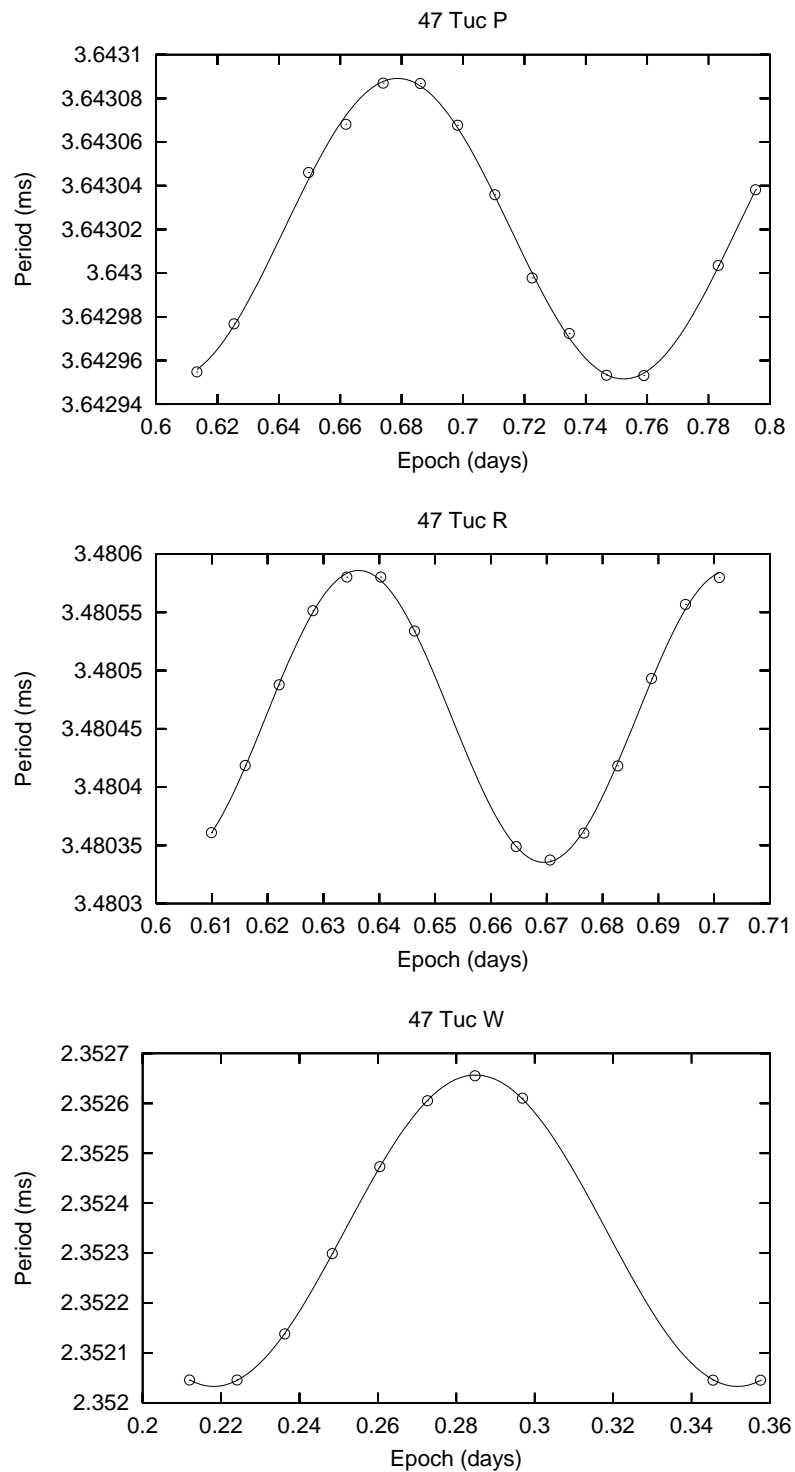
Figure 2.3: Observed barycentric periods for three newly discovered pulsars that are seldom detected. Each period is based on 17.5 min of data, with the exception of 47 Tuc R (8.7 min), and corresponds to $(S/N) \geq 6$. Times are given in fractions of a day after the date indicated in Table 2.3.
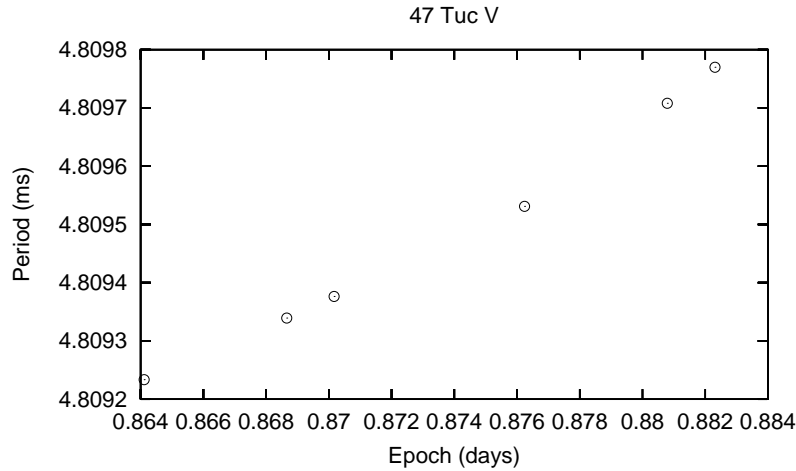
Figure 2.4: Observed barycentric periods for 47 Tuc V. Each period is based on 2.2 min of data and corresponds to $(S/N) \geq 6$. Times are given in fractions of a the day of first observation (see Table 2.3).

change of up to $\sim 80 \, \mathrm{km \, s^{-1}}$ in under one hour. The observed change in period during this time leads us to believe that the orbital period is several hours, suggesting a relatively massive companion. Another unusual aspect of this system is that it was detected on both occasions with relatively large signal-to-noise ratios in several 2 min sub-integrations, but interspersed with non-detections (Fig. 2.3), as if it were being irregularly eclipsed, despite its orbital phase[2].

Pulsar 47 Tuc W, with an orbital period of 3.2 h, may resemble short-period binary systems such as 47 Tuc J, and the pulsed radio signals are apparently eclipsed for a fraction of its orbit, as in some of these systems (see § 7.4). However its implied companion mass, at $\sim 0.15 \, \mathrm{M_\odot}$, is a factor of ~ 6 higher than that of those systems, more typical of a low-mass white-dwarf. But if the companion

---

[2]In practice it is usually easy to distinguish among interstellar scintillation and eclipses by a companion as the cause for the temporary non-detection of a pulsar. Eclipses tend to occur with the pulsar roughly centered at superior conjunction, while scintillation has no preferred orbital phase. Also, scintillation has characteristic time-scales and amplitudes. No other pulsar in 47 Tuc displays the deep intensity modulations on time-scales of about a minute observed for 47 Tuc V, and we therefore suggest the eclipse interpretation.

Pulsar	Date (MJD)	Number of integrations	Detections/(S/N)
47 Tuc P	50689	16	5/6.3
47 Tuc R	50742	8	7/8.9
47 Tuc S	50741	8	3/9.9
47 Tuc V	51012	8	2/3.4
	51055	16	3/4.4
47 Tuc W	51214	16	9/10.0

Table 2.3: Pulsars detected less than three times by AS23.

were indeed a white dwarf, we would not expect eclipses. We consider it possible that this system is somewhat akin to PSR B1744$-$24A, located in the globular cluster Terzan 5, with $P_b \sim 1.8\,\mathrm{h}$, $m_c \sim 0.10\,\mathrm{M_\odot}$, and displaying irregular eclipses (Lyne et al. 1990, Nice & Thorsett 1992).

2.4   Results of AS25

Two of the pulsars, 47 Tuc S and T, were detected by AS23 with $(S/N) > 6$ on one and three occasions respectively. During these observations, these pulsars did not change their accelerations noticeably, so they were thought to have orbital periods longer than a few hours. However, the orbital parameters for these pulsars remained indeterminate for some time.

When AS25 started, its aims were to detect these pulsars more often and to search more efficiently for unknown isolated pulsars and pulsars in binary systems with periods longer than $\sim$ eight hours. AS25 provides a doubled sensitivity to the target population. For these systems, measurements of rotational period are more precise by a factor of four, and measurements of acceleration are more precise by a factor of 16. This search, however, cannot detect the short period binaries efficiently.

As expected, the faint slow-moving pulsars were detected more often. 47 Tuc S, for example, was detected again in its discovery observation and in three other

Pulsar	T (MJD)	P (ms)	A (m s^{-2})	(S/N)
47 Tuc S	50741.644	2.8304388	-0.78 ± 0.06	16
	50741.693	2.8304061	-0.86 ± 0.06	14
	51000.765	2.8304721	0.72 ± 0.04	14
	51000.814	2.8304984	0.58 ± 0.04	11
	51002.899	2.8303046	0.56 ± 0.08	9
	51216.176	2.8305188	-0.50 ± 0.08	9
47 Tuc T	50740.654	7.5878889	-0.92 ± 0.08	12
	50740.703	7.5878334	-0.24 ± 0.08	13
	50746.626	7.5884100	1.68 ± 0.04	12
	50746.675	7.5885810	1.67 ± 0.06	19
	50981.811	7.5878836	0.72 ± 0.06	9
	50983.932	7.5878552	-0.44 ± 0.08	11
	51005.893	7.5891029	0.52 ± 0.08	13
	51040.857	7.5891350	0.00 ± 0.04	66
	51335.904	7.5891358	0.00 ± 0.02	11

Table 2.4: Measured periods and accelerations for 47 Tuc S and T. 47 Tuc S was detected on four different observations, and 47 Tuc T on seven different observations. We could obtain 6 and 9 measurements of accelerations and apparent rotational period respectively.

observations (See Table 2.4). 47 Tuc T was detected in the three previously known observations and also on four other observations. The re-detections made by AS25 are important, because they provide better (S/N), and we also obtain more precise periods and accelerations.

The purpose of detecting pulsars like 47 Tuc S and T more often is to allow the determination of their orbital parameters. The measurements of rotational period in Table 2.4 are, unfortunately, rather sparse. However, we know the acceleration of the pulsar for each measurement, and this allowed the determination of the orbital parameters of these binaries, therefore fulfilling the main initial objective of AS25. In chapter 4 we describe how the orbital parameters of these pulsars were determined.

AS23 produced about 30 periodic signals that displayed several pulsar-like characteristics, but that were detected on only one integration of one day. We regard several of these as good pulsar candidates, potentially to be confirmed by future observations. Two of them have already been confirmed as binary millisecond pulsars by AS25, their characteristics will be published elsewhere

when this search program is finished. AS25 has detected no additional isolated MSPs so far.

2.5   Survey limitations

Although the recent observations of 47 Tuc have been successful beyond our most optimistic expectations, it is important to keep in mind the many and severe selection effects inherent in the data and analyses reported on in this work. The greatest of these, particularly for short-period binary systems, has to do with the extent of parameter space that has been covered by our "acceleration searches".

2.5.1   Sensitivity to binary pulsars

In addition to the improvements in sensitivity over previous searches of 47 Tuc enabled by the new 20 cm observing system, use of acceleration searches has significantly improved the ability to find binary pulsars. Previously, only four out of 11 (36%) millisecond pulsars known in 47 Tuc were members of binary systems. The new discoveries bring the number of binary pulsars in 47 Tuc to 13 (two-thirds of the total). We consider it highly significant that all of the new millisecond pulsars reported here are members of binary systems. These discoveries are in spite of the fact that, as demonstrated in § 2.2, the sensitivity of AS25 to isolated pulsars is significantly improved over the previous surveys by Manchester et al. (1990, 1991) and Robinson et al. (1995). We note that three of the five brightest pulsars in 47 Tuc at 20 cm are isolated (Table 2.1); if significant, this may suggest that isolated pulsars in 47 Tuc have a relatively high intrinsic luminosity cutoff. Also, isolated pulsars in 47 Tuc might have, on average, a larger spectral index than binary pulsars. Finally, the specific incidence of isolated pulsars in 47 Tuc might be low. A combination of these factors could

explain why AS25 has failed to find additional isolated pulsars.

The improved sensitivity of AS23 to short-period binaries is demonstrated by the fact that four of the nine binary systems we found, 47 Tuc P, R, S and V would not have been discovered without the use of the acceleration code since, in each case, the signal-to-noise ratio never rose above the threshold of 9 at a trial acceleration of zero[3]. Despite searching an acceleration range of $|a| < 30\,\mathrm{m\,s^{-2}}$ in the, most of the new discoveries and detections of previously known pulsars occurred at $|a| < 5\,\mathrm{m\,s^{-2}}$. Three notable exceptions are 47 Tuc R, V, and W, that displayed maximum line-of-sight accelerations of 11.4, 23.7, and $21.3\,\mathrm{m\,s^{-2}}$ respectively (e.g., Fig. 2.1).

While it is clear that AS23 has improved the knowledge of the true fraction of binary pulsars in 47 Tuc, an outstanding question that remains is the extent of binary parameter space probed by the present search strategy. In this section we attempt to answer this by exploring the limits of AS23 with respect to a variety of short orbital period binary systems. In what follows, when we use the term "acceleration search" we are explicitly referring to AS23 (§ 2.1).

For the purposes of this discussion it is useful to note that most observed binary pulsar systems in 47 Tuc fall broadly into two categories: those with orbital periods of order 0.4–2.3 d and companion masses $\sim 0.2\,\mathrm{M_\odot}$ (47 Tuc E, H, Q, U, S and T) and 47 Tuc I, J, O, P, and R, which are characterized by shorter orbital periods (1.5–5.5 h) and lighter companions ($m_c \sim 0.03\,\mathrm{M_\odot}$). (The nature of 47 Tuc V and W is unclear at present.) We shall refer to these types here respectively as the "normal" and "short-period" binary systems, investigating the sensitivity of our search to both types in turn. In addition, since all the presently

---

[3]In effect this suggests that without the acceleration code we would have discovered five new pulsars, an increase of $\sim 50\%$ over the previously known population. This is surprising, considering the factor of ~ 2 improvement in sensitivity claimed in § 2.2. This estimate relied on assuming a spectral index of -1.6 for pulsars in 47 Tuc. Perhaps this assumption is not valid, and the average spectral index for millisecond pulsars in 47 Tuc is smaller than -1.6.

known binary systems have essentially circular orbits, we also investigate the search sensitivity to putative binary systems in which the pulsar is in an eccentric orbit about a more massive companion.

The first, and really only, detailed study of the degradation in sensitivity of a radio pulsar search for short orbital period systems was carried out by Johnston & Kulkarni (1991; hereafter JK). By calculating the decrease in amplitude of the signal in the Fourier power spectrum for a binary pulsar relative to a solitary one, and mathematically describing the signal recovery technique involved in the acceleration search, JK were able to quantify the degradation in sensitivity of pulsar search codes with and without acceleration schemes of the type used here. As their main example, JK considered a $1000\,$s observation of a $1.4\,M_\odot$ pulsar in a circular orbit with a $0.3\,M_\odot$ companion for a wide variety of orbital and pulse periods. Given that our $17.5\,$min analyses correspond to a similar integration time, JK's results are highly relevant to this discussion. In addition, the $0.3\,M_\odot$ companion considered by JK closely resembles the class of normal binary systems defined above.

We focus on Figure 4 of JK, which shows the net gain in sensitivity of an acceleration search when making multiple observations of the same system. In their example, JK assumed five independent observations of the binary at random orbital phases. From this figure we see that, for a $10\,$ms pulsar, the acceleration search allows one to detect binary systems with orbital periods of order four times shorter than a standard pulsar search code. The gain increases still further for shorter period pulsars, where the blurring of harmonics in the power spectrum becomes even more pronounced. For a $3.5\,$ms pulsar, similar to 47 Tuc E and H, we infer from Figure 4 of JK that the acceleration analysis allows the detection of a binary with an orbital period about six times shorter than the standard search.

The results of JK are not directly applicable to the population of short-period

binaries in 47 Tuc. Presently, the 3.48 ms pulsar 47 Tuc R, with an orbital period of 96 min, is the shortest orbital period system of this type. In order to estimate the sensitivity of our search code to even shorter period binaries with low-mass companions like 47 Tuc R, we generated a number of time series containing a synthetic 3.48 ms pulsar whose period was modulated as in a circular Keplerian orbit with a low-mass companion. We considered four separate cases corresponding to orbital periods of 90, 60, 30 and 15 min. The first value considered is similar to that of 47 Tuc R; the last value is close to that of the shortest orbital period known for any binary system: the 11 min orbit of the X-ray burst source X1820−303 in the globular cluster NGC 6624 (Stella et al. 1987).

In each case the mass function was held constant at 8.68×10^{-6} M$_\odot$ (similar to that of 47 Tuc R). To quantify the improvement gained by using the acceleration code, we generated a control time series containing a fake 3.48 ms pulsar with a fixed period but otherwise identical to the other simulations. In a similar sense to JK, we define the efficiency factor γ as the detected (S/N) of the binary pulsar divided by that of the control pulsar. In order to compare the relative efficiency of the non-accelerated and accelerated analyses, separate values of γ were computed: γ_0 is the efficiency for the non-accelerated analysis, and γ_A is the equivalent parameter for the acceleration search in the analysis of the same data, performed as described in § 2.1. By definition $0 \leq \gamma \leq 1$, with a value of unity signifying that no loss of signal occurred. In each case, the simulations were performed over all orbital phases to establish the response of the search code to the full range of orbital accelerations.

The results of the simulations are summarized in Table 2.5, where we list the range of efficiencies, as well as the mean values averaged over all orbital phases. As expected, the efficiencies for both the normal (γ_0) and acceleration search code (γ_A) are strong functions of orbital phase. In Table 2.5 we also list the

Case	Period (ms)	P_b (min)	f ($M_\odot$)	e	$\gamma_{0,\min}$ (%)	$\overline{\gamma_0}$ (%)	$\gamma_{0,\max}$ (%)	$\gamma_{A,\min}$ (%)	$\overline{\gamma_A}$ (%)	$\gamma_{A,\max}$ (%)	I
1	3.48	90	$8.68{\times}10^{-6}$	0.0	33	48	75	80	88	99	1.8
2	3.48	60	$8.68{\times}10^{-6}$	0.0	26	39	58	68	75	86	1.9
3	3.48	30	$8.68{\times}10^{-6}$	0.0	24	33	41	38	45	51	1.4
4	3.48	15	$8.68{\times}10^{-6}$	0.0	18	23	28	30	32	35	1.4
5	34.8	60	0.13	0.7	0	48	78	18	63	92	1.3
6	34.8	30	0.13	0.7	0	33	63	20	43	69	1.3

Table 2.5: Search code tests on simulated data. For each case considered, the columns list the assumed pulse period, orbital period, mass function, and orbital eccentricity. The remaining columns show the range and average values of efficiencies of the search code for a normal analysis, γ_0, and using an acceleration search, γ_A. The averaged "improvement factor" $I \equiv \gamma_A/\gamma_0$ is also given. Averaging over orbital phases has been appropriately weighted by the time spent at each phase.

"improvement factor" $I \equiv \gamma_A/\gamma_0$, the net gain in signal achieved by employing the acceleration search, averaged by time spent at each orbital phase. These simulations show a significant improvement in sensitivity gained when using an acceleration search. In particular for orbital periods as short as one hour (cases 1 and 2) the efficiency of the acceleration search is at least 70% for any orbital phase, more than twice the efficiency of the normal search code.

For the shortest orbital periods of this type considered (cases 3 and 4), the acceleration search continues to be more efficient than the normal search although the improvement factor is smaller. In these cases the integration is becoming an increasingly significant fraction of the orbital period. As a result, the constant acceleration approximation used in the search (§ 2.1) ceases to hold. Among possible improvements to this strategy, the most straightforward approach is to perform one-dimensional acceleration searches on shorter segments of data. One can also include the acceleration derivative term in the prescription for $v(t)$. Although this necessarily adds a dimension to the search, it may provide a dramatic improvement in coverage of orbital parameter space for radio pulsars with binary characteristics akin to X1820$-$303.

Finally, in Table 2.5 we also summarize the results of simulations carried out to test the efficiency of our code at detecting a putative relativistic binary double-neutron star system in a highly eccentric short-period orbit (cases 5 and 6). As would be expected, for certain orbital phases a normal search has no hope of detecting such systems, while the acceleration search maintains a detection efficiency of at least 20% at all orbital phases. Our search would therefore have found a relatively bright relativistic binary pulsar in 47 Tuc at any orbital phase, but none was detected. This provides some empirical evidence that the population of pulsars in the central regions of 47 Tuc is composed exclusively of bona fide millisecond pulsars: those with rotation periods under ~ 10 ms, and in relatively circular orbits with low-mass companions, or with no companions at all.

2.5.2   Other selection effects

An interesting issue from the point of view of the origin and evolution of the pulsars in 47 Tuc is their intrinsic pulse period distribution. The observed distribution shown in Figure 2.5 spans a remarkably narrow range and suggests that there may be a deficit of pulsars below 2 ms. This interpretation should be viewed with some caution, however, given the small number statistics, and it is clear from Figure 2.2 that we begin to lose sensitivity to pulsars with $P \leq 2$ ms. Therefore, the observations made between August 1997 and August 1999 do not unambiguously address the question of what the shortest pulsar periods might be. Pulsar 47 Tuc W, for example, was originally detected at a period of 1.18 ms, showing that we are sensitive to some rather short periods. However, the observations of 47 Tuc made since August 1999 (see Table 1.3) have three times higher time resolution. The processing of these observations for searching purposes is still incomplete, but it is already clear that this data will enable us to detect any moderately bright pulsars with periods larger than ~ 0.6 ms that might exist in
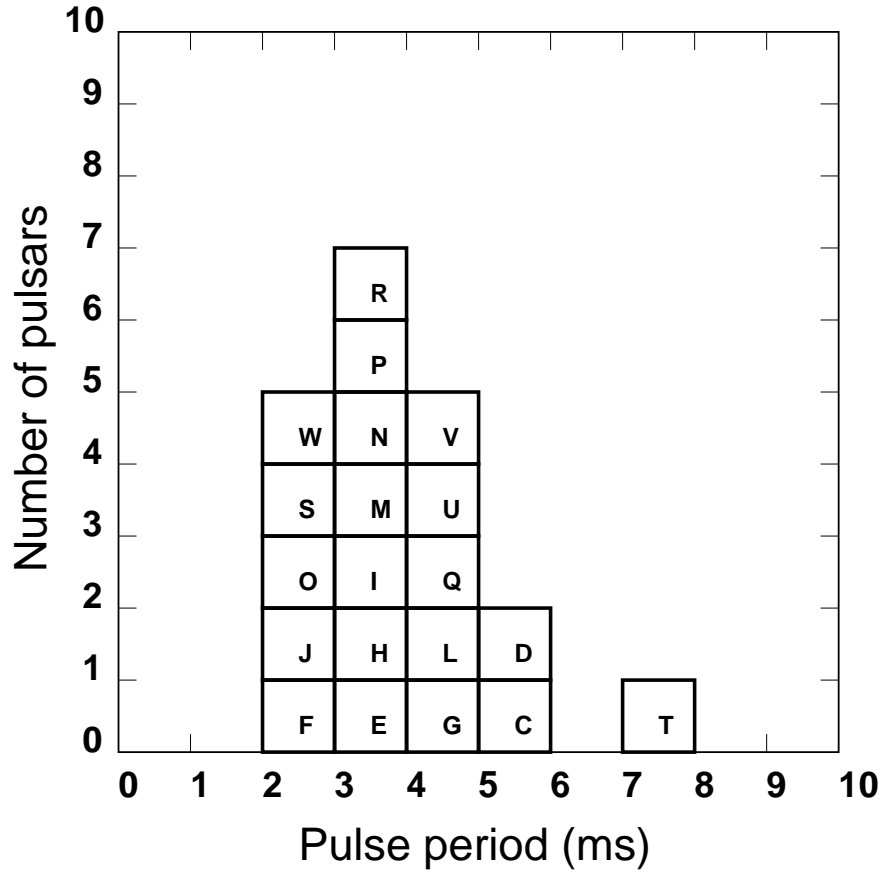
Figure 2.5: The observed period distribution of the 20 pulsars known in 47 Tuc. It is presently unclear to what extent the apparent deficit of pulsars with periods below 2 ms is a result of period-dependent selection effects (see §2.5.2).

the cluster (see Fig. 2.2).

It is likely that the vast majority of all pulsars in 47 Tuc are to be found within the area covered by the 14′-wide 20 cm telescope beam pattern. In § 6.1, the timing analysis reveals that 15 of the pulsars lie within 1′2 of the centre of the cluster. Therefore, it is not likely that we are missing any discovery by not probing further out.

There are a number of additional selection effects having to do with the manner in which we have reduced the data so far. For isolated pulsars, the sensitivity limits might still be improved by a factor of up to $\sim \sqrt{4}$ over the sensitivity

limits of AS25 by reducing the entire 4.66 h data sets in a coherent manner. This could be done at reasonable computing expense because only the trivial zero-acceleration case would have to be addressed (once the Earth's rotation is accounted for). However, since flux densities for pulsars in 47 Tuc certainly vary significantly due to scintillation on time-scales of hours or less, the gain in sensitivity might be quenched by periods within the 4.66 h during which we would be adding mostly noise to the time series being analyzed. In extreme cases, the sensitivity could actually be degraded! Optimally then, each session's data stream should be analyzed with a multiplicity integration spans. This can, however, degenerate into a huge overall data reduction task. These considerations also apply to the case of binary pulsars, where the additional need to perform sensitive acceleration searches over longer time intervals further exacerbates the overall computing load.

Finally, as already noted, we have analyzed most of the data at only one value of DM. The DMs for known pulsars in 47 Tuc span about 0.5 cm^{-3} pc (Table 2.1), and this already introduces some loss of signal for the shortest period pulsars we have considered (§ 2.2). This is particularly important for searches of sub-millisecond pulsars in data with very high time resolution. It would also be advantageous to broaden the range of DM searches because greater variance in the value of measured DMs might add to the understanding of the properties of the ionized intra-cluster, and interstellar, medium. Most of the variance observed for DMs of pulsars in globular clusters is expected to be due to slightly different lines-of-sight across the Galaxy, because most clusters are believed to be evacuated of gas (Spergel 1991), but there is evidence for intracluster plasma in 47 Tuc (see § 6.4). This could broaden the range of DMs of the pulsars in the cluster, and a search with different values of DM might prove worthwhile in the future.

2.5.3   Isolated pulsars in 47 Tuc

Mindful of the comments in the previous section, we can still make some general statements about the likely intrinsic population of pulsars in 47 Tuc. The observed population of pulsars, all with millisecond periods, divides at present roughly into one-third isolated pulsars, one-third normal binary systems ($P_b \sim$ 0.4–2.3 d and $m_c \sim 0.2\,\mathrm{M_\odot}$), and one-third short-period binary systems ($P_b \sim$ 0.06–0.2 d and $m_c \sim 0.03\,\mathrm{M_\odot}$).

As mentioned previously, the fraction of isolated pulsars known in 47 Tuc prior to AS23 and AS25 was 64% of the total. Use of acceleration code has improved the detectability of binary systems, but we are still selecting severely against binaries of the short-period variety, when compared to isolated pulsars, and we consider it probable that the actual fraction of isolated pulsars in 47 Tuc is less than the 35% found at present. By comparison, the fraction of isolated millisecond pulsars in the disk of the Galaxy is $\sim 20\%$ (e.g., Camilo 1998?). The surveys of the Galactic disk, because of their short integration times, are relatively more sensitive to short-period binaries, so the isolated fraction for disk pulsars, up to small-number statistics, is already known with some confidence.

The overall small fraction of isolated millisecond pulsars in 47 Tuc suggests an interesting puzzle: long-period binaries ($P_b \sim 10$–10^3 d) are expected to be formed at high rates in dense clusters through exchange interactions between old isolated neutron stars and "hard" primordial binaries (Hut et al. 1992, Sigurdsson & Phinney 1993). The long-period binaries have, however, high cross-section to disruption in a globular cluster, and should eventually leave behind isolated millisecond pulsars. We detect no long-period binaries, and relatively few isolated pulsars. Perhaps most wide binaries are disrupted before the neutron star companions can evolve into red giants, followed by mass transfer and birth of millisecond pulsars, as in the standard scenario (e.g., Verbunt 1993). This is an

open question. In any case, even if the isolated fraction of millisecond pulsars in 47 Tuc and in the Galactic disk are comparable it is surely a coincidence, given the different evolutionary pressures present in both environments.

Date (MJD)	Number of integrations	C	D	E	F	G	H	I	J	L	M	N	O	Q	T	U
50683	16	0/4.6	2/7.0	14/19.8	0/2.3	0/2.5	10/17.0	0/2.4	6/8.8		0/2.5		0/2.9		0/2.2	
50686	16	4/7.6	0/3.2	0/4.4	16/33.5	0/3.4			16/12.2	0/3.1			4/10.1		0/2.1	
50689	16	5/9.8		0/3.1	0/3.4	0/2.9		3/6.0	11/12.9	0/2.8		16/18.2	0/2.7			
50690	16	16/21.9	0/2.8	0/3.2	0/6.1	0/3.3			1/6.6				3/8.6	0/2.0	0/4.1	
50739	5	5/20.9	3/10.2					0/7.4	5/31.5						0/4.0	
50740	8	0/4.4	1/7.2	0/7.2		0/3.7		2/8.8	8/13.4		0/3.8		0/5.3	7/13.5	0/6.9	0/4.2
50741	8		8/11.9	8/19.7				2/9.8	8/46.5				0/4.1	0/4.5		0/3.0
50742	8	8/15.7	0/4.1		2/6.5	0/3.1	8/16.6	0/6.1	6/12.6	0/4.0						0/4.0
50743	3	0/7.9			3/21.9	3/12.8			3/17.8						0/5.9	
50744	8	8/15.3		0/3.2	0/3.6	8/14.7	0/4.2	0/2.9	4/11.1				0/3.2			
50745	8	0/2.8	8/22.6		0/5.4		5/11.3	0/3.7	8/26.7				0/3.5			
50746	8	0/5.4	8/17.7		0/3.1		0/6.5	0/3.6	8/32.2					0/6.0	4/9.3	
50748	4	4/10.5	0/3.7			0/3.9					4/14.5		0/4.3			
50980	8	8/22.5	8/33.4	8/20.7	1/4.9				0/3.8			0/3.4	0/3.0	2/2.7	0/2.2	1/8.4
50981	16	16/63.2	5/9.3		15/18.8	1/4.2			7/7.9		1/6.3		0/3.0	0/3.5		
50982	16	2/5.8	16/22.7	9/13.3	1/5.7		0/2.5		3/5.4		1/8.5		0/4.3			
50983	4	0/5.0		3/12.6	0/6.3								0/7.4		0/6.0	0/5.6
50992	8	0/5.4	0/6.7		6/12.9				0/4.7							0/3.3
50993	8	8/40.2	0/7.2	0/5.4	0/2.9			1/9.1	8/22.8	7/11.8					0/6.0	0/3.0
50998	16	0/2.1	3/6.6	1/5.4	2/5.4				0/2.7	0/2.7		14/11.8				

(Continued in next page)

Table 2.6: Log of detections for the 47 Tuc pulsars with a coherent timing solution for the period MJD = 50683 to MJD = 51218 analysed in Camilo et al. (2000). For each observing date we list the number of 17.5 min integrations that were independently searched by AS23. For each pulsar and each day we list the number of integrations in which the pulsar was detected with the search code according to the criteria summarized in § 2.3; and the signal-to-noise ratio (S/N) scaled to a 17.5 min integration, obtained from summing the entire day's data set using the best pulsar ephemeris available (e.g., on MJD 51004, 47 Tuc C was not detected in any of 16 integrations with $(S/N) \geq 9$, but all data added together using the pulsar's ephemeris yielded $(S/N) = 23.2$, or an average of $(S/N) = 5.8$ per integration. Hence the 0/5.8 notation. For 47 Tuc D, even adding all data did not yield an unambiguous detection - one with $(S/N) \simeq 7$ - and so the respective entry is blank).

Date (MJD)	Number of integrations	C	D	E	F	G	H	I	J	L	M	N	O	Q	T	U
(Continued from previous page)																
50999	5	0/6.4	5/14.6		4/10.8			0/4.1	0/6.8				0/4.8			0/3.7
51000	16	0/6.7	0/2.1					0/2.7	2/6.7	0/3.1		0/2.3	0/2.6		0/2.3	0/2.2
51001	10	5/10.2	0/3.2				0/6.0		0/3.1					1/2.9		4/10.9
51002	16		2/5.5	1/7.4				0/2.8	16/146.3		0/2.2		3/6.4			3/7.7
51003	16		4/8.6	4/8.8	0/6.1	0/2.8	0/3.2	0/2.6	16/36.1				0/4.9			0/5.3
51004	16	0/5.8		0/5.7	12/12.6				13/16.2					10/10.2	0/2.1	0/3.0
51005	12	2/7.7	0/3.0		0/2.5				9/12.8	0/2.7			2/4.4		0/6.6	
51007	10	0/4.3	0/5.2						10/23.5					0/2.9	0/2.2	
51012	8	5/11.4		0/7.1	4/10.9	1/6.2			8/186.1				3/7.2			0/4.7
51026	16	16/25.1	0/4.4	0/4.0	0/3.0	0/3.6			4/8.3		0/2.2		0/3.2			0/2.4
51027	7	6/15.7	7/36.0	3/9.9				0/7.2	7/14.3		0/3.4					0/3.1
51029	5	0/4.4		1/9.5	0/5.4			0/4.1	5/26.2							
51031	6	0/3.1		0/4.7	4/10.2			0/6.7	3/8.0				0/5.1			0/7.1
51033	6		3/12.8			0/5.5			0/3.4					6/20.7		
51036	7	0/3.5	7/15.2		4/9.9				0/4.5				0/5.8	2/9.6		0/3.9
51037	16		16/34.1				0/2.6	0/4.6	16/29.7		0/3.8					0/2.2
51038	6	6/18.3	5/10.2		1/8.1			0/3.8					0/6.2	10/10.7		
51039	3	3/17.2	3/19.9	1/8.6			0/8.4	1/10.3								
51040	4	4/18.0	4/16.8			2/12.1		0/8.3	4/42.0				0/5.0		4/30.1	0/8.2
51085	16	5/8.9	10/9.6	0/2.8	0/3.0			0/2.1	16/16.5		0/3.2	0/3.2	0/4.4			0/3.4
51086	16	16/27.9	0/2.9			0/2.2	15/17.4		16/44.5	0/5.0			1/6.2			0/2.3
51088	19	0/2.2	0/2.9		0/2.8	0/1.9	1/5.7	0/1.9	8/13.0		0/2.2		0/2.7			
51089	4	4/13.6			0/4.8			3/10.3	0/5.1		0/4.6				0/3.9	
51090	4	4/23.2	4/20.5		0/5.7				4/16.7							0/7.9
51091	4	4/49.3	4/21.3				4/21.2		1/9.3						0/3.4	
51092	8	8/29.4	7/15.5	1/7.7	8/29.3			5/13.4	0/4.8		0/6.4			0/2.8	0/5.5	0/4.5
51093	8	0/6.8	0/3.5		0/3.2			0/4.6					3/6.7		0/3.8	
51095	4	4/18.0		0/6.8				3/11.8	1/10.7							
51096	5	4/30.5	5/16.4		0/4.5				0/4.8							
51097	12	3/9.8	4/12.2		7/18.2		1/5.2		12/88.3		8/11.2		0/3.7			0/2.6

(Continued in next page)

Date (MJD)	Number of integrations	C	D	E	F	G	H	I	J	L	M	N	O	Q	T	U
(Continued from previous page)																
51098	16	15/17.8	0/2.4	0/3.7					0/2.9	2/6.6	2/6.2					
51099	19	0/2.7	4/6.9	18/28.6	1/3.8				0/3.6				0/2.6		0/3.2	10/8.2
51100	16	0/3.5		0/2.4		0/3.5	1/6.0		16/16.5							0/6.3
51101	17	16/23.5	0/2.3						10/8.7							0/2.8
51145	16	0/3.0	10/15.8	14/13.4	16/15.8				16/18.4			0/2.3			0/3.1	
51146	16	3/6.8	0/4.9		0/3.4				2/6.6				0/2.3			
51147	8	0/3.5		0/5.5												6/11.6
51148	5	1/3.6	5/31.2						0/13.4							0/6.4
51149	16	0/5.4	0/5.1			0/2.4		0/2.6	13/11.4	0/2.9	0/2.1				0/2.5	1/5.2
51150	16	0/5.4		0/2.8				0/2.2	14/22.7	0/2.3			0/4.0			
51151	9	2/7.7	9/15.1						2/5.3							
51152	17	1/6.2	4/7.6		0/2.8			0/2.5	16/14.5				0/4.6		0/1.9	3/7.3
51153	16	0/3.0	0/4.0	0/2.7		0/5.4	1/4.8		15/16.1			0/2.0				
51154	19	19/69.6	5/9.0				6/8.9	0/2.3	12/14.5				0/2.7		0/3.0	
51155	16	14/18.1	0/2.1	0/4.8			0/2.5	0/2.9	11/9.9			0/6.2	1/6.0		0/2.2	0/3.0
51156	16	10/49.0	3/6.1	4/14.4	16/32.0				16/52.2							
51157	6	0/6.9	6/23.2					0/3.2	6/53.2							
51211	16	0/5.5	2/6.4	15/20.3	4/6.4	0/2.0	0/4.6	0/3.2	0/2.2	0/2.2			1/4.1			0/2.7
51212	16	3/5.6	0/3.8		0/2.1	0/2.9		0/2.1	16/38.6			0/2.7	0/2.3	0/2.8	0/2.4	
51213	16		4/6.0	0/2.6	0/2.1	0/7.1		0/2.8	0/2.8				15/13.7			13/14.1
51214	16	2/5.9	0/2.5		0/2.9		0/2.1	0/3.7	16/18.5				0/3.3		0/3.3	
51215	16	3/6.2	0/2.1	0/2.5	15/13.2	0/2.1	0/3.0	0/2.1	2/5.4				11/12.4		0/2.2	
51216	16	9/9.7	1/6.1	10/10.0	9/9.4			0/2.8	9/10.4				15/19.7			
51217	16	0/4.0	0/4.3	0/3.6		0/2.7	7/8.4	0/2.8	14/28.8				0/3.1			0/2.9
51218	16	2/8.6	0/2.6	0/3.9	0/5.0			0/2.8	16/24.1				0/4.7			4/7.0

Chapter 3

Emission characteristics

This chapter is an update on sections 3 and 6 of Camilo et al. (2000).

3.1   Profile morphology

Previous 1400 MHz pulse profiles for the pulsars in 47 Tuc have been published
by Camilo et al. (2000). Since then, and starting in August 1999, we have been
observing 47 Tuc with the new $2 \times 512 \times 0.5$ MHz filterbank (see § 1.4, Table
1.3), which improved the resolution of these 1400 MHz pulse profiles by a factor
of three. In Figs. 3.1 and 3.2, we present the best available pulse profiles for the
20 known pulsars at 430 MHz, 660 MHz and 1390 MHz, obtained after processing
all the data in Table 1.3.

A wealth of details are emerging at 20 cm. A clear example is 47 Tuc C. Two
precursors at phases of 0.1 and 0.3 can now be distinguished before the main pulse
of this pulsar (see Fig. 3.3). An emission bridge connects the precursor at 0.3 to
the main pulse. A new shoulder-like component can now be seen after the second
component of the main pulse, at about phase 0.6. We also notice an emission
tail, probably consisting of several distinct emission features, immediately after
the three components of the main pulse. The minimum in emission comes at a

phase of 0.9. Together, the detectable features cover at least 90% of the rotational phase.

47 Tuc D also revealed a faint and very sharp interpulse (see Fig. 3.3). The main component of the pulse is still unresolved, and the sharp drop in measured intensity after it provides for excellent timing. 47 Tuc E proved to have at least three components, with the two main ones now seen to be completely separated. The main components are still unresolved. 47 Tuc H, I, J and O still display a single component, but some structure is now clearly discernible in their pulses.

47 Tuc L, M, Q and U were already know to have complex pulse profiles, the full structures can now be seen far more clearly. The pulse profile of 47 Tuc L is such that it is unclear which component should be called the "main" component, the one with highest peak flux has a width of 7%, the other component, which appears a third of a rotation before, has a width of 16% and has, overall, more power, although spread in time twice as much. This component has the highest peak flux in data with lower time resolution. In 47 Tuc Q, the emission features cover at least 90% of the rotation cycle. 47 Tuc U displays a still unresolved main pulse and a prominent interpulse, the remaining components are weak and rather wide, and collectively cover at least 80% of the rotation cycle.

Also, with the probable exception of 47 Tuc E, these pulse profiles don't seem to change much with frequency, a common characteristic of MSPs in the disk of the Galaxy (Kramer et al. 1999). Therefore, the values for the DMs presented in this work are likely to reflect the true column densities between the individual pulsars and the solar system. This is an important fact for the discussion in § 6.4.

Chen & Ruderman (1993) suggested that the formation mechanism for millisecond pulsars in the Galactic disk and in globular clusters might be different. The observational evidence to support this idea relied on supposed differences in the observed radio beams (and hence magnetic field geometry, and origin)
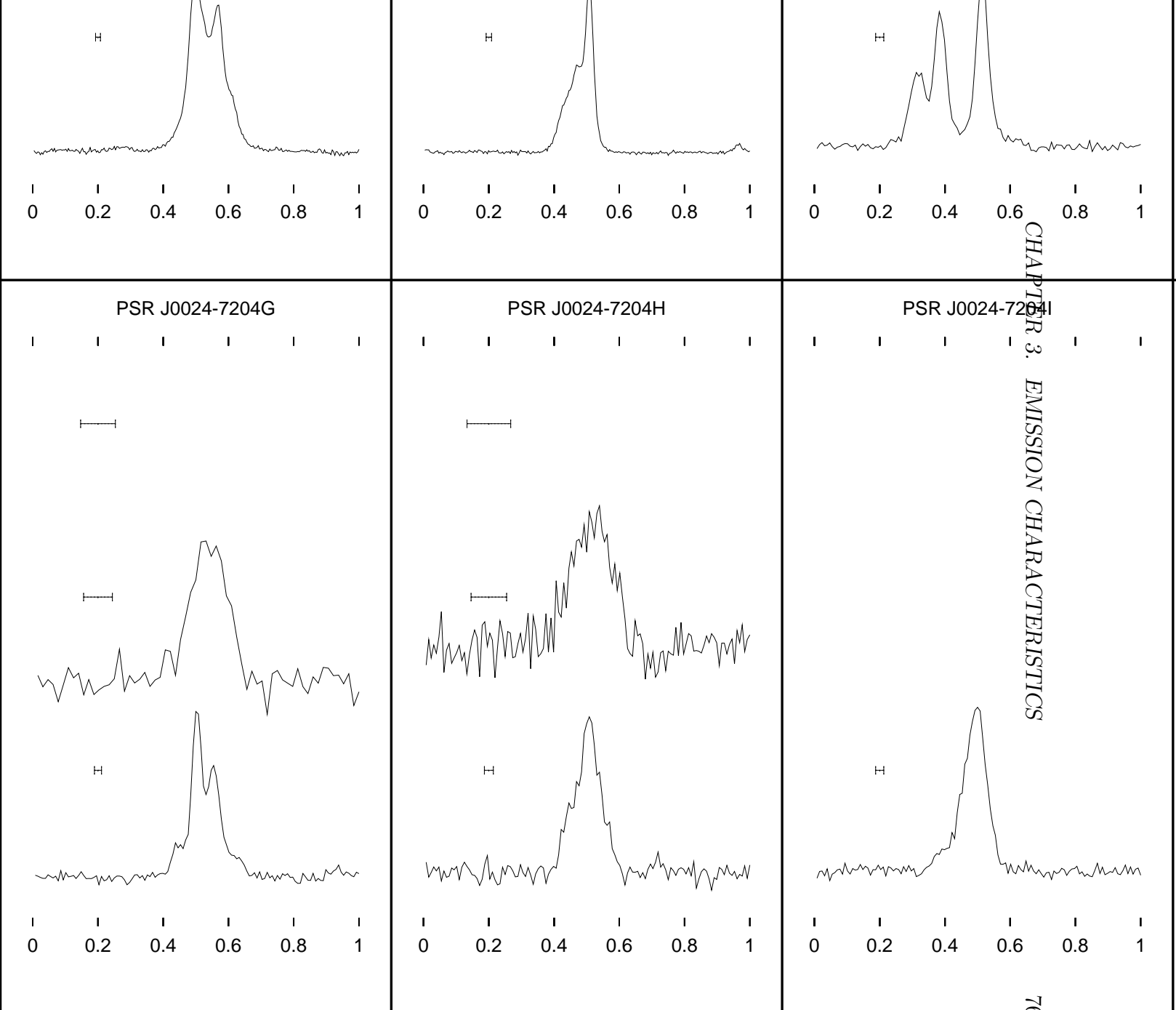
Figure 3.1: Pulse profiles for 47 Tuc C-J, L and M at three radio frequencies: 430 MHz (top), 660 MHz (middle) and 1390 MHz (bottom). The horizontal bars indicate the time resolution of the data at each frequency.

PSR J0024-7204G

PSR J0024-7204H

PSR J0024-7204I
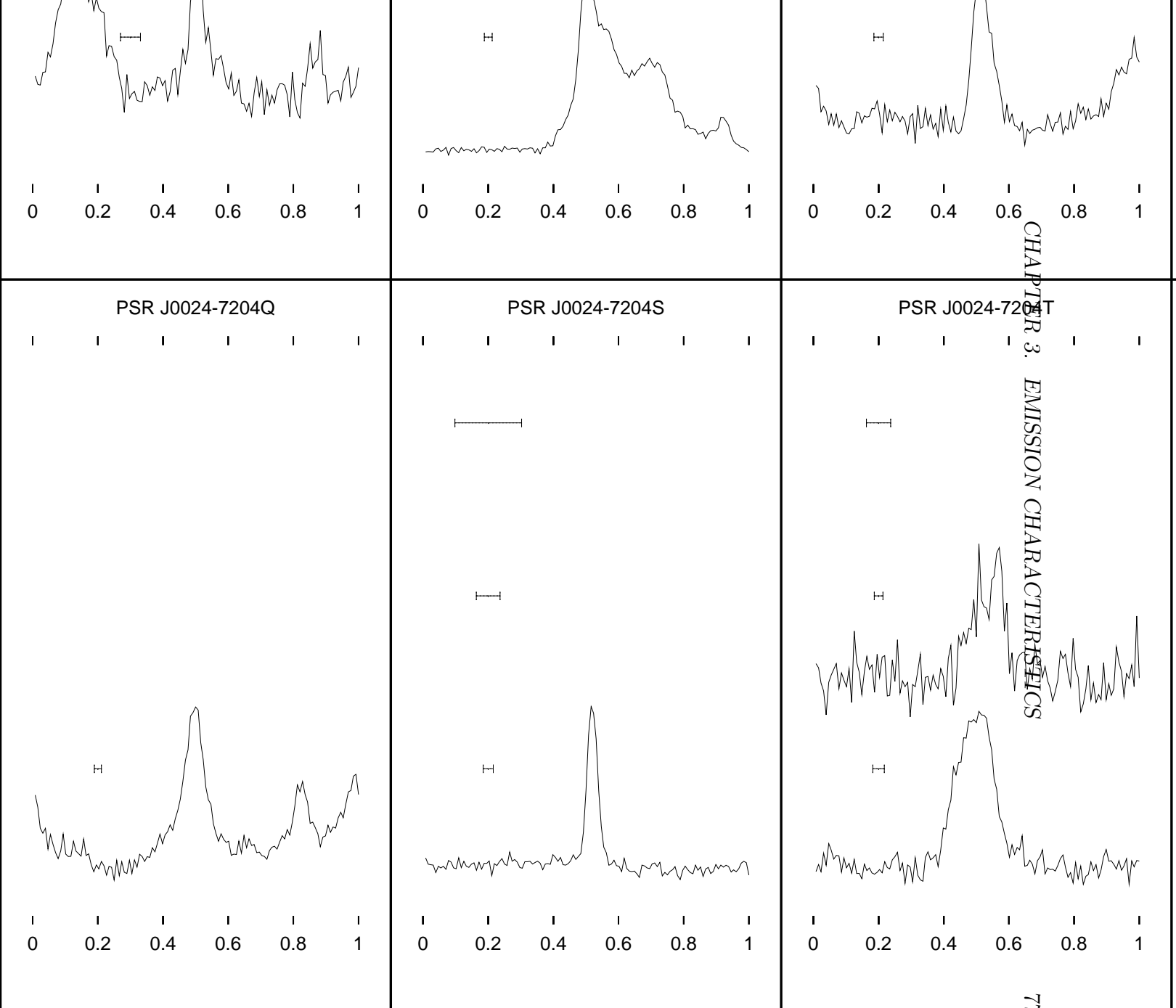
Figure 3.2: Pulse profiles for 47 Tuc N-W at three radio frequencies: 430 MHz (top), 660 MHz (middle) and 1390 MHz (bottom). The horizontal bars indicate the time resolution of the data at each frequency.
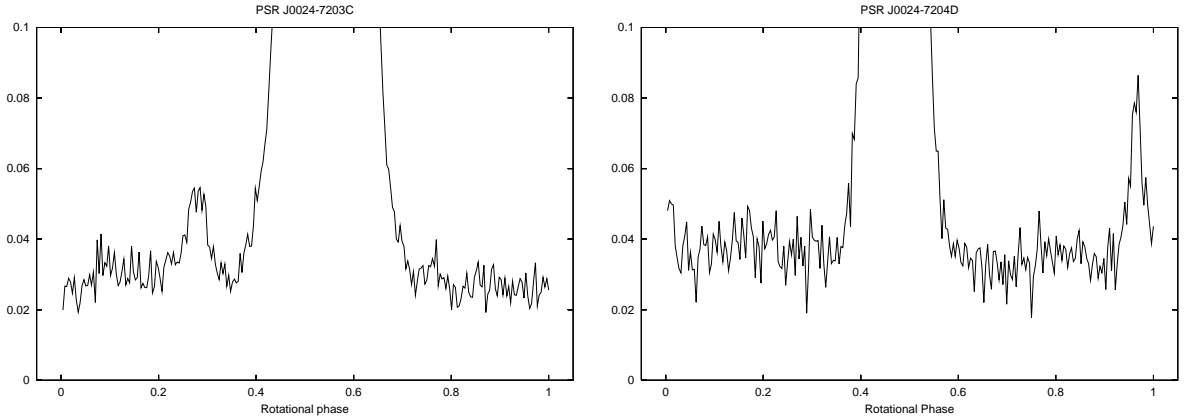
Figure 3.3: Details of the 1400 MHz pulse profiles of 47 Tuc C and D. 47 Tuc C displays weak emission during most of the rotational cycle, while 47 Tuc D shows a weak but sharp interpulse.

when comparing the collection of pulse profiles then available for disk millisecond pulsars and those in 47 Tuc, and in particular the supposed dearth of interpulses among the pulsars in 47 Tuc. More recently, Jayawardhana & Grindlay (1996) also presented evidence suggesting that the observed pulse width distribution of disk and cluster millisecond pulsars may be different.

Our collection of profiles for pulsars in 47 Tuc is larger and of higher quality than that presented by Manchester et al. (1991), on which Chen & Ruderman (1993) and Jayawardhana & Grindlay (1996) based their conclusions. In addition, there are now many more high-quality pulse profiles available for disk millisecond pulsars (Kramer et al. 1998, Stairs et al. 1999). Given these observational improvements, it is appropriate to review the situation regarding possible morphological differences. In an attempt to ensure homogeneity, we choose to compare our 1400-MHz profiles with those reported by Kramer et al. (1998) which were also obtained from 1400-MHz observations. We excluded globular cluster pulsars, double-neutron star systems and PSR 1257+12, which has planets. The

remaining 20 millisecond pulsars supposedly had a formation mechanism similar
to that of the pulsars in 47 Tuc.

In order to test the suggestion that the pulse widths of the pulsars in 47 Tuc
are broader than their counterparts in the Galactic disk, we compared the pulse
width distribution measured at the 50% intensity level (w_{50}) for the 20 pulsars
listed in Table 2.1 with that of the 20 disk millisecond pulsars presented in Table 2
of Kramer et al. (1998). The pulsewidths in Table 2.1 were measured in the same
way as those in Kramer et al. (1998) for consistency. A Kolmogoroff-Smirnoff test
returns a probability of 77% for both distributions being drawn from the same
underlying distribution (see Figure 3.4). This result must be taken with caution:
in spite of the improved time resolution of the $2 \times 512 \times 0.5$ MHz filter-bank,
not all the profiles shown in Figures 3.1 and 3.2 are fully resolved. Five pulsars
(47 Tuc P, R, S, V and W) were only observed with the $2 \times 96 \times 3$ MHz filterbank,
so their pulsewidths are probably smaller.

It should be noticed that the extreme faintness of the pulsars in 47 Tuc intro-
duces a further selection effect against the detection of pulsars with broad pulse
profiles, which must have a higher flux density in order to be detectable with the
minimum stipulated normalized (S/N) (see equation 2.8). This effect probably
causes the dearth of pulsars in 47 Tuc with fractional pulsewidths between 0.15
and 0.25.

From the discussion in the beginning of this section, we notice that the pro-
files of 4 pulsars (47 Tuc D, N, P and R) consist of a simple configuration pulse-
interpulse; other pulsars, like 47 Tuc L, M, Q, U and W, have morphologies that
are notoriously more complex. Inspecting the sample of Galactic disk millisecond
pulsars presented by Kramer et al. (1998), we find five clear interpulses in the
pulse profiles of the 24 pulsars that do not belong to double neutron-star systems.
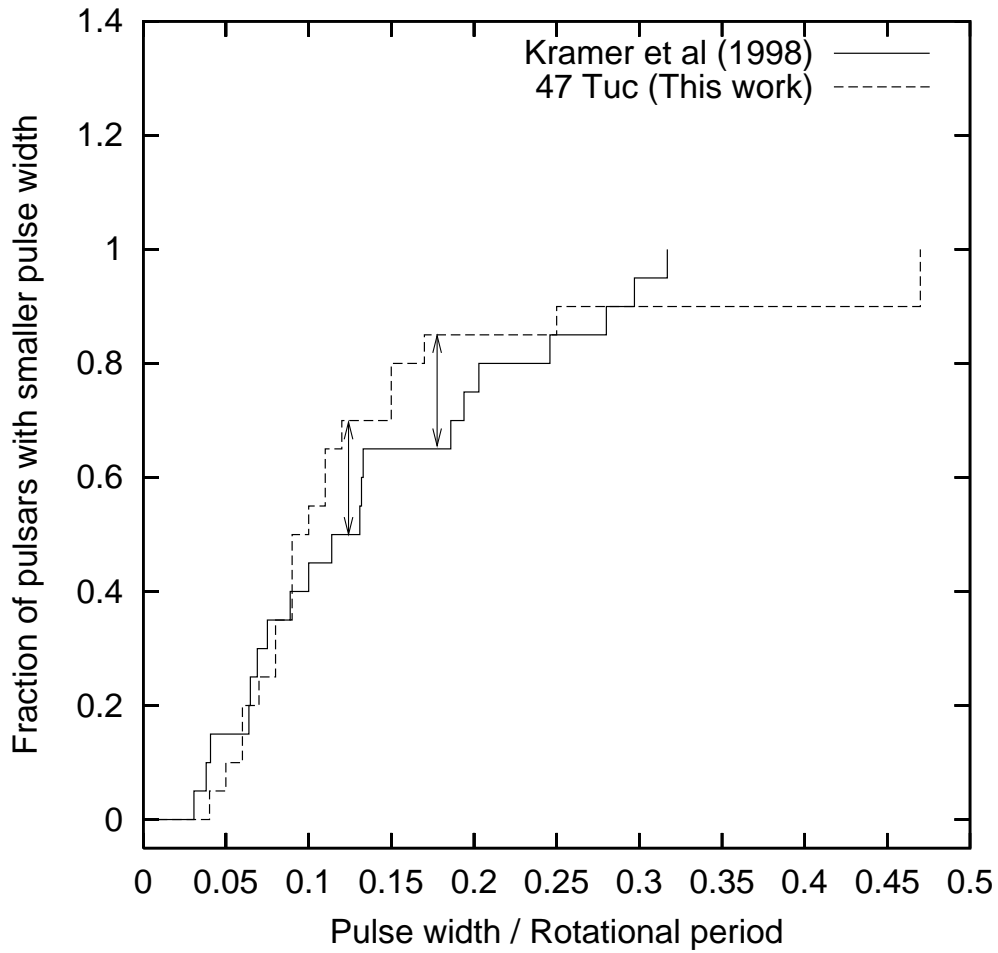
Figure 3.4: Cumulative distribution of fractional pulsewidths for the 20 selected millisecond pulsars in Kramer et al. (1998) and the equivalent distribution of pulsewidths for the pulsars in 47 Tuc. The maximum difference is 0.2, which is indicated with arrows.

Given the present statistics, this is entirely consistent with the fraction of inter-pulses we observe in 47 Tuc, refuting the morphological differences suggested by Chen & Ruderman (1993).

3.2 Pulsar luminosities

Except for 47 Tuc C, D, and J, pulsars in 47 Tuc are detected on fewer than 75% of observing days, and we have detected some of the pulsars on only one observing day (see Table 2.6). Given this fact, it is not appropriate to estimate average flux densities for most pulsars by simply averaging the detected signal-to-noise ratios and converting to flux densities using the approximately known system noise and detection apparatus characteristics. In this section we present a more rigorous method to estimate mean flux densities of the pulsars in 47 Tuc.

The variability in apparent flux densities, apart from the occurrence of eclipses, results from interstellar scintillation (Rickett 1977), and we proceed further by assuming that scintillation affects all pulsars in 47 Tuc similarly, since they are all located in relatively close proximity.

Given this assumption, we construct cumulative histograms in $\log(S/N)$ for the frequently-detected pulsars in the cluster, and attempt to synthesize a "standard" histogram which we take to be representative of the relative flux variations due to interstellar scintillation for a pulsar in 47 Tuc. Initially the standard histogram is defined to be that of 47 Tuc J, the brightest pulsar. The histograms of other frequently-appearing pulsars are then shifted by a scaling factor in a fitting procedure so as to match the standard as closely as possible, in a least-squares sense. A new standard is then defined where normalized (S/N) of the nth strongest "observation" is the average of the respective values from each of the individually shifted histograms, and this procedure is iterated until the scaling factors are stationary and a self-consistent solution is obtained. The

scaling factors with respect to the final standard (see Fig. 3.5) therefore provide an estimate of the average relative signal-to-noise ratios of the various pulsars.

For 47 Tuc J we obtain the actual average normalized (S/N) from the observations (Table 2.6), but correct it downwards to take into account the $\sim 10\%$ of observing days in which we do not detect the pulsar. We do this by assuming that on these days, on average, the pulsar has a flux density that is half of the lowest value detected, resulting in a 10% correction. After applying the scaling factors and converting to a flux density scale using the methodology outlined in § 2.2, we obtain the average flux densities listed in Table 2.1 for 14 pulsars.

One obvious problem with this method is that for the less-frequently appearing pulsars only part of the cumulative histogram is being fitted to — and to the extent that the standard histogram is in fact not precisely descriptive of the scintillation behavior of all pulsars, this may particularly skew the average normalized (S/N) for such pulsars. We have accounted for this in the uncertainties listed in Table 2.1. In addition, until we calibrate the sensitivity of the observing system with a pulsed source of known strength, the conversion between normalized (S/N) and flux density is subject to a systematic uncertainty that we judge to be of the order of $\sim 25\%$.

Pulsars 47 Tuc C, D, and J, for which we have the most reliable flux density estimates, display maximum "daily" flux densities that are factors of 4–8 greater than the average values. This is the only information we have available that is of some use to estimate, very roughly, the average flux density for the pulsars that are detected very infrequently (Table 2.3). We obtain estimates of $\sim 0.04\,\mathrm{mJy}$ for the average flux density of these pulsars. We note this plausible estimate simply to suggest that the flux densities of these pulsars need not be much lower than those of the weakest among the more frequently-appearing pulsars.

The weakest pulsars we have been able to detect in 47 Tuc have flux densities
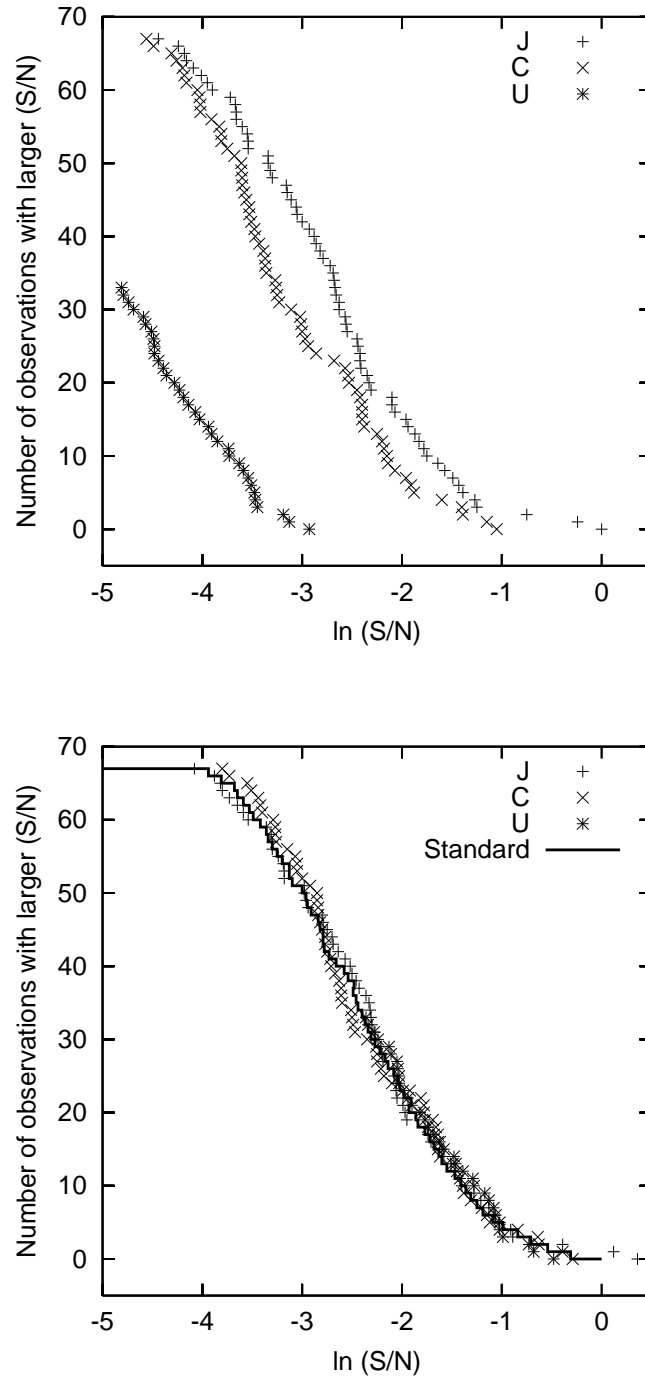
Figure 3.5: Cumulative histograms of $\log(S/N)_R$ for the observations of three pulsars in 47 Tuc (not all were represented, for clarity). Top: $(S/N)_R$ is the signal-to-noise ratio of an observation divided by the maximum signal-to-noise ratio detected for the brightest pulsar, $(S/N)_{\max}$. Bottom: The cumulative histograms of each pulsar were shifted to the right so they closely coincide with the average "standard" distribution typical of the cluster (indicated by the stairs), which is obtained by averaging all the shifted histograms. The value for this shift indicates the relative flux density. The plot also shows that scintillation produces similar effects for all pulsars. See §3.2 for details.
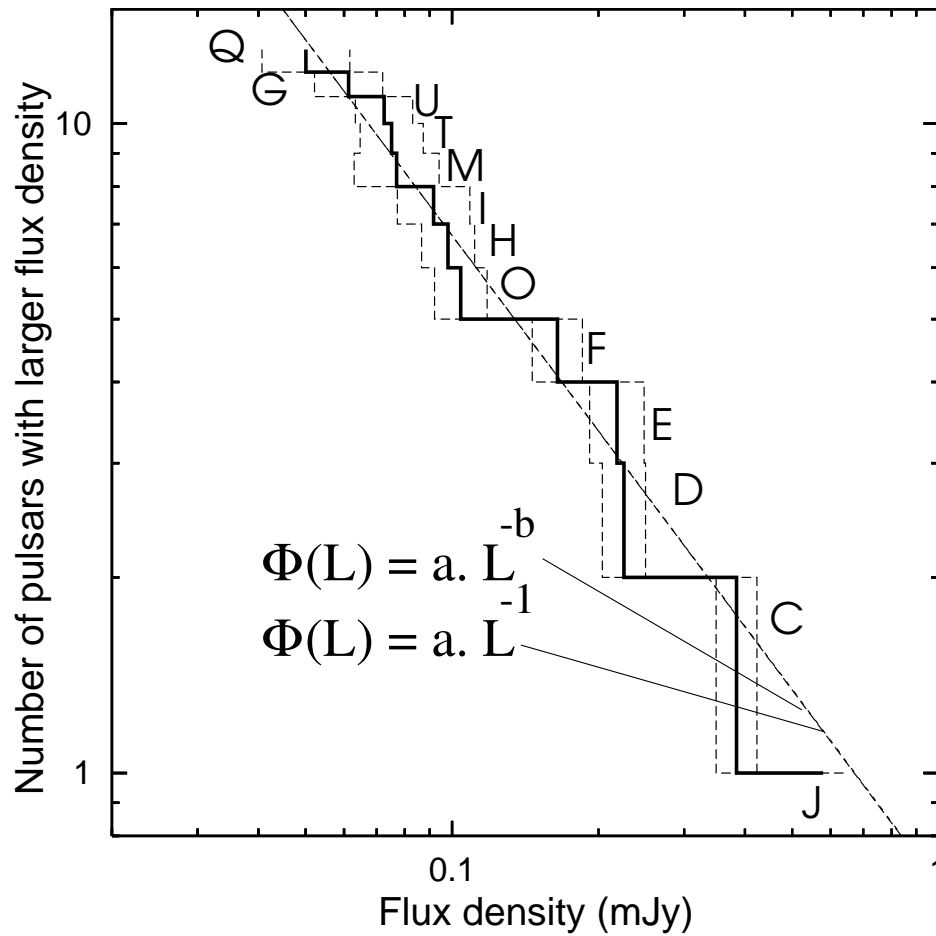
Figure 3.6: Cumulative histogram of 1400 MHz flux densities and their associated errors for the brightest pulsars in 47 Tuc. It can be seen that the observed distribution is indistinguishable from $\Phi(L) \equiv dN/d \log L = a.L^{-1}$; the fitted values are a $= 0.67 \pm 0.12$ and b $= 1.00 \pm 0.07$, consistent with what is found in M15 and the disk of the Galaxy (see text). The two weakest pulsars with a well-measured timing solution and flux density, 47 Tuc L and N, were not included because in their range of luminosities (i.e., below 50 μJy) it is difficult to determine coherent timing solutions for the binary pulsars, hence it is difficult to meaningfully measure their flux densities. Thus, in that range of flux densities the number of such measurements is smaller than the true number of pulsars, therefore the whole range should not be taken into account.

at 1400 MHz of about $S_{1400} = 0.04$ mJy, while the strongest, 47 Tuc J, has $S_{1400} = 0.54$ mJy. At the distance of 47 Tuc (Table 1.2), these correspond to luminosities at 1400 MHz, $L_{1400} \equiv S_{1400}d^2$, of 0.8–11 mJy kpc^2. Translated to luminosities at frequencies ~ 400 MHz, assuming a spectral index for the pulsars in 47 Tuc of -2.0, these correspond roughly to $10 < L_{400} < 130$ mJy kpc^2.

The limiting minimum luminosity for Galactic disk pulsars at ~ 400 MHz is about 1 mJy kpc^2 or lower (Lorimer et al. 1993, Lyne et al. 1998). For the Galactic disk (Lyne et al. 1985) and M15 (Anderson 1992), the differential luminosity distribution for pulsars is found to be consistent with $dN = L^{-1} d \log L$. These findings apply to 47 Tuc as well, as indicated in Figure 3.6 and its caption. Thus we estimate that in 47 Tuc there are about 10 times as many potentially observable pulsars in the luminosity decade 1–10 mJy kpc^2 as there are in 10–100 mJy kpc^2, where we already know of about 20 pulsars. Hence we estimate a potentially observable population of pulsars in 47 Tuc, similar to the ones already detected, of about 200, above a minimum luminosity $L_{400} \sim 1$ mJy kpc^2. When beaming and selection effects are accounted for we judge it likely that 47 Tuc contains several hundred pulsars with $L_{400} \leq 1$ mJy kpc^2.

A more accurate determination of the luminosity distribution, and a detailed discussion of flux densities, spectral indices, and scintillation properties for the pulsars in 47 Tuc, will rely on more complete multi-wavelength data sets, and will be addressed in Freire et al. (2000f). It is already clear, however, that we have detected only the few brightest pulsars in 47 Tuc, and continued searches of this cluster, particularly with greater sensitivity, should yield a bounty of new discoveries.

Chapter 4

Determining the orbits of the new pulsars

A previous version of this chapter has been accepted for publication in the Monthly Notices of the Royal Astronomical Society (**?**). It describes a new and simple procedure to estimate the orbital parameters of binary systems in low-eccentricity orbits, which was devised by the author and implemented by himself, M. Kramer and A. G. Lyne. A section on the conventional pulsar period analysis is here added for the sake of completeness.

4.1 The problem

If a newly discovered binary system has an orbital period comparable to the length of an observation, then it is possible to make a unique determination of the orbital parameters of the pulsar using data from a single observation and conventional period analysis (see § 4.4). This happened for the newly-discovered binaries 47 Tuc O, P, R and W, whose orbital parameters are presented in chapter 2 (see Figure 2.3). However, 47 Tuc H and some of the newly-discovered binaries (47 Tuc Q, S, T and U) have orbital periods considerably longer than one
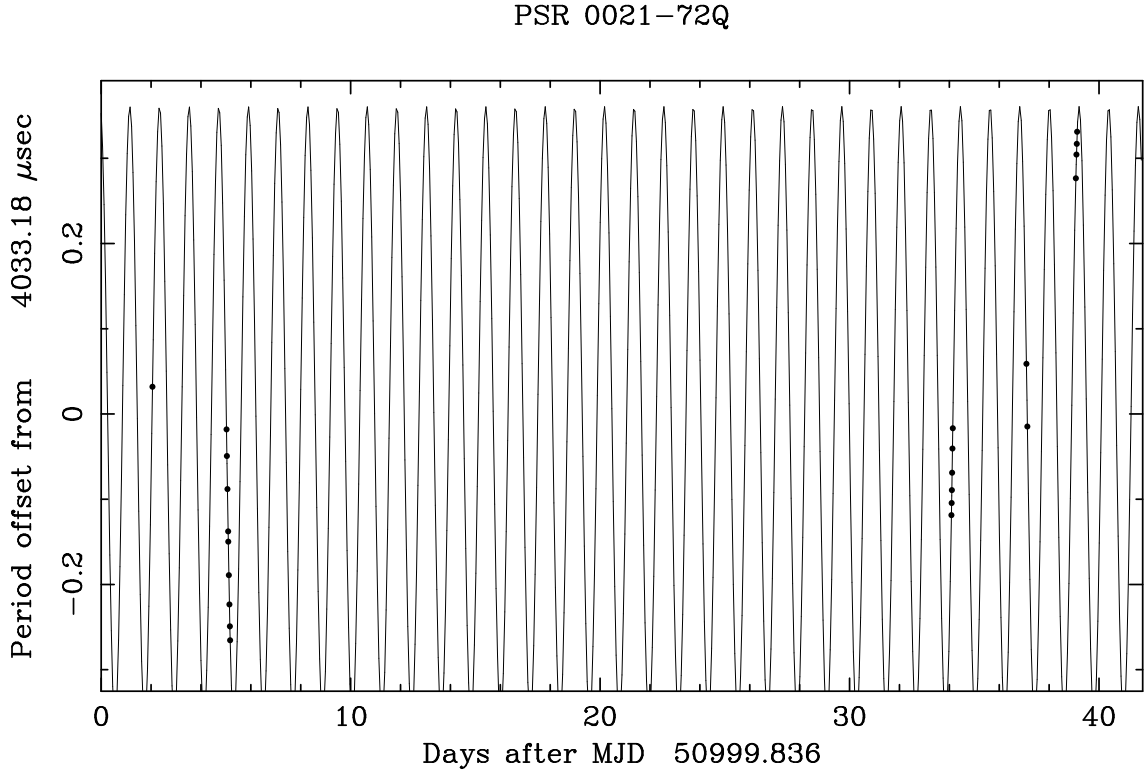
Figure 4.1: Plot of observed barycentric spin periods as a function of epoch for 47 Tuc Q (dots); the solid line is the prediction of the orbital model. It was with this set of periods that the orbit of this binary was first determined. The observed rotational period of the pulsar changes because of its variations in line-of-sight velocity, which cause a Doppler shift in the period.

observation. For 47 Tuc H, Q and U, the orbits could be determined using the known period analysis techniques because the pulsars happened to be detected on several closely spaced observations (see Figure 4.1).

This did not happen for 47 Tuc S and T, essentially because we cannot choose when to detect the pulsars - that is primarily determined by scintillation. Therefore, it has been impossible so far to determine the orbital parameters of these pulsars: even in table 2.4 their detections are very rare and extremely sparse.

We have sought a way of employing the hitherto unused information contained

in the measured orbital accelerations to obtain a full, coherent solution for the Keplerian orbital parameters.

In this chapter, we present a simple procedure for estimating the orbital parameters of a binary that is completely independent of the epochs of the individual observations, provided that the pulsar accelerations are known in each case. In §4.2, we present the equations for the period and acceleration of a pulsar in an eccentric binary system as a function of its position in the orbit. We also provide an analysis of the circular case and show how the orbital parameters can be obtained from a plot of the acceleration of the pulsars against rotational period, and determine the orbital parameters of 47 Tuc S and T. In § 4.3, we show how to improve the estimates of the orbital parameters, and refine the orbits of the two binaries. In § 4.4, we finish by presenting the principles of conventional period analysis, which was used to further refine the ephemerides of 47 Tuc S and T and determine the orbital parameters of the remaining binaries.

4.2 Binary orbits in the acceleration/period plane

Figure 4.2 represents the orbit of a binary pulsar (point P) around the centre of mass of the system (O) projected onto a plane that contains the direction towards the Earth (i.e., perpendicular to the plane of the sky, Π) and the line of nodes, where the orbital plane intersects Π. The orbit is an ellipse of eccentricity e and projected semi-major axis $a_P = a'_P \sin i$ (i is the unknown inclination of the orbit relative to the plane of the sky). $\mathbf{r}$ is the vector connecting O to P, and $r = |\mathbf{r}|$ is the distance of the pulsar to O, $r_l = |\mathbf{r_l}|$ is the projection of this in the line-of-sight. ω is the longitude of periastron and f is the angle of the pulsar to the periastron measured at O, also called "true anomaly". According to Roy (1988), the equation for r_l as a function of f is given by
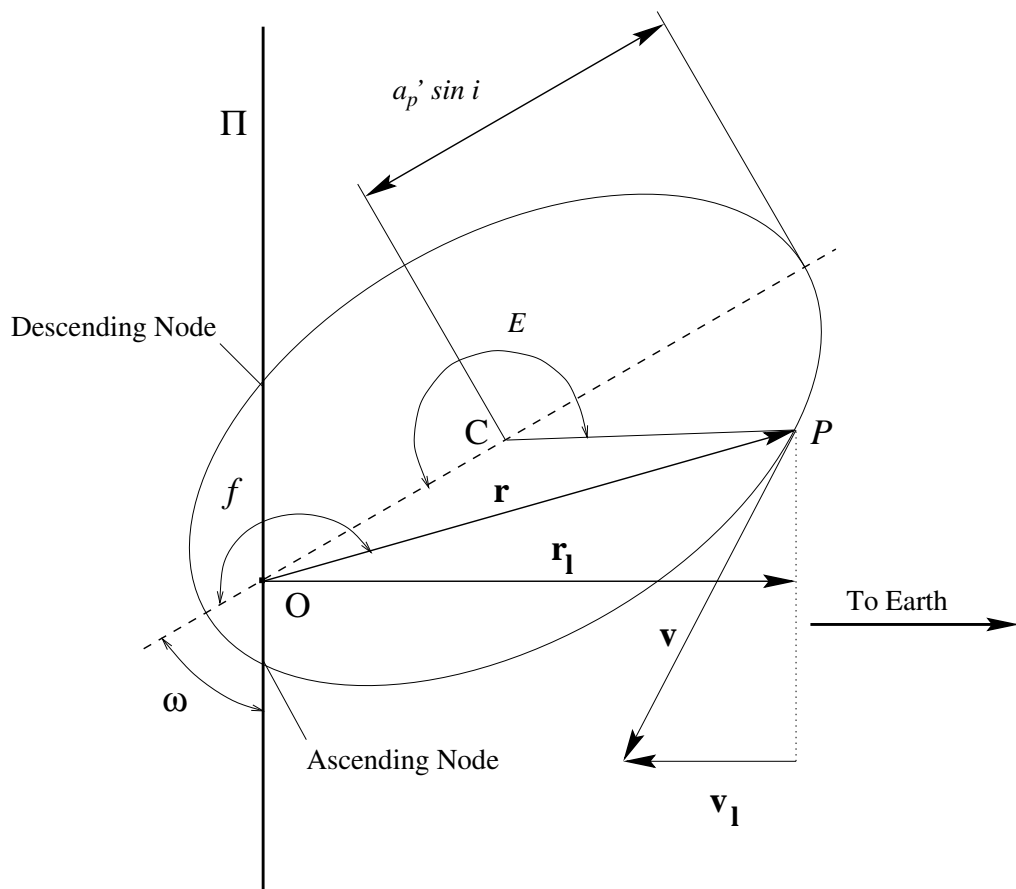
Figure 4.2: Geometrical parameters for an elliptical orbit.

$$r_l(f) = r\sin(\omega + f) = a_P \frac{\sin(\omega + f)}{1 + e\cos f} \qquad (4.1)$$

The time derivative of $r_l(f)$ is the line-of-sight velocity, $v_l(f)$, which is just a component of the total velocity of the pulsar $v(f)$. Using the following equations (Roy 1988)

$$\dot{r} = h'e\sin f \qquad (4.2)$$

$$r\dot{f} = h'(1 + e\cos f) \qquad (4.3)$$

$$h' = \frac{n_B a_P}{\sqrt{1 - e^2}} \qquad (4.4)$$

where $n_B \equiv 2\pi/P_B$ is the mean angular velocity; and P_B denotes, as usual, the orbital period of the system, we obtain:

$$v_l(f) = n_B \frac{a_P}{\sqrt{1 - e^2}} \left[\cos(\omega + f) + e\cos\omega\right] \qquad (4.5)$$

The observed rotational period of the pulsar as a function of f and its intrinsic rotational period P_0 is given by the classic Doppler equation

$$P(f) \simeq P_0 \left(1 + \frac{v_l(f)}{c}\right) \qquad (4.6)$$

if $v_l(f)/c$ is small.

Differentiating equation 4.5 in time, we can again use equations 4.2 to 4.4. We obtain the acceleration along the line of sight A_l as a function of the true anomaly, f:

$$A_l(f) = -n_B^2 \frac{a_P}{1 - e^2}(1 + e\cos f)^2 \sin(\omega + f) \qquad (4.7)$$

Plotting $A_l(f)$ as a function of $P(f)$, we obtain a parametric curve that does not depend on time, and therefore does not require the solution of Kepler's equation. This curve is illustrated in Figure 4.3 for a binary pulsar of spin period 10 ms and orbital parameters $e = 0.9$, $\omega = 140°$, $P_B = 1$ day and $x \equiv a_P/c = a'_P \sin i/c = 1s$.
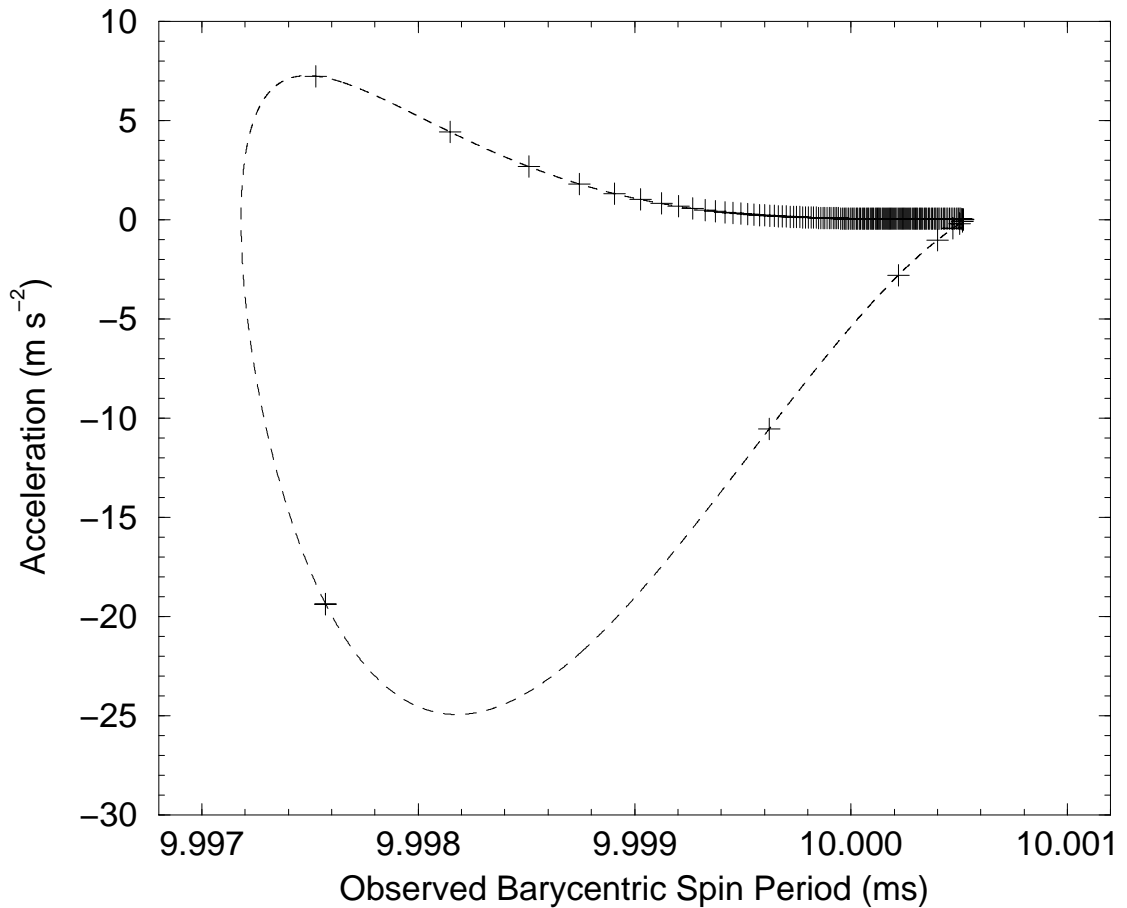
Figure 4.3: A simulated binary system with an orbital period of 1 day, $x = 1$s, $e = 0.9$ and $\omega = 140°$. The pulsar has an intrinsic rotational period of 10 ms. The dashed line represents the acceleration as a function of the observed barycentric rotational period. The pulsar was "observed" every ten minutes, each observation is here represented as a + sign. The zones with a smaller concentration of observations correspond to the periastron, where the pulsar spends relatively little time, but where accelerations are largest. The apastron is to the left of the cusp, where the binary spends most of its time, accelerations there are rather small.

All known binaries containing "true" millisecond pulsars, i.e., those with periods below 20 ms, have rather circular orbits (Camilo 1995*b*, Kulkarni & Anderson 1996). Therefore, in most cases, we have $e = \omega = 0$ in the equations above, so that equations 4.6 and 4.7 reduce to

$$P(f) = P_0 + P_0 x n_B \cos f \equiv P_0 + P_1 \cos f \tag{4.8}$$

and

$$A(f) = -n_B^2 x c \sin f \equiv -A_1 \sin f. \tag{4.9}$$

The track followed by the pulsar in the period/acceleration space is therefore an ellipse centred on the point $(P_0, 0)$ and having as horizontal and vertical semi-axes the values P_1 and A_1 respectively, with the pulsar moving in a clockwise direction.

Generally, once an ellipse has been found to fit a set of measurements of barycentric period and acceleration for a given pulsar, we can easily recover the two relevant orbital parameters in a circular orbit:

$$P_B = \frac{P_1}{P_0} \frac{2\pi c}{A_1} \tag{4.10}$$

$$x = \left(\frac{P_1}{P_0}\right)^2 \frac{c}{A_1} \tag{4.11}$$

Using these newly determined orbital parameters, we can calculate the angular orbital phase for each kth data point, i.e. for each pair of acceleration and period measured (A_k, P_k):

$$\phi_k = \arctan\left(-\frac{A_k}{A_1} \frac{P_1}{P_k - P_0}\right) \tag{4.12}$$

where $-\pi < \phi_k \leq \pi$. Since the barycentric time T_k of each observation is also known, we can determine the time of the nearest ascending node, or simply $T_{\mathrm{asc,k}}$ for each observation:
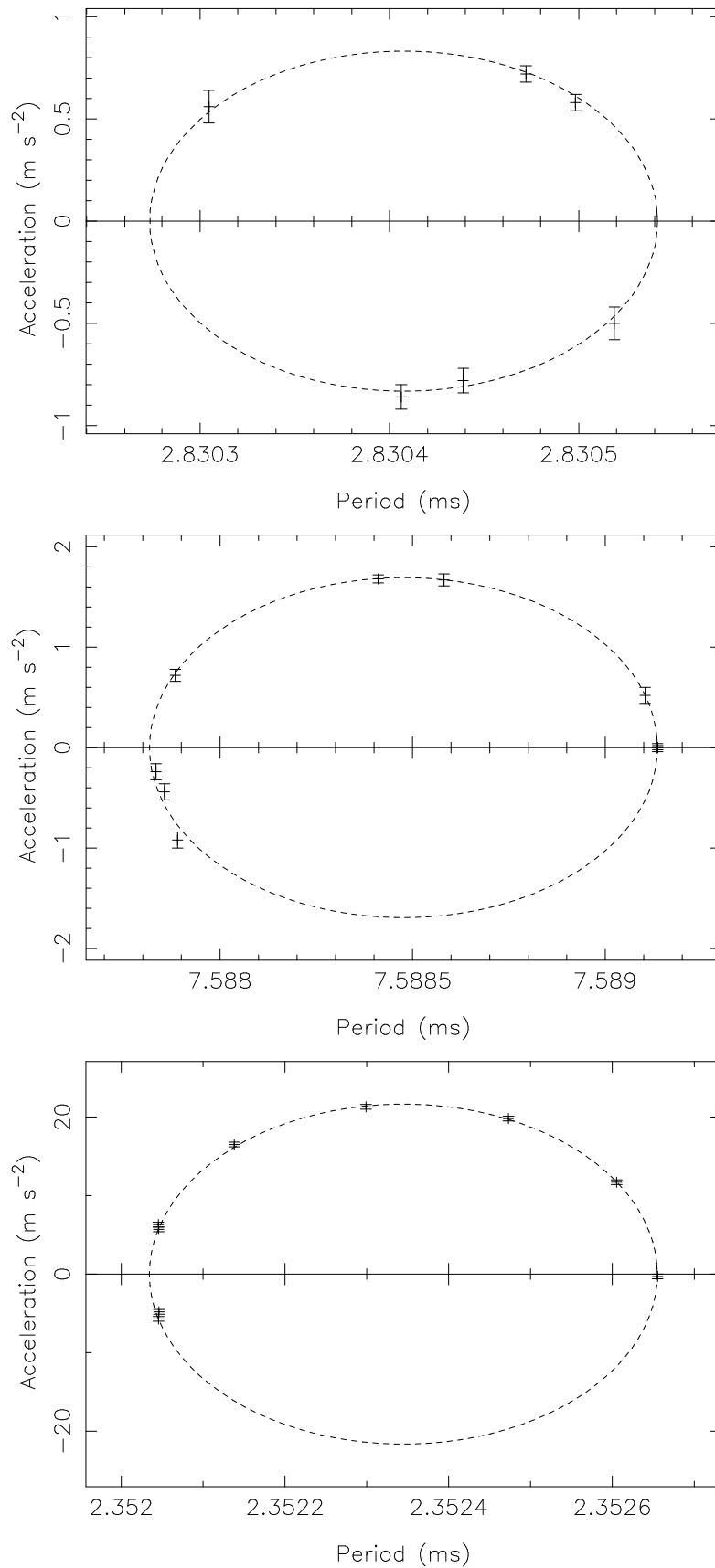
Figure 4.4: Observed accelerations plotted against barycentric spin period for 47 Tuc S (top), 47 Tuc T (middle) and 47 Tuc W (bottom), three binary millisecond pulsars in the globular cluster 47 Tuc.

$$T_{\mathrm{asc,k}} = T_k - \frac{\phi_k}{n_B} \qquad (4.13)$$

We can use these values to refine the orbital period (§ 4.3).

Using this procedure, the few and very sparse detections in Table 2.4 made by AS25 proved enough to make a preliminary determination of the orbits of 47 Tuc S and T (the details of the fitting algorithm are presented in Appendix A). In Fig. 4.4, the accelerations are plotted as a function of barycentric period, and they clearly delineate well-defined ellipses. The orbital parameters resulting from the best fitting ellipses for these three pulsars are given in Table 4.1. 47 Tuc S and, particularly 47 Tuc T seem to be very similar to the 47 Tuc Q system. The 47 Tuc W binary system already had determined orbital parameters, it was included to illustrate the fact that using only the positive accelerations is enough to determine the orbit of a binary using this method. We could not observe this pulsar at large negative accelerations, although we know that it went through these twice during the discovery observation; this indicates the presence of eclipses in this system, which cover more than 30 % of the whole orbit.

From the data in this last Table, we conclude that the procedure presented in § 4.2 is accurate within the error bars derived from Monte Carlo simulations (see Appendix A). Although timing provides far more precise values for the orbital parameters, the new procedure is the only one capable of giving any estimates of the orbital parameters when the data samples the orbital period sparsely. For this purpose, the epochs of the individual period/acceleration measurements are completely irrelevant as long as the measurements have reasonable orbital phase coverage; their values are only needed to make the appropriate corrections of the periods (and, in some cases, the accelerations) to the barycentre of the solar system.

Parameter	J	U	W	S	T
P_0^a (ms)	2.1006335(6)	4.342831(1)	2.3523445(8)	2.830407(8)	7.588476(4)
P_0^b (ms)	2.1006336	4.342827	2.3523445	2.830406	7.588481
P_B^a (d)	0.119(3)	0.41(2)	0.1322(16)	1.24(14)	1.12(3)
P_B^b (d)	0.121	0.43	0.1330	1.20	1.13
x^a (s)	0.0396(13)	0.49(4)	0.240(3)	0.79(14)	1.33(4)
x^b (s)	0.0404	0.53	0.243	0.77	1.34
T_0	51000.7979	51003.0587	51214.9496	51000.9649	51000.3173
N	31	13	9	6	9

Table 4.1: Comparison of the orbital parameters for several binaries in the globular cluster 47 Tuc. The parameters indicated by an "a" were determined by the procedure presented in § 4.2, the parameters indicated by a "b" were determined by the timing analysis. The latter are far more accurate (see chapter 5), and their true value is within half of the last significant digit quoted. For 47 Tuc S the "b" parameters are still derived from the period analysis. N is the number of individual measurements of acceleration and period; for 47 Tuc J and U these were randomly selected from the many measurements of these pulsars made by AS23; for 47 Tuc S and T all the data used is in Table 2.4.

4.3   Refining the ephemeris

As mentioned at the end of § 4.2, it is possible to refine the orbital period using the local values of the $T_{\mathrm{asc,k}}$, in the same manner that a group of times of arrival of pulses from an isolated pulsar (henceforth TOAs) can be used to improve the estimate of the rotational period of the pulsar, once a reasonable estimate of the rotational period is available. This also allows the determination of a more precise value for a global T_{asc}.

As in the pulsar case, the problem is that we don't know precisely how many orbits have occurred between any two observations. With data as sparse as that of 47 Tuc S and T, this task is normally impossible. However, we already know approximate orbital periods for the binary systems from the procedure outlined in § 4.2 and Appendix A. We also know more than two times of ascending node for each binary, calculated using equation 4.13. So all we have to do is to

estimate a binary period and global T_{asc} that produces the observed $T_{\text{asc,k}}$, with the restriction that the orbital period should be consistent with that determined in the previous section.

This can be done in a very intuitive manner. All the (positive) differences between any two times of ascending node are integer multiples of the orbital period. Dividing all these differences $D_{j,k}^+ = |T_{\text{asc,k}} - T_{\text{asc,j}}|$ (with $j \neq k$ and $D_{j,k}^+ = D_{k,j}^+$) by the set of integers that provide an orbital period consistent with the estimate obtained in the previous section, we obtain a set of possible orbital periods for each $D_{j,k}^+$. The "true" orbital period should be common to all these sets.

To illustrate this, we now proceed to refine the orbital period of 47 Tuc S using this method. From equation 4.13, we obtain for this pulsar the following $T_{\text{asc,k}}$ (with a precision of 0.01 days approximately):

$$T_{\text{asc,1}} = 50741.38,$$
$$T_{\text{asc,2}} = 51000.98,$$
$$T_{\text{asc,3}} = 51003.39,$$
$$T_{\text{asc,4}} = 51216.05.$$

There are six $D_{j,k}^+$. We will now use only four of these:

$$D_{2,1}^+ = 259.6 \text{ days},$$
$$D_{3,2}^+ = 2.41 \text{ days},$$
$$D_{4,3}^+ = 212.7 \text{ days},$$
$$D_{1,4}^+ = 474.7 \text{ days}.$$

From $D_{2,3}^+$, we obtain an approximate estimate for P_B of 1.205 ± 0.010 days. In Figure 4.5, we can see that the true orbital period is probably equal to $D_{2,1}^+/216 = 1.2018(1)$ days, or $D_{4,3}^+/177 = 1.2017(1)$ days or $D_{1,4}^+/395 = 1.20177(5)$ days. This can be confirmed by using the two other $D_{j,k}^+$. This improved orbital period can
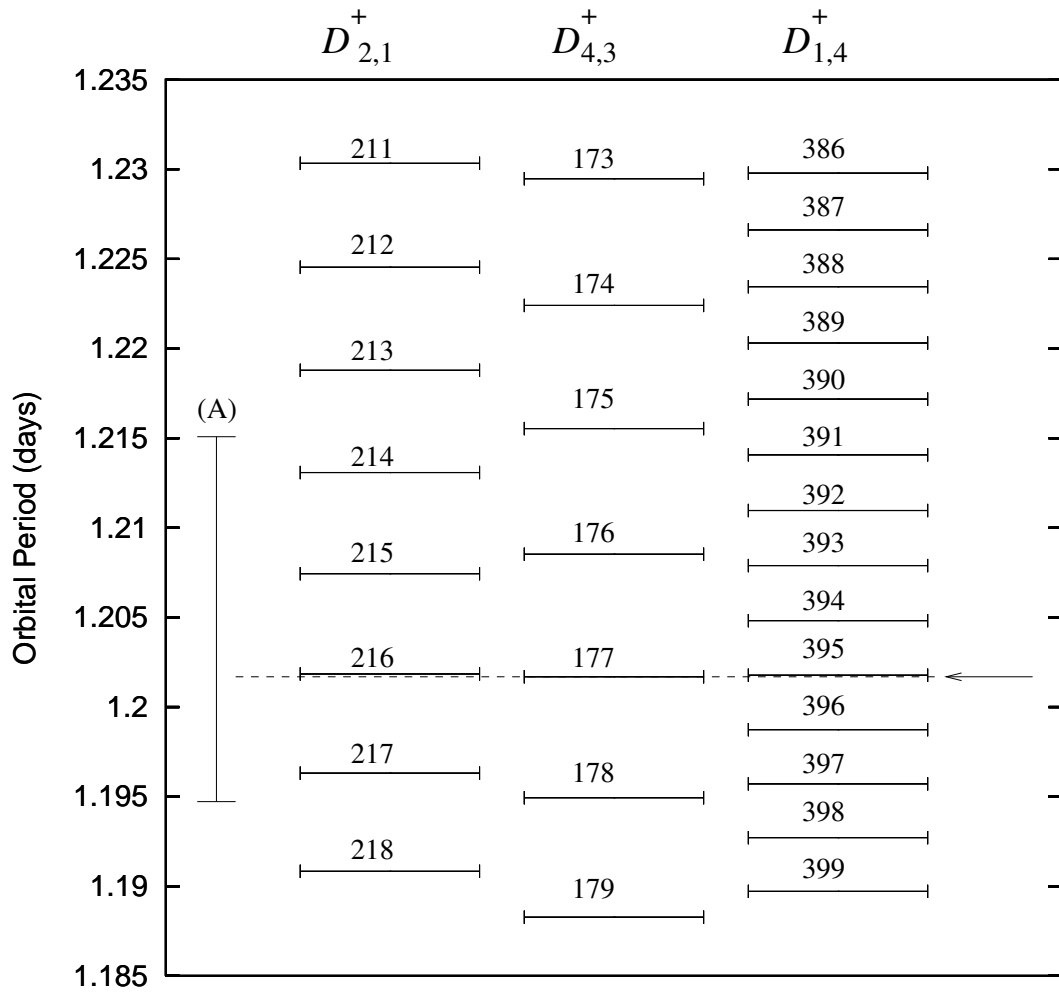
Figure 4.5: Periodogram for 47 Tuc S. The vertical errorbar indicated with an "(A)" is the range of orbital periods consistent with $D_{3,2}^+$ and the estimate made in the previous section, the height of the horizontal bars indicates the orbital periods obtained by dividing the $D_{j,k}^+$ indicated on top of the picture by the integer immediately above each bar. The period common to the three sets is near 1.2017 days.

now be used in equation 4.13 to improve the estimates of the $T_{\rm asc,k}$, therefore leading to a still better estimates for P_B.

In practice, there are more precise (although computationally more intensive) ways of doing this refinement of the orbital period of the binary. Two such algorithms, which were implemented in a program called "ORBITFIT", are presented in Appendix A; these provided good values of P_B for 47 Tuc S and T and also provide a good estimate of $T_{\rm asc}$, these values were later confirmed (and refined) by the period analysis described in the following section.

4.4 Conventional period analysis

With the improved estimates of P_B and $T_{\rm asc}$ obtained in the previous section, the orbital parameters can be refined even further using conventional period analysis. We now describe this sort of analysis in more detail, the software used to make this analysis is described in Appendix A.

The first step of the analysis is to compute, for a set of orbital parameters, the observed rotational period of the pulsar as a function of time. Because the true anomaly of a binary system f varies with time T, equation 4.6 means that the Doppler shift affecting P changes with time. The model for such time variations will therefore include equations 4.5 and 4.6, with a suitable description of $f(T)$. The true anomaly at a given time $f(T)$ is related to the eccentric anomaly $E(T)$ by

$$\tan\frac{f(T)}{2} = \sqrt{\frac{1+e}{1-e}}\tan\frac{E(T)}{2} \qquad (4.14)$$

The eccentric anomaly $E(T)$ is the angle pulsar - centre of orbit (Point "C") - periastron (see Figure 4.2). It can be obtained solving Kepler's equation

$$M(T) = n_B(T - T_0) = E(T) - e\sin E(T) \qquad (4.15)$$

where $M(T)$ is known as the mean anomaly. Equation 4.15 must be solved

PSR 0021−72S
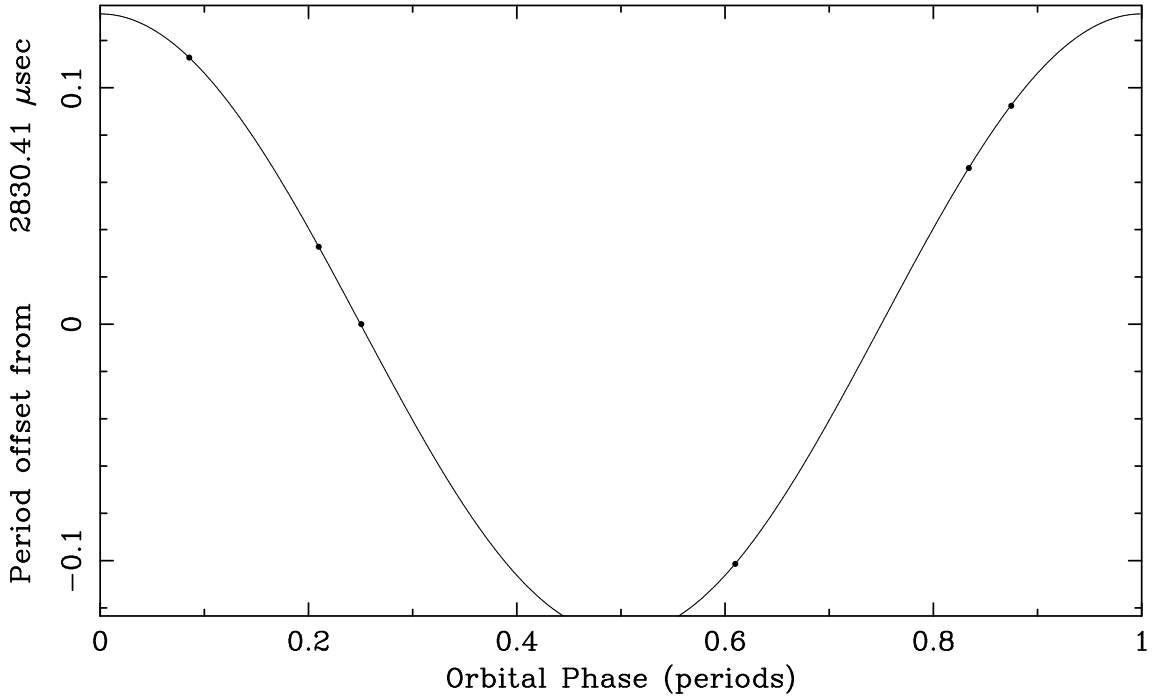
Figure 4.6: Plot of barycentric spin period against orbital phase (measured in time) for 47 Tuc S. The pulsar has no eclipse. From the data in Table 2.4.

by some iterative method, in order to compute $E(T)$. From that, we calculate $f(T)$ using 4.14, $v_l(T)$ from $f(T)$ using equation 4.5 and $P(T)$ from $v_l(T)$ using equation 4.6.

For the simple case of a circular orbit, we have $e = 0$, thus equation 4.15 becomes $E(T) = n_B(T-T_0)$, and equation 4.14 is simply $f(T) = E(T)$. Equation 4.8 then applies:

$$P(T) = P_0 + P_0 x n_B \cos\left[n_B(T - T_0)\right] \tag{4.16}$$

In this case, T_0 no longer means the time of passage through a given periastron. As mentioned previously, in this case T_0 is the time of passage through an ascending node, T_{asc}. This sinusoidal wave is the curve seen in Figures 2.3, 4.1 and 4.6. Most binary millisecond pulsars have very low eccentricity orbits, and the variations of their observed rotational period are perfectly described by equation 4.16.

Let us now suppose that our knowledge of the orbital parameters of a binary

system is only approximate. For a new pulsar, which is being studied for the first time, this knowledge normally comes from an educated guess of the values of the orbital parameters, which is improved by trial-and-error. One of the novelties in the work presented so far in § 4.2 and § 4.3 is that, apart from being able to estimate the orbital parameters when the orbit is poorly sampled, we now have a scientific and rigorous way of making the first estimate of the orbital parameters, which is useful even when the orbit is reasonably sampled. The quality of this estimate obviously depends on orbital phase coverage and the precision of the measurement of accelerations.

If our knowledge of the parameters is only approximate, there should be differences between the observed rotational period of the pulsar and the prediction of the model $P(T)$. Using a program called FITORBIT (see Appendix A), we can use these differences to improve the estimates of the orbital parameters of the pulsars, provided that the original estimate of orbital parameters is close enough to the solution (this was the case for the orbital ephemerides of 47 Tuc S and T after applying the procedure described in § 4.3). All the data needed to do this orbital fitting (epochs and apparent rotational periods at the barycentre) is in Table 2.4 already. Figures 4.1 and 4.6 show a comparison between predicted and observed barycentric periods for pulsars 47 Tuc Q and S after the orbital parameters were fitted using FITORBIT.

After this stage, and for all pulsars in long-period binaries, we fold the raw data with the known detections according to the ephemeris determined in the previous step. The TOAs obtained can be used to make much more precise estimates of apparent rotational period; to do this we use a timing program implemented at Jodrell Bank called PSRTIME. We then use these improved apparent rotational periods to refine the orbital ephemeris of the binary using FITORBIT

once more. We used this method to make a precise estimate of the orbital parameters of 47 Tuc S and T. For 47 Tuc S, the ephemeris obtained at this stage is still the most precise available: $P_B = 1.20172465(7)$ days, $x = 0.766338(9)$ s and $T_{\mathrm{asc}} = 51000.964588(8)$ (MJD), the current estimate for the rotational period is $P = 2.830406030(3)$ ms.

The process of further refinement of the ephemeris is described in chapter 5; it is no longer period analysis but essentially TOA analysis, or "pulsar timing". We could already determine a coherent timing solution for 47 Tuc T, the orbital, positional and rotational parameters for this pulsar are presented in chapter 5.

An analysis of the orbital parameters determined at this stage (see Table 2.2) is mentioned in § 7.1. It is clear from that section that the mere determination of orbital parameters, even with no coherent timing solution, like in the case of 47 Tuc P, R, S and W; is scientifically interesting, apart from being a necessary step to obtaining a timing solution.

Chapter 5

Coherent timing solutions for 15 pulsars

Sections 5.2 and 5.3 of this chapter have been published before as sections 2 and 3 of Freire et al. (2000b)?, a paper containing the timing results for the pulsars in 47 Tuc. This paper has been recently submitted to Monthly Notices of the Royal Astronomical Society.

5.1 Pulsar Timing

Millisecond pulsars are exquisitely precise rotators, rivalling the best time standards available today in timescales of several years (see, e. g., Kaspi, Taylor and Ryba 1994). The stability of their spin rate is thought to derive from their comparatively weak magnetic field, which produces no strong stresses in the crust. Timing residuals of $10^1 - 10^2 \mu s$ are common, and of the same order of the residuals we obtain for the pulsars in 47 Tuc. It is a fortunate coincidence that such a precise rotation can be measured from the Earth by monitoring the radio pulses arriving from the pulsar. This precise rotation can be put to a variety of uses.

Timing of the binary pulsars PSR B1913+16 and PSR B1534+12 has been

used to test the strong field predictions of general relativity. Pulsar timing can also be used to search for any variations of the gravitational constant G, to set stringent upper limits to the gravitational wave background and to study inhomogeneities in the interstellar medium. In can also be used to study the motions in classical, newtonian systems. One important such case is PSR B1257+12, which has its own planetary system. Other cases are the pulsars in globular clusters, which can be used as exquisite accelerometers immersed in the gravitational field of the cluster. It is a nice coincidence that Nature tends to form millisecond pulsars precisely in the places where such measurements are more interesting, such as binary systems and globular clusters.

5.1.1 Topocentric Times-of-Arrival

Although single pulses from any given pulsar fluctuate in both intensity and shape, the pulse profile of the pulsar, obtained by adding several minutes of pulses, is remarkably stable for a given observation band. This is quite convenient in the case of the pulsars we are studying in 47 Tuc: they are so weak that several million pulses need to be added to obtain a single TOA (this depends strongly on scintillation).

A "standard pulse profile", representing the best available profile at a given frequency, is generated from several hours worth of data from the observing system, and is an important element in the TOA calculation procedure. During data analysis, the data are added according to the dispersion measure known for the pulsar (i.e., the lower frequencies are artificially anticipated in time so the arrival times of the pulses are similar at all frequencies, see eq. 5.21) and then folded modulo the predicted topocentric pulse period to form an integrated pulse profile. The resulting observed total intensity of the signal as a function of time, $p(t)$, may be written as (Taylor 1992):

$$p(t) = a + bs(t - t_0) + g(t), \qquad (5.1)$$

where $s(t)$ is the standard profile, $g(t)$ is Gaussian noise, a is a constant DC level, b measures the intensity of the pulsar signal and t_0 is a time offset $(0 \leq t \leq P$, where P is the pulse period). The constants a, b and t_0 can be obtained by making a least-squares fit; for timing purposes, the interesting quantity is t_0. This is added to the time stamp at the beginning of the observation to obtain the topocentric TOA. The fit of t_0 can either be made in the Fourier domain or in the time domain. In this work, we use time domain fitting, which was done with a program called TREDUCE.

The topocentric TOA is then referred to UTC (Coordinated Universal Time) by adding the difference between the observatory clock and UTC. These TOAs are therefore arrival times of pulses measured in the reference frame of the radio telescope. Let us now look at how the pulses are emitted in the reference frame of the pulsar.

5.1.2   Pulsar rotation model

For any pulsar, the rotational phase $(0 < \phi < 1)$ in the rest frame of the pulsar can be described by

$$\phi(T) = \int_0^T \frac{dt'}{P(t')} \quad = \quad \frac{T}{P(0)} - \frac{1}{2}\dot{P}(0)\left(\frac{T}{P(0)}\right)^2 +$$
$$+\frac{1}{6}\left[2\dot{P}(0)^2 - P(0)\ddot{P}(0)\right]\left(\frac{T}{P(0)}\right)^3 + ... + n(T), \text{ (5.2)}$$

where T is the time in the pulsar rest frame, P is the rotational period and $n(T)$ is a term that accounts for glitches and timing noise, and excludes, by definition, all long-term behaviour. Third and higher order period derivatives are normally attributed to $n(T)$, as they normally decrease with increasing observing time T. $n(T)$ is normally very small or undetectable for millisecond pulsars, and the same

is true for $\ddot{P}$. These terms have not been detected for the pulsars in 47 Tuc, and therefore we won't discuss their implications here.

Thus the behaviour of most millisecond pulsars in their reference frames is of remarkable simplicity, including only the first two terms on the right side of equation 5.2. The reason for the spindown term $\dot{P}$ is due to rotational energy loss, in § 1.1 we related this term to the radiative braking torque that is supposed to act upon each pulsar.

5.1.3 Transformation between the pulsar and topocentric frames

5.1.3.1 Transformation to solar system barycentre

The task of pulsar timing is to relate a simple rotation law like 5.2, which is valid in the rest frame of the pulsar, to what is observed at the telescope. In order to do this, we first subtract the effect of the motion of the telescope relative to an inertial reference frame. As usual, we choose this to be the barycentre of the solar system (henceforth SSB). We later discuss some limitations of this as an inertial rest frame.

The transformation from observatory time t_0 to barycentric time t'_b is given by

$$t'_b = t_0 + \triangle_{R\odot} + \triangle_{E\odot} - \triangle_{S\odot} \tag{5.3}$$

$\triangle_{R\odot}$ is the Roemer delay, which is due to the fact that the path from the pulsar to SSB has a different length than the path from the pulsar to the telescope. This term is given by

$$\triangle_{R\odot} = \frac{\mathbf{r}.\mathbf{n}'}{c} + \frac{(\mathbf{r}.\mathbf{n}')^2 - |\mathbf{r}|^2}{2cD} \tag{5.4}$$

where $\mathbf{r}$ is the vector from SSB to the telescope, this is computed using a solar system ephemeris, $\mathbf{n}'$ is the assumed unit vector from SSB to the pulsar. This

depends on right ascension α, declination δ, proper motion μ, parallax π and time. The effect of parallax is taken into account by the second term of the Roemer delay, but for distant pulsars like those studied in this work it is negligible.

$\triangle_{E\odot}$ is the Einstein delay term. This is due to changes in the speed of time at the telescope (as seen from a very distant observer at rest in the SSB frame) due to the special relativistic effect of its speed relative to SSB, and the changing solar system gravitational potential (caused by the Sun, Moon and planets) experienced by the Earth. It is therefore given by the integral of the expression

$$\frac{d\triangle_{E\odot}}{dt} = \sum_i \frac{\mathrm{G}m_i}{c^2 r_i} + \frac{v_\oplus^2}{2c^2} - constant \tag{5.5}$$

where the m_i are all the significant masses of the solar system, excluding the Earth, and r_i are the distances of those masses to the Earth. $v_\oplus$ is the velocity of the Earth relative to SSB and the additive constant is chosen so that the average value of the right-hand side over long time intervals is zero. If we don't introduce this constant, we compare the time on Earth with the time measured by a distant observer (which is not influenced by the gravitational potential of the solar system) at rest in the frame of the SSB (the distant observer does not suffer any special relativistic time dilation caused by its velocity); the difference between these two measured times grows monotonically with time.

$\triangle_{S\odot}$ is the Shapiro delay. As said in the previous paragraph, from the viewpoint of a distant observer, time runs slower near the Sun, because of the increased gravitational potential, this is the cause of part of the Einstein delay. Conversely, this can be seen as gravitational redshift. In either interpretation, a signal from a pulsar propagating in the vicinity of the Sun travels slowly from the point of view of a remote observer, therefore delaying its arrival at the Earth. The precise effect is given by

$$\triangle_{S\odot} = -2T_\odot \ln(1 + \cos\theta) \tag{5.6}$$

where $T_\odot \equiv \mathrm{G}M_\odot/c^3 = 4.925490947\,\mu s$ (see § 2.3.2), ln indicates the natural (base

e) logarithm and θ is the pulsar-Sun-Earth angle at the time of observation, this is normally calculated neglecting the eccentricity of Earth' orbit.

After this stage, and assuming the position of the Earth relative to SSB was properly subtracted, i.e., that the assumed direction to the pulsar $\mathbf{n}'$ is correct, all remaining deviations of the TOAs in the SSB from equation 5.2 will be a characteristic of the motion of the pulsar. If $\mathbf{n}'$ is incorrect, a yearly modulation $d(t)$ will be apparent in the residuals, this will be given by

$$d(t) = \mathbf{r}(t).(\mathbf{n}' - \mathbf{n})/c \qquad (5.7)$$

for instance, an error in position of 1 arcsecond can lead to a maximum modulation in arrival times of 2.4 ms, which is of the order of the rotational period of most of the pulsars under study in this work. Such modulations can be removed by fitting for α, δ, and in some cases proper motions and parallaxes.

5.1.3.2   Binary pulsars

If the pulsar is in a binary system, we have to make a further transformation from its rest frame to the frame of the centre of mass of the binary (CM). If the pulsar is isolated, we call its rest frame CM as well.

The form of this transformation will depend on the particular binary model being used. For 47 Tuc H, we use the D'Amour-Deruelle (DD) orbital model (Damour & Deruelle 1986, Taylor & Weisberg 1989). In this model, as in other orbital models, the transformation of CM time t_c to pulsar time T is given by

$$t_c - t_{\text{ref}} = T + \triangle_R + \triangle_E + \triangle_S + \triangle_A \qquad (5.8)$$

As in the case of the solar system, the subscripts R, E and S indicate the Roemer, Einstein and Shapiro delays respectively. The extra term is the so-called "aberrational-delay", caused by the rotation of the pulsar. Without taking into

account this last delay and a set of small parameters which have never been separately measured for any pulsar, these delays are given by

$$\triangle_R = x\sin\omega(\cos E - e) + x\sqrt{1-e^2}\cos\omega\sin E \tag{5.9}$$

$$\triangle_E = \gamma\sin E \tag{5.10}$$

$$\triangle_S = -2r\ln\{1 - e\cos E -$$
$$-s[\sin\omega(\cos E - e) + \sqrt{1-e^2}\cos\omega\sin E]\} \tag{5.11}$$

where, as in the remaining of this work, $x \equiv (a_1 \sin i)/c$ is the projected semi-major axis of the orbit of the pulsar, in time units, e is the eccentricity and ω is the longitude of periastron. t_{ref} is an arbitrary time chosen to coincide with phase 0 in equation 5.2. The γ factor measures the combined effect of gravitational redshift and special-relativistic time dilation and r and s ("range" and "shape") are the two parameters needed to describe the Shapiro delay. E is the eccentric anomaly, which can be calculated as a function of time using equation 5.15. The model accommodates the change of ω and P_B in time by setting

$$\omega = \omega_0 + kf(E) \tag{5.12}$$

$$\dot{\omega} = 2\pi k/P_B \tag{5.13}$$

$$P_B = P_B(T_0) + \dot{P}_B(t_c - T_0) \tag{5.14}$$

$$E - e\sin E = 2\pi\left[\left(\frac{t_c - T_0}{P_B}\right) - \frac{\dot{P}_B}{2}\left(\frac{t_c - T_0}{P_B}\right)^2\right] \tag{5.15}$$

where $f(E)$ is the true anomaly for a given eccentric anomaly E, this can be calculated using equation 4.14.

If we assume general relativity to be correct, then the following relations hold (Taylor & Weisberg 1989, Arzoumanian 1995):

$$\dot{\omega} = 3n_B^{5/3}(MT_\odot)^{2/3}\left(1-e^2\right)^{-1} \tag{5.16}$$

$$\gamma = n_B^{-1/3}em_c(2m_c + m_p)M^{-4/3}T_\odot^{2/3} \tag{5.17}$$

$$\dot{P}_B = -\frac{192\pi}{5}n_B^{5/3}f_em_pm_cM^{-1/3}T_\odot^{5/3} \tag{5.18}$$

$$s \equiv \sin i \;=\; x n_B^{2/3} m_c^{-1} M^{2/3} T_\odot^{-1/3} \tag{5.19}$$

$$r \;=\; m_c T_\odot, \tag{5.20}$$

where m_p and m_c are the masses of the pulsar and of its companion respectively (in solar masses), $M = m_p + m_c$ and $f_e = \left(1 + \frac{73}{24}e^2 + \frac{37}{96}e^4\right)\left(1 - e^2\right)^{-7/2}$. This model works well for eccentric binaries, because in that case we can make precise determinations of ω and T_0. However, with the notable exception of 47 Tuc H, all remaining binaries in 47 Tuc have small eccentricities. In these cases, the determination of a precise ω and T_0 is rather difficult, and these quantities will have large intrinsic uncertainties. These orbital parameters are highly covariant in standard binary fits, and in order to maintain phase coherence, they must be specified with many decimal places, no matter how imprecise is their determination. This happens because the time of ascending node $T_{asc} = T_0 - P_B\omega/2\pi$ can (and must) be specified with high accuracy to maintain phase-coherence.

To solve this problem, we used the binary model ELL1 as implemented in TEMPO by Norbert Wex (see Appendix B). In this model, the parameters being fit are the time of passage through ascending node ($T_{\rm asc}$) and the two Laplace-Lagrange parameters, $\eta \equiv e \sin \omega$ and $\kappa \equiv e \cos \omega$. This orbital model was first used to study radial velocities in low-eccentricity spectral binaries (Wilsing 1893), and was more recently used to time the X-ray pulses of Hercules X-1 (Deeter et al. 1981); its use eliminates all large covariances in the timing parameters of a binary pulsar with a small eccentricity.

5.1.3.3   Transformation between SSB and CM time

We know make the final transformation between SSB and CM. This transformation comprises three terms. The first concerns the fact that whatever happens on the pulsar is only seen hundreds, or thousands, of years later on the Earth. This term in the transformation (D/c) is normally ignored, unless the effect of parallax

can be measured; but we must bear in mind that c it is not exactly is the same for all frequencies, because higher frequencies propagate faster through the ionized plasma in the interstellar medium than lower frequencies (see § 2.1.1), therefore the signals at lower frequencies arrive with a delay. This frequency-dependent delay is normally removed during the transformation to barycentric time; this is the correction to infinite frequency, and it is given by

$$t_b = t'_b - dt(F) \tag{5.21}$$

being $dt(F)$ given by equation 2.3.

The second term originates in the time derivative of the distance of CM to SSB ($\dot{D}/c$, see e.g. Phinney 1992). This term comprises only the relative line-of-sight velocity between these two frames, which given by $v_l(t) = (\mathbf{v}_{\mathrm{CM}} - \mathbf{v}_b).\mathbf{n}$, while $\mathbf{v}(t) = \mathbf{v}_{\mathrm{CM}} - \mathbf{v}_b$, and $v^2(t) = \mathbf{v}(t).\mathbf{v}(t)$. An amount of time dt_c is seen in the SSB as a Doppler-shifted amount of time dt_b given by

$$dt_b = dt_c \frac{1 + \frac{v_l(t)}{c}}{\sqrt{1 - \frac{v^2(t)}{c^2}}} = dt_c \left\{ 1 + \frac{v_l(t)}{c} + \frac{1}{2} \left[\frac{v(t)}{c} \right]^2 + \frac{1}{2} \left[\frac{v_l(t)v^2(t)}{c^3} \right] + ... \right\}. \tag{5.22}$$

If $v_l(t)/c$ and $v(t)/c$ are small, the rotational period of a pulsar measured in the SSB will be given as a function of the rotational period in CM (P_0) by equation 4.6, which is an expression of the well-known classical Doppler effect.

Some parameters, like x and P_B, will be affected in the same way. Other parameters, like e and ω, are not affected by the transformation. The rate of advance of periastron will transform according to $\dot{\omega}_b = \dot{\omega}_c/(1 + \frac{V_l(t)}{c})$, but the correction is quite small compared to the uncertainty in the measurement of this parameter. Apart from these parametric transformations, the equations of motion for binary systems described in the previous section still apply perfectly after a Doppler transformation, this happens because of the principle of relativity: all laws of physics are invariant under Lorentz transformations. Generally, neither $v_l(t)/c$ or $v(t)/c$ are known, so these terms are not taken into account.

The third term in this correction concerns the second derivative of the distance between both frames $\ddot{D}/c$. The SSB and CM are both accelerated by the gravitational field of the Galaxy, so for our purposes, they cannot be considered inertial reference frames. Furthermore, for the pulsars in 47 Tuc, the gravity of the cluster also induces further accelerations to the CM reference frame. In equation 4.6, we have no knowledge of $V_l(t)$, so the "real" parameters P_0, P_B, etc are not known. However, differentiating equation 4.6 we obtain

$$\frac{\dot{P}}{P} = \frac{\dot{P}_0}{P_0} + \frac{\mathbf{a.n}}{c} + \frac{V_\perp^2}{cD} \tag{5.23}$$

$\dot{P}$ is the pulsar period derivative measured in the SSB. This is due to the pulsar spin-down in the CM reference frame ($\dot{P}_0$) and to $\ddot{D}/c$, which is the sum of the relative accelerations of SSB and CM ($\mathbf{a} = (\mathbf{a}_{\mathrm{CM}} - \mathbf{a}_b).\mathbf{n}$) and the centrifugal acceleration caused by the speed of the pulsar perpendicular to the line-of-sight $V_\perp$. The last term represents a fictitious acceleration, which is present even when the two reference frames SSB and CM have no mutual acceleration, and it is called the Shklovskii effect (Shklovskii 1970).

Apart from the change in $\dot{P}$ (some pulsars in globular clusters have negative observed $\dot{P}$s), no other effects (like what is expected for $\dot{P}_B$) are discernible in the residuals of the pulsars in 47 Tuc. For other pulsars, like PSR B1913+16, the contribution of Galactic acceleration for $\dot{P}_B$ of the binary has been detected (Damour & Taylor 1991), these authors have also calculated in detail the influence of the relative velocity and acceleration upon all timing parameters affected by the relative motion.

The gravitational field of the galaxy and the cluster is such that we can consider the acceleration terms to be constant in time. The reason for this approximation is purely observational: no second period derivatives have been measured for the pulsars in the cluster. If these are present for any pulsar, that will indicate the presence of a star near that particular pulsar.

The effect of equation 5.23 on the rotational period of the pulsars, or on other timing parameters, is not taken into account by the program used to determine the ephemeris of the pulsar, TEMPO. This is the reason why in § 6.3 we calculate the different terms in that equation for the particular case of the pulsars in 47 Tuc.

5.1.4   TEMPO

The TOAs are fit to the timing model using the TEMPO program (Taylor & Weisberg 1989, see also http://pulsar.princeton.edu/tempo). This software package was written by J. Taylor in the 1970's, and has been continually evolving since, with major contributions from R. Manchester, D. Nice, J. Weisberg, A. Irwin and N. Wex. We have used the latest version of this program, 11.005, which comprises the ELL1 orbital model.

The program first corrects the topocentric TOA by reading a file that contains the differences between the local time standard and UTC. It then converts this corrected topocentric TOA to SSB time (called TDB) using equation 5.3, at this time it also corrects to infinite frequency. Then, assuming that t_c (time in the reference frame CM) is identical to t_b, a transformation from t_c to T is made using a specific orbital model, with its specific set of orbital parameters x^i. This whole transformation and the parameters it depends on can be written as a sum, which results from equations 5.8, 5.21 and 5.3:

$$
\begin{aligned}
T \;=\; & t_0 - t_{\text{ref}} - 4.14 \times 10^{15}\frac{\text{DM}}{F^2} + \triangle_{R\odot}(\alpha, \delta, \mu_\alpha, \mu_\delta, \pi) + \triangle_{E\odot} - \triangle_{S\odot}(\alpha, \delta) \\
& - \triangle_R\left(x^i\right) - \triangle_E(\gamma) - \triangle_S(r, s).
\end{aligned} \tag{5.24}
$$

When a T_i is calculated for each TOA, the pulsar rotational phase $\phi(T_i)$ is determined from equation 5.2. The goodness of the fit is measured using

$$
\chi^2 = \sum_{i=1}^{N}\left(\frac{\phi(T_i) - n_i}{\sigma_i/P}\right) \tag{5.25}
$$

In this equation, n_i is the closest integer to each computed $\phi(T_i)$, and σ_i is the estimated uncertainty in T_i, which depends on the uncertainties of the parameters used to obtain T_i (The uncertainty in the topocentric TOA, uncertainties in RA, Dec, proper motion and parallax in the transformation to SSB, uncertainties in the orbital parameters to obtain T from t_b). The program attempts to minimize χ by changing the assumed timing parameters in equation 5.24,therefore changing the calculation of T. These changes are calculated using standard numerical techniques. Success is achieved when we can count the individual pulses, i.e., when there is no ambiguity in how many times the pulsar rotated between any two observations. In that case, the minimization algorithm converges smoothly to the true set of timing parameters.

After this stage, we still need to quantify the uncertainties in the parameters. To accomplish this task, we use the Monte-Carlo Bootstrap method implemented in TEMPO. For a set of TOAs, each with an uncertainty e_i, the program generates a number $n_s = 2^j$ of synthetic data sets, where j is a number specified by the user. In these synthetic data sets, the synthetic TOAs cluster around the true TOAs, with a given distribution $\mathcal{D}$ and width e_i. This distribution $\mathcal{D}$ is derived from the distribution of the TOAs around the values predicted by the ephemeris, and it is normally close to a Gaussian.

For each of these synthetic data sets, a fit for the timing parameters is made. The resulting distribution of values for each fitted parameter is then used to derive optimal values for the parameters and their uncertainties. The uncertainties thus estimated are generally more conservative than those calculated using TEMPO, and are given to an intended precision of $1 - \sigma$. Most of the uncertainties for timing parameters presented in this work are obtained in this way.

5.2   Data processing

In § 1.4, we described the characteristics of the data obtained during the recent observations of 47 Tuc. This data is recorded as it is generated by the digitizer, without any processing. Recording raw data has two benefits: firstly, it allows off-line searches for new pulsars to be carried out (see chapter 2). Secondly, for timing purposes, it allowed us to refine the timing models iteratively, resulting in the ephemerides reported here.

In the timing analysis carried out specifically for this work, the raw data are de-dispersed and folded according to an initial ephemeris for each pulsar; this is done using a program called "FCH3". In the early stages, this ephemeris is determined from variations in the rotational period of the pulsar in the discovery and confirmation observations (see chapter 4).

It is important that the pulsars be detected frequently, otherwise it is impossible to count unambiguously the number of pulsar rotations between two different epochs. The 20-cm observations made after August 1997 made use of the excellent sensitivity of the Parkes multi-beam system and resulted in a large increase in the detection rate for all the previously known pulsars in 47 Tuc when compared to the earlier observations at 660 MHz. This was despite the lower flux densities at 1400 MHz.

The individual pulse profiles obtained by folding the data at the predicted pulse period are then cross-correlated with a low-noise "standard" pulse profile (see chapter 3) in the manner described in § 5.1.1, using a program called "TRE-DUCE". We then use the TEMPO software package described above to calculate the corresponding barycentric TOAs using the assumed pulsar position in the sky and the DE/LE 200 solar system ephemeris (Jet Propulsion Laboratory, http://ssd.jpl.nasa.gov). The differences between the measured and predicted

Pulsar	Orbital	Coherent timing solutions		
(J2000)	solution	Start MJD	Final MJD	rms (μs)
0023$-$7204C	isolated	48464	51693	15
0024$-$7204D	isolated	48464	51693	11
0024$-$7205E	known	48464	51693	13
0024$-$7204F	isolated	48464	51692	16
0024$-$7204G	isolated	48493	51637	15
0024$-$7204H	known	48517	51693	28
0024$-$7204I	known	50683	51693	31
0023$-$7203J	known	48473	51693	3
0024$-$7204L	isolated	50686	51634	31
0023$-$7205M	isolated	48491	51693	46
0024$-$7204N	isolated	50689	51634	14
0024$-$7204O	known	50683	51693	10
47 Tuc P	known	. . .	. . .	. . .
0024$-$7204Q	known	50689	51692	36
47 Tuc R	known	. . .	. . .	. . .
47 Tuc S	known	. . .	. . .	. . .
0024$-$7204T	known	50683	51751	82
0024$-$7203U	known	48515	51637	13
47 Tuc V	not known	. . .	. . .	. . .
47 Tuc W	known	. . .	. . .	. . .
Reference MJD for all timing solutions: 51000				

Table 5.1: Timing status for the pulsars in 47 Tuc. No J2000 names have been assigned to pulsars for which there is presently no timing solution. A horizontal line separates the pulsars discovered in the early 1990s (Robinson et al. 1995) from those reported in this work. "rms" is the weighted root mean square of the residuals.

TOAs are then used to improve the parameters of the pulsar (binary and rotational) ephemeris, as described in § 5.1.4. In the early stages, the improved ephemeris is used to reprocess the raw data. This iterative process increases the number and quality of the TOAs, which in turn are used to improve the ephemeris.

After determining the timing solutions for the 1997–1999 period, we re-analysed the raw data from the earlier observations (see Table 1.3). This resulted in a substantial increase in the number and quality of TOAs, especially for the binary pulsars, because of the much improved orbital ephemerides. Essentially all the data in Table 1.3 has been processed with the purpose of obtaining TOAs for the pulsars that have coherent timing solutions.

5.3   Coherent timing solutions for 15 pulsars

The timing solutions obtained from the analysis described in the previous chapter result in a wealth of high-precision astrometric, spin and (for the binary pulsars) orbital information. Table 5.1 summarises the current timing status for the known pulsars in 47 Tuc. Detailed parameters of these solutions are presented in what follows.

In Table 5.2, we present the positions, DMs and rotational parameters for the 15 pulsars with known timing solutions. We call all these parameters "common", because they are are shared by isolated and binary pulsars.

The DMs in this Table were calculated using only 20-cm data. The wide 1400-MHz bands provided by both filterbanks used were divided in four sub-bands, and TOAs were generated for each of these sub-bands. A fit for DM was then made with TEMPO. We did not use data collected at other frequencies to measure the DM because it is difficult to align the pulse profile templates at different frequencies to the precision of about 5% in phase. For the pulsars with the shortest period (e.g., 47 Tuc J), a 5% error in phase causes an error in TOA of about $100\,\mu$s which, in turn, causes an error in the measured DM of $\sim 0.01\,\mathrm{cm}^{-3}\,\mathrm{pc}$. For the most recent high-resolution data, this error is larger than the DM uncertainty using the 20-cm data only. For pulsars with longer periods, similar uncertainties in phase translate to larger uncertainties in alignment, thus resulting in larger uncertainties for the DM.

The orbital parameters for the eight pulsars which are members of binary systems and have known coherent timing solutions are presented in Table 5.4. For each pulsar, we list the five Keplerian parameters: orbital period P_B, projected semi-major axis light travel time x, time of passage through the ascending node T_{asc} and, where measurable, longitude of periastron ω and eccentricity e. For 47 Tuc H we actually indicate the time of passage through periastron, rather

Pulsar	Right Ascension (h m s)	Declination (° ′ ″)	Period (ms)	$\dot{P}$ (10^{-20})	DM (cm^{-3} pc)
C	00 23 50.3511(1)	−72 04 31.4868(6)	5.7567799980975(3)	−4.9842(4)	24.600(5)
D	00 24 13.8777(1)	−72 04 43.8349(6)	5.3575732850392(4)	−0.3381(6)	24.727(4)
E	00 24 11.1014(1)	−72 05 20.1316(7)	3.5363291476530(3)	9.8520(4)	24.234(2)
F	00 24 03.8521(1)	−72 04 42.8005(7)	2.6235793491667(2)	6.4520(2)	24.385(5)
G	00 24 07.9572(4)	−72 04 39.683(1)	4.0403791457480(5)	−4.2172(8)	24.442(4)
H	00 24 06.6994(3)	−72 04 06.793(2)	3.2103407094399(6)	−0.158(1)	24.37(2)
I	00 24 07.9309(5)	−72 04 39.662(2)	3.4849920640394(7)	−4.589(5)	24.433(18)
J	00 23 59.40412(6)	−72 03 58.7725(5)	2.10063354585877(6)	−0.97843(6)	24.5856(3)
L	00 24 03.7701(8)	−72 04 56.906(4)	4.346168005785(2)	−12.20(1)	24.36(3)
M	00 23 54.4854(8)	−72 05 30.733(4)	3.676643219592(1)	−3.843(1)	24.44(3)
N	00 24 09.1838(3)	−72 04 28.876(2)	3.0539543473929(4)	−2.177(3)	24.571(17)
O	00 24 04.6491(2)	−72 04 53.748(1)	2.6433432956675(3)	3.037(2)	24.359(4)
Q	00 24 16.4867(5)	−72 04 25.146(3)	4.033181182804(1)	3.419(7)	24.33(3)
T	00 24 08.541(1)	−72 04 38.915(7)	7.588479792132(5)	29.44(3)	24.41(5)
U	00 24 09.8328(2)	−72 03 59.6684(8)	4.3428266914509(3)	9.5239(7)	24.325(7)

Table 5.2: Common timing parameters for 15 pulsars in 47 Tuc, at the reference epoch of MJD 51000 (cf. Table 5.1). In this and in the following tables, the numbers in parentheses are the formal 1-σ confidence level uncertainties in the last digits quoted. The positions are given in the J2000 reference frame. For all pulsars, these parameters were fitted assuming that the pulsar has the proper motion of the cluster given in Table 1.2 (see §6.2).

than through ascending node, and we also list the measured rate of advance of periastron $\dot{\omega}$.

The following steps were involved in refining these parameters:

1. A fit to the entire 1991–2000 data set was made. All relevant parameters except DM were fitted at this stage using TEMPO, including the proper motions. The values for the proper motions thus obtained are indicated in Table 5.3. This fit provides good estimates of period and period derivative, as well as very precise values for the orbital parameters.

2. We use the weighted average of the proper motions previously derived to refine the remaining parameters for all pulsars. We therefore assume that all pulsars have the same proper motion as that of the cluster. The reasons for this assumption are discussed in § 6.2. The values for all parameters obtained in this last step are consistent with those obtained in step 1, and all uncertainties

Pulsar	μ_α (mas yr^{-1})	μ_δ (mas yr^{-1})
C	6.1(0.4)	−3.6(0.3)
D	5.6(0.4)	−4.3(0.5)
F	6.7(0.6)	−4.2(0.7)
J	5.5(0.3)	−4.3(0.3)
4-Average	5.9(0.6)	−4.1(0.6)

Table 5.3: Proper motions of four pulsars in 47 Tuc. The error for the average represents the dispersion of the values of proper motion and the expected dispersion of proper motions for the pulsars added in quadrature.

Pulsar	P_B (days)	x (sec)	$T_{\rm asc}$ (MJD)	ω (°)	e	$\dot{\omega}$ (° yr^{-1})
E	2.256844822(1)	1.981841(1)	51002.6763043(3)	218.8(2)	0.000316(1)	...
H	2.35769716(8)	2.152824(4)	51000.97354(2)	110.487(2)	0.070565(3)	0.073(3)
I	0.229792249(3)	0.038453(4)	50740.579411(8)	...	< 0.001	...
J	0.1206649381(2)	0.040403(2)	51000.7656781(8)	...	< 0.0002	...
O	0.1359743038(3)	0.045153(1)	50691.903381(2)	...	< 0.0004	...
Q	1.189084046(3)	1.462196(4)	51002.174932(1)	130(4)	0.000080(6)	...
T	1.126176785(5)	1.33850(1)	51000.317049(2)	63(3)	0.00038(2)	...
U	0.4291056832(2)	0.526951(1)	51002.6451351(2)	347(2)	0.000151(5)	...

Table 5.4: Orbital parameters for the eight binary pulsars in 47 Tuc with a known coherent timing solution. For 47 Tuc H the value listed under $T_{\rm asc}$ indicates the time of passage through periastron.

presented in Table 5.2 are obtained using a Monte Carlo bootstrap calculation implemented in TEMPO (see § 5.1.4).

In Figs. 5.1 and 5.2, we present the timing model residuals as a function of date for each of the 15 pulsars. The residuals as a function of orbital phase are shown for the binary pulsars in Fig. 5.3.

The main factors limiting the precision of the coherent timing solutions presented in this work are the relatively low signal-to-noise ratio of the pulsars and the low detection rate, particularly in the observations of the early 1990s. For some of the pulsars, the observed 20-cm flux densities are so low that they are detectable only in about 10% of all observations (chapter 2). Additionally, the data obtained between July 1989 and May 1991 were not used in any of the fits because the difference between the Parkes clock and UTC is not known to within $50\,\mu$s. This introduces significant errors that would compromise several of the measurements.
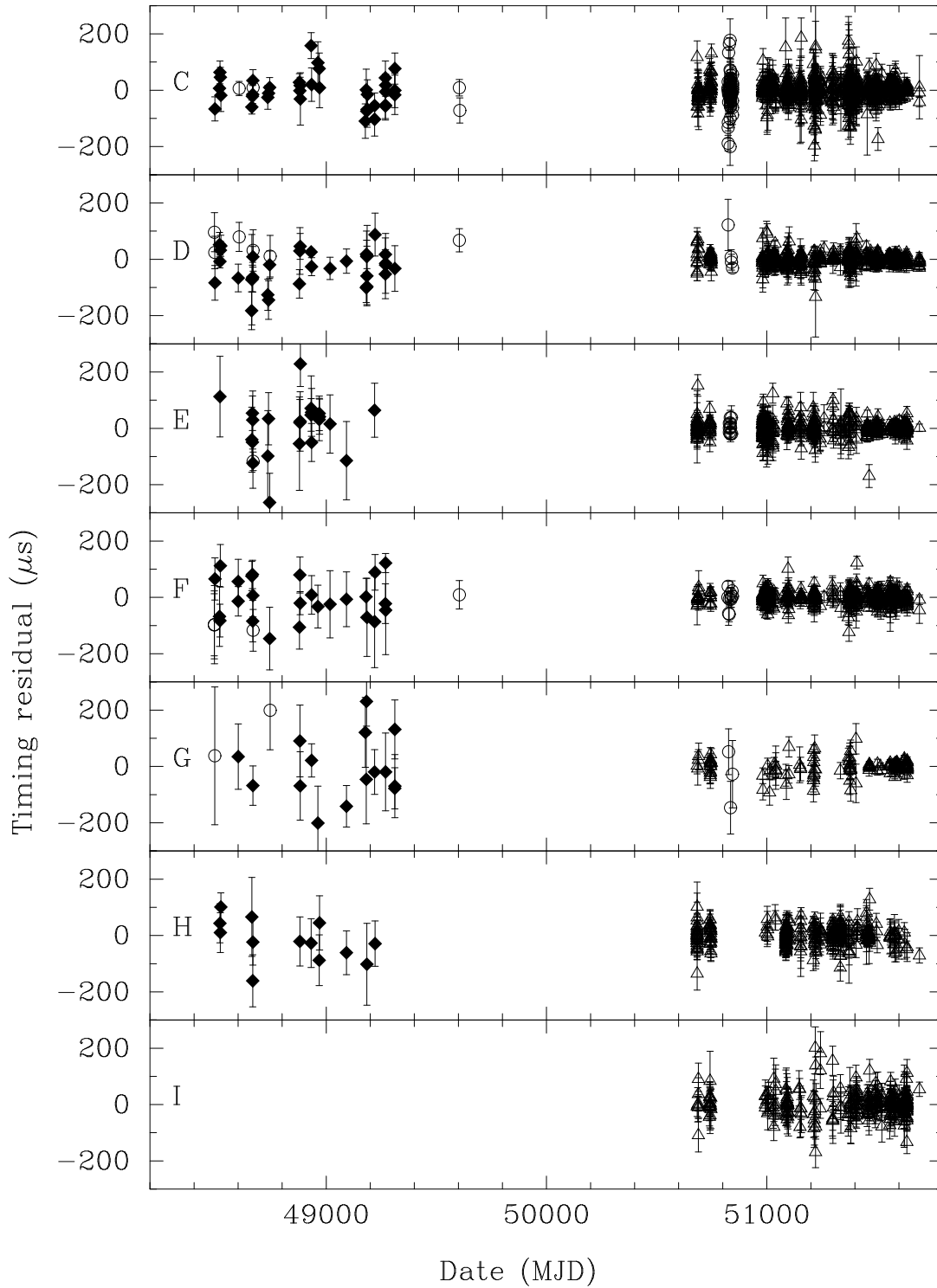
Figure 5.1: Post-fit timing residuals as a function of date for pulsars 47 Tuc C-I. In this and in Figs. 5.2 and 5.3 the triangles, circles and filled diamonds represent residuals at 1400, 660 and 430 MHz respectively.
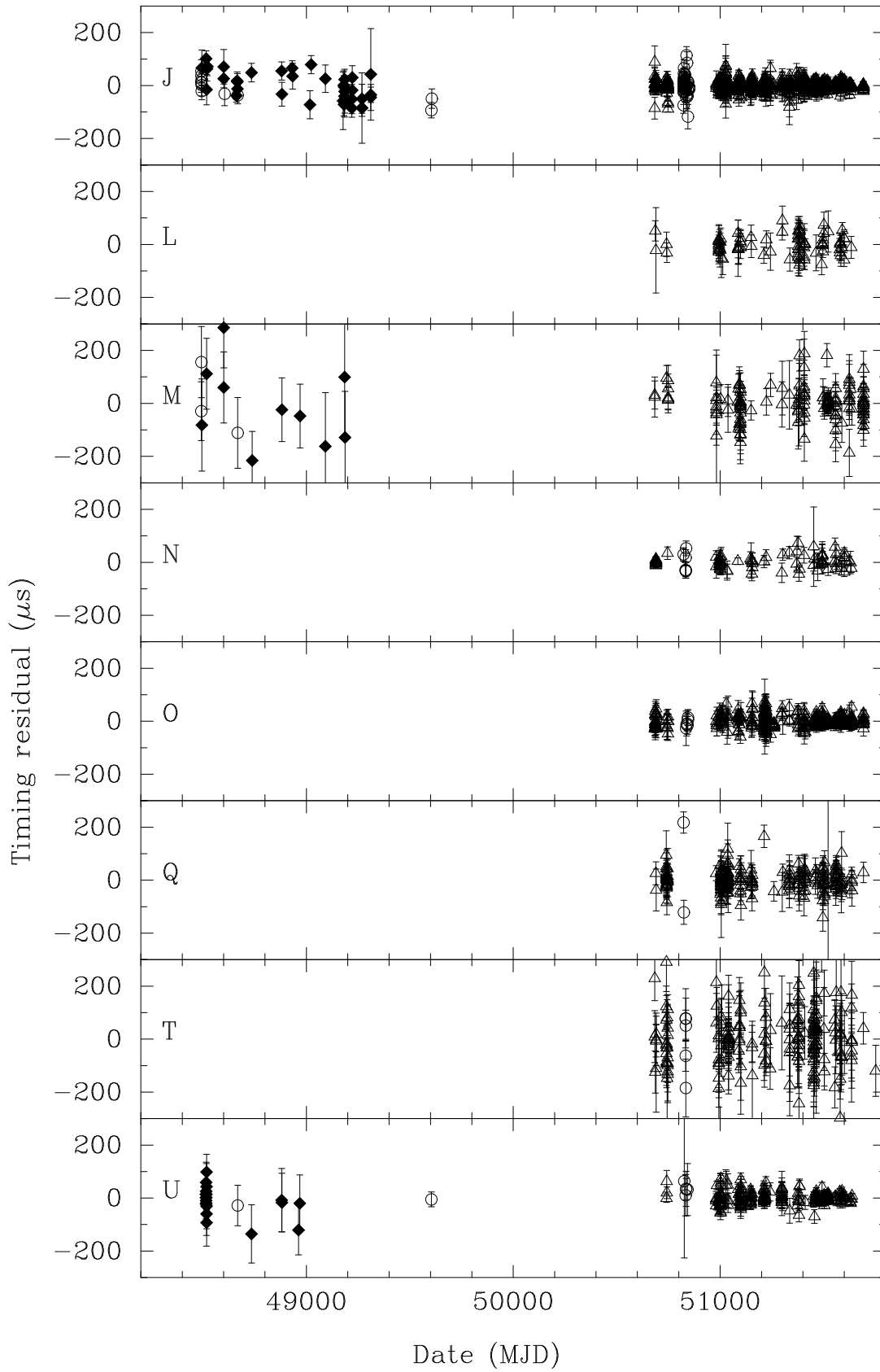
Figure 5.2: Post-fit timing residuals as a function of date for pulsars 47 Tuc J, L-O, Q, T and U.
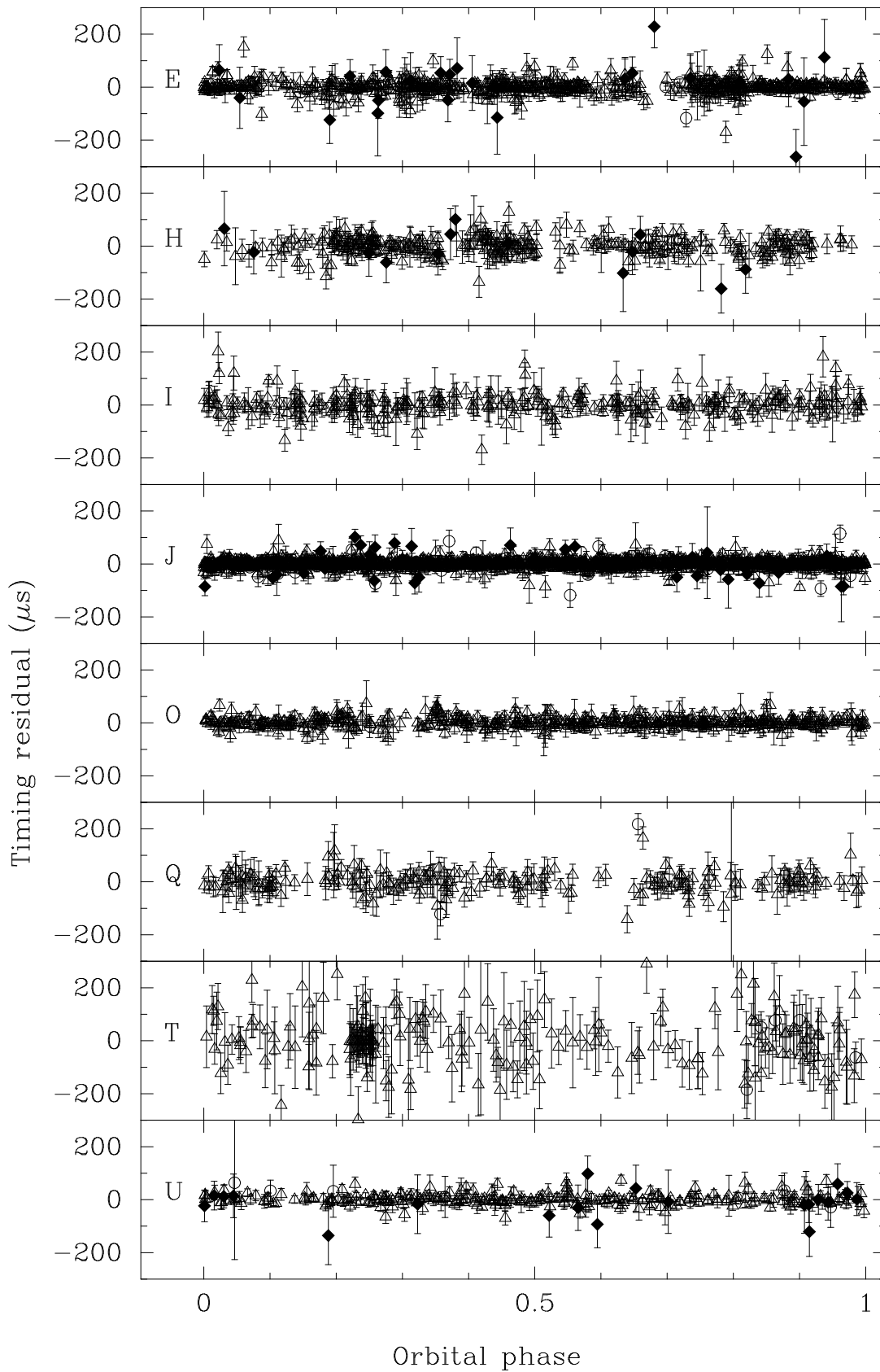
Figure 5.3: Post-fit timing residuals as a function of orbital phase for the eight binary pulsars in 47 Tuc with a known coherent timing solution.

Chapter 6

The common parameters

A previous version of this chapter (with the exception of § 6.4) has been included as sections 4 and 5 of Freire et al. (2000b), a paper containing the timing results for the pulsars in 47 Tuc. This has been submitted to Monthly Notices of the Royal Astronomical Society.

6.1 Positions

The timing solutions presented in the previous chapter bring the number of pulsars in 47 Tuc with accurately known positions to 15, and with measured proper motions to four. For easy reference, we derive from the right ascensions and declinations presented in Table 5.2 the east-west (x) and north-south (y) offsets of the pulsars relative to the centre of the cluster. These are presented in Table 6.1 and depicted graphically in Fig. 6.1. In the remainder of this section, we discuss the implications of these positional measurements.

6.1.1 Radial distribution

The cumulative radial distribution for the present sample of 15 pulsars is shown in Fig. 6.2, where we plot $N(< \theta_\perp)$ against $\theta_\perp$. Two simple inferences can be

Pulsar	x	y	$\theta_\perp$
	(')	(')	(')
C	−1.1541	0.3469	1.21
D	0.6634	0.1411	0.68
E	0.4490	−0.4639	0.65
F	−0.1111	0.1583	0.19
G	0.2060	0.2103	0.29
H	0.1089	0.7585	0.77
I	0.2040	0.2106	0.29
J	−0.4547	0.8921	1.00
L	−0.1174	−0.0768	0.14
M	−0.8347	−0.6405	1.05
N	0.3008	0.3904	0.49
O	−0.0495	−0.0241	0.06
Q	0.8650	0.4526	0.98
T	0.2512	0.2231	0.34
U	0.3509	0.8772	0.94

Table 6.1: North-south (y) and east-west (x) offsets of the pulsars with a coherent timing solution from the centre of the cluster, assumed to be *exactly* at $\alpha = 00^{\rm h}\,24^{\rm m}\,05\overset{\rm s}{.}29$ and $\delta = -72°\,04'\,52\overset{''}{.}3$. The errors in the offsets are of 2 or smaller in the last digits quoted. The angular distance of each pulsar from the centre of the cluster is indicated by $\theta_\perp$, the precision for this parameter is limited by the uncertainty in the absolute position of the centre of the cluster, indicated in Table 1.2.
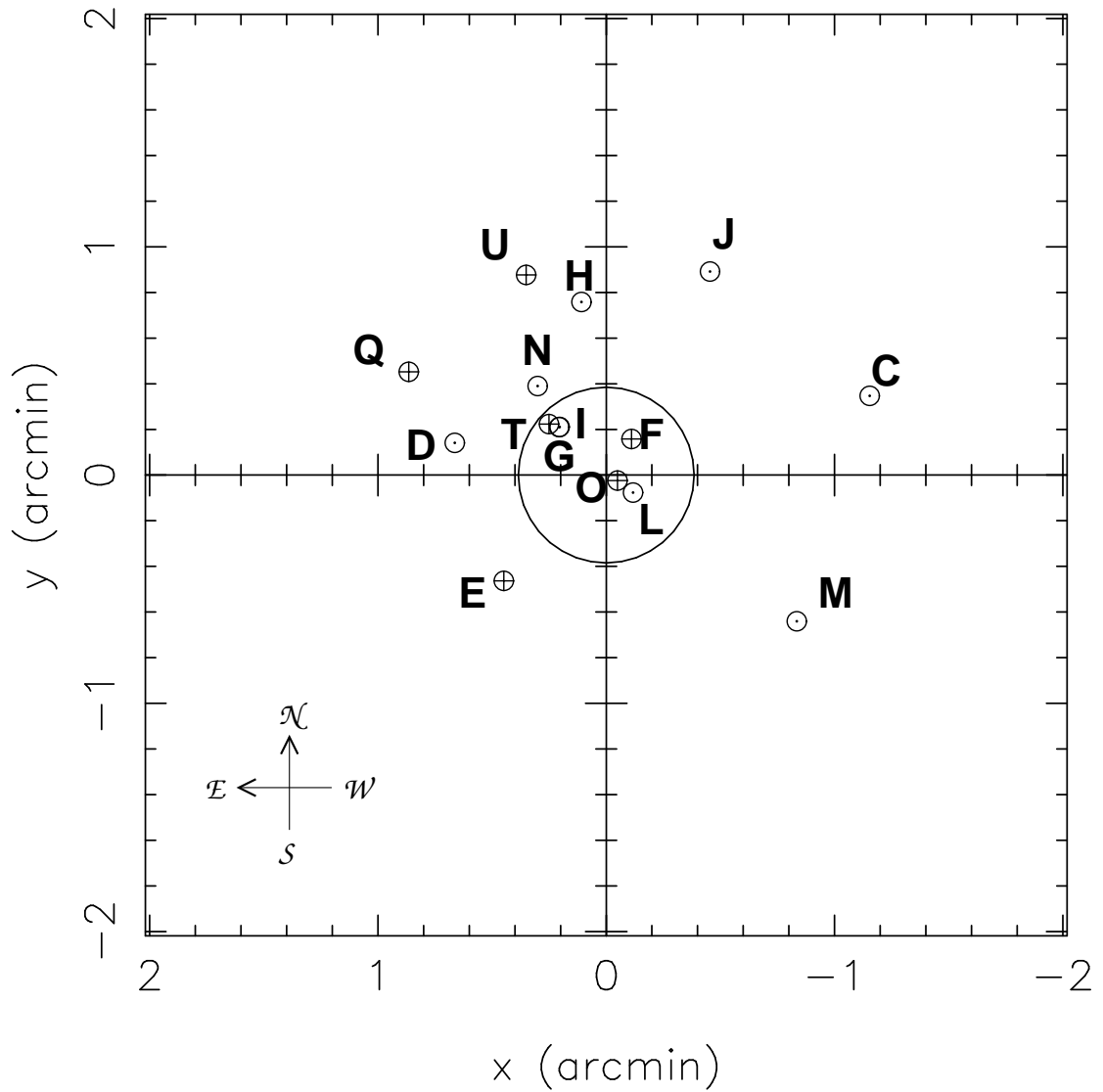
Figure 6.1: North-south (y) and east-west (x) offsets of the pulsars from the centre of the cluster (see Table 6.1). The pulsars indicated with $\oplus$ have positive period derivatives ($\dot{P}$), while those indicated with $\odot$ have negative $\dot{P}$. The circle indicates the core radius.

made from this distribution: first, the distribution is linear within $1\rlap{.}'2$ (3.1 core radii) where a simple fit to the data yields $N(< \theta_\perp) = (4.71 \pm 0.08) \times (\theta_\perp/\theta_c)$. Second, no pulsars are found outside 3 core radii. We discuss this surprising result later in this section and show that it is not caused by small-number statistics or observational selection effects.

Should such a linearity within 3 core radii be expected? For a cluster of stars with a predominant individual mass m_i in thermal equilibrium, the expected outcome is an "isothermal distribution" with the total mass inside radius r given by

$$M(< r) = 8\pi \rho_c \kappa^2 r, \tag{6.1}$$

where ρ_c is the central density and $\kappa = r_c/3$ is the Jeans length of the cluster (Spitzer 1987). This relation applies approximately for $r \geq 3r_c$, and implies a density of

$$\rho(r) = \frac{2}{9}\rho_c \left(\frac{r_c}{r}\right)^2. \tag{6.2}$$

Since most stars in such a cluster have the same mass m_i, the number density is of the form $n_i(r) \propto r^{-2}$ as well.

A less numerous population of stars in the cluster, with individual mass m_j, has a distribution of the form

$$n_j(r) \propto r^{-2m_j/m_i}, \tag{6.3}$$

provided that these stars are in thermal equilibrium with the remaining population (Spitzer 1987; Phinney 1993). Generally, for any two types of stars we have $n_j(r) \propto n_i(r)^{m_j/m_i}$.

In terms of projected distance from the core, the isothermal distribution is

$$N(< R_\perp) \propto M(< R_\perp) \propto R_\perp \propto \theta_\perp, \tag{6.4}$$

where $\theta_\perp$ is the projected angular distance of the pulsars from the centre of the cluster. This is precisely what is seen in Fig. 6.2. This linearity, also observed for

blue stragglers and binary stars (Edmonds et al. 1996), is somewhat surprising because equation 6.2 should apply only for $\theta_\perp \geq 3\theta_c$, while virtually all pulsars are located at $\theta_\perp < 3\theta_c$. However, the core radius given in Table 1.2 is determined from the distribution of giant stars, with masses of about $0.8\,M_\odot$. Neutron stars, with mass $\sim 1.5\,M_\odot$, should have a more compact distribution.

Thus, within 3 core radii, the pulsars have the same distribution that is expected for the dominant stellar species in thermal equilibrium. Using equation 6.3 we conclude that near the centre of the cluster both the pulsars and the dominant stellar species have approximately the same individual stellar mass. Neutron stars in binary radio pulsar systems have average mass $1.35 \pm 0.04\,M_\odot$ (Thorsett & Chakrabarty 1999), and the binary pulsar systems in 47 Tuc have companion masses $\sim 0.02\,M_\odot$ to $0.25\,M_\odot$ (Camilo et al. 2000), so we expect the pulsar systems in 47 Tuc to have total masses 1.3–$1.6\,M_\odot$. This expectation is independently confirmed by the fact that blue stragglers have similar masses (Gilliland et al. 1998) and are observed to have a distribution that is very similar to that of the pulsars (Rasio 2000). However we know that the dominant stellar species are not the detectable pulsar or blue straggler populations: they are not large enough. It is therefore more likely to be undetectable neutron stars, massive white dwarfs, or faint binary systems with mass $\sim 1.5\,M_\odot$; they cannot be single main-sequence stars because the turn-off mass for 47 Tuc is about $0.8\,M_\odot$ (De Marchi et al. 1996).

The radial distribution observed in 47 Tuc is in sharp contrast to what is observed in M15. According to equation 6.3, stars lighter than the dominant stellar species have shallower distributions, while heavier stars are more concentrated in the core. In M15 the pulsar distribution is given by $n_j(r) \propto r^{-3.1}$, indicating that the dominant mass species is lighter than the pulsars (Anderson 1992). Using equation 6.3, the mass of the dominant stellar species in M15 is derived by

Anderson (1992) to be $2/3.1 \times 1.4\,M_\odot = 0.9\,M_\odot$. This represents a fundamental difference between the two clusters.

We now turn our attention to the striking observation that all of the pulsars in 47 Tuc with measured positions lie within $1\overset{'}{.}2$ (3 core radii) from the centre of the cluster, despite the fact that the tidal radius of 47 Tuc is about $40'$ (Table 1.2).

This distribution is not an artifact introduced by the size and shape of the Parkes telescope radio beam pattern, which has a half-power radius of $\sim 7'$ at 1400 MHz. The flux densities for most of the pulsars have been calculated in chapter 3. Among the pulsars with a known solution, 47 Tuc N has the lowest flux density (0.03 ± 0.01 mJy). Let us suppose that this value is the lower limit for the flux density of a pulsar for which we can obtain a timing solution. In that case, weak pulsars like 47 Tuc U, with a flux of 0.07 ± 0.01 mJy, are detectable in a circle with a radius of at least $7'$, and there are 11 pulsars with at least this flux density. The fact that none of these is seen outside a radius of $1\overset{'}{.}2$ is therefore a true feature of the pulsar distribution, and not an artifact due to the shape of the beam. To quantify the statistical significance of this result, let us assume that the isothermal distribution applies within the $7'$ radius of the primary telescope beam. Also, each pulsar inside this limiting radius brighter than 0.06 mJy is detectable everywhere in the region. Using the isothermal distribution law, the probability of detecting such a pulsar in the inner $1\overset{'}{.}2$ is simply $1.2/7 = 0.17$. The probability of detecting a second pulsar in the same region is independent of the position of the first pulsar, and is also 0.17. The probability of finding all the 11 brightest pulsars within $1\overset{'}{.}2$ is therefore $0.17^{11} = 3.4 \times 10^{-9}$. The actual chance probability of the observed distribution is smaller still, because the brightest pulsars can be observed in circles with radii larger than $7'$, and the four fainter pulsars also appear concentrated in the core, following the same distribution as the brighter ones, and not around 47 Tuc C, where the telescope beam is centred during the
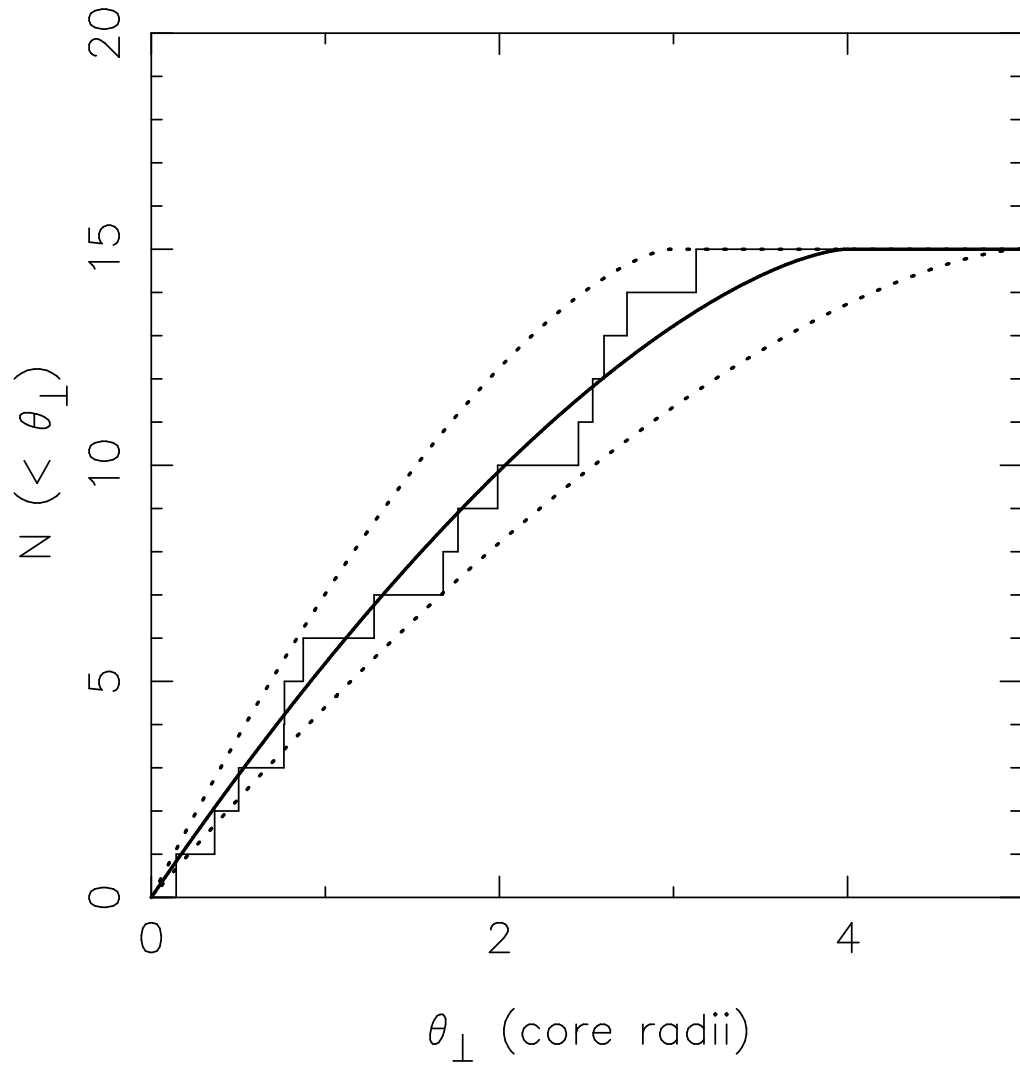
Figure 6.2: Cumulative histogram of the radial positions of the pulsars in 47 Tuc. The solid line represents the best linear fit, $N(< \theta_\perp) = 4.71(\theta_\perp/\theta_c)$.

observations. Therefore, the observed distribution is not due to the beam shape nor to a mere chance gathering of bright pulsars in the centre of the cluster — it is a real feature of the pulsar distribution.

Although the reason for the compactness and abrupt end to the pulsar radial distribution is not understood, we offer the following hypothesis. To begin, we note that the relaxation time (the time necessary for an effective re-distribution of kinetic energies between different groups of stars in the cluster via two-body interactions) in the core of 47 Tuc is of order 10^8 yr (Djorgovski 1993). Since the ages of the pulsars are significantly greater than this (see § 6.3.3) their present distribution within the cluster is not related to the distribution of their birthplaces. This also implies that the average kinetic energy of the pulsars should be the same as that of the lighter main-sequence stars, and therefore the pulsars have lower average velocities and tend to dwell deeper in the gravitational potential of the cluster.

We know that the kinetic energy of the heavy main-sequence stars observed in the cluster core, with mass m_{ms}, is limited by the escape velocity v_e. Equating the resulting limit of kinetic energy to that of the pulsars results in a limit to the velocity of pulsars bound in the cluster core:

$$v_{p\,\max}^2 = (m_{ms}/m_p)v_e^2, \tag{6.5}$$

where m_p is the pulsar mass. As pulsars move away from the centre of the cluster under the influence of the cluster's gravitational potential their velocities decrease, eventually reaching zero at a maximum possible distance $r_{\lim}$ from the centre of the cluster.

The potential energy $U(r)$ at $r_{\lim}$ is calculated using conservation of energy to be

$$U(r_{\lim}) \equiv m_p W(r_{\lim}) = m_p W(0) + m_p v_{p\,\max}^2/2, \tag{6.6}$$
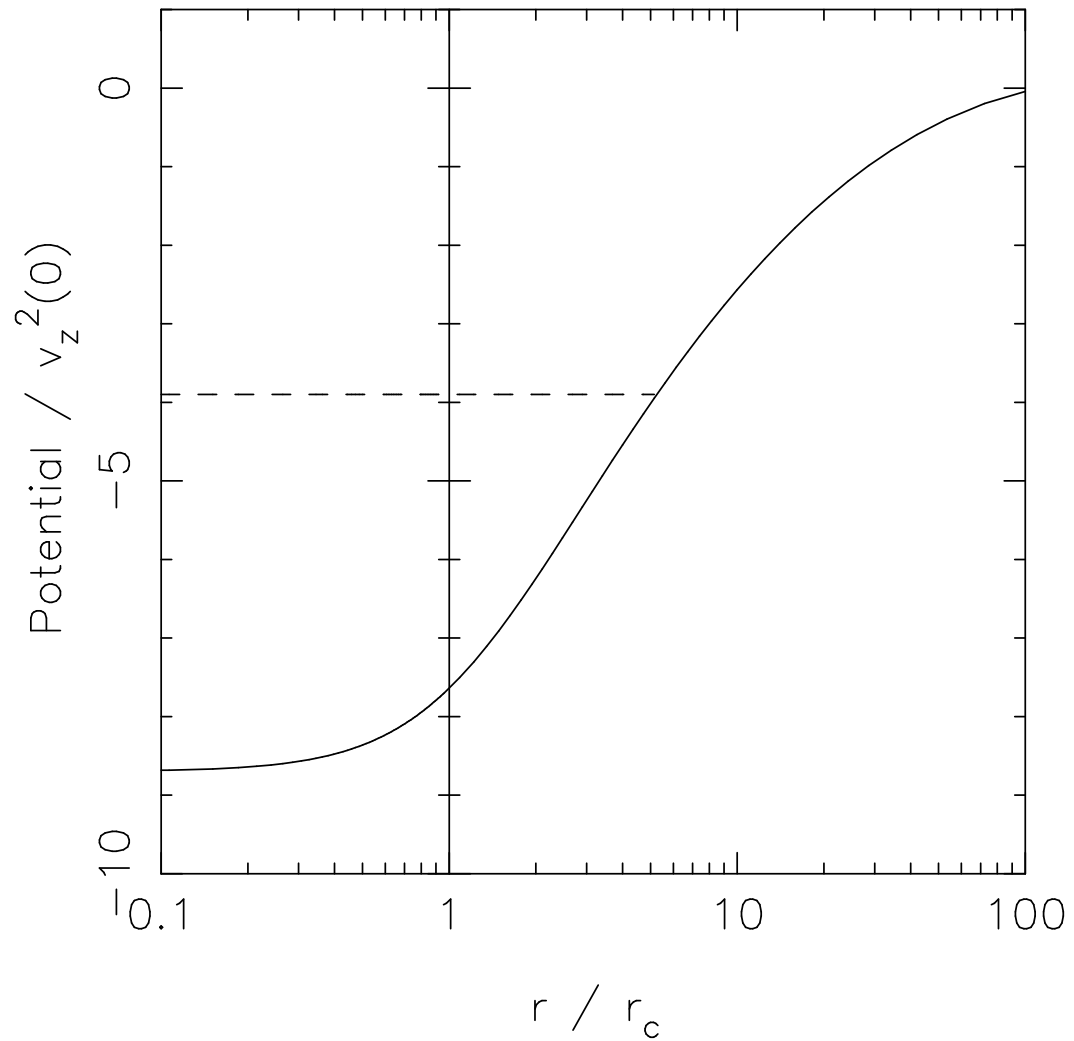
Figure 6.3: Globular cluster potential as a function of distance from the centre given by a King model of 47 Tuc. The maximum squared pulsar velocity at the centre is indicated by the height of the dashed line above $W(r = 0) = -8.7v_z^2(0)$. The pulsars cannot travel further than about 5 core radii from the centre (see § 6.1.1).

where $W(r)$ is the cluster potential. Using equation 6.5 we obtain

$$W(r_{\text{lim}}) = W(0) \left(1 - \frac{m_{ms}}{m_p}\right). \tag{6.7}$$

This limit, with $m_{ms} = 0.8\,\text{M}_\odot$ and $m_p = 1.45\,\text{M}_\odot$ (the average mass for isolated and binary pulsars), is represented by a dashed line in Fig. 6.3, where we use a King model for the gravitational potential of 47 Tuc (King 1966; Phinney, priv. comm.). From this we derive $r_{\text{lim}} \sim 5r_c$. While this simple argument has the virtue that the resulting limiting radius for the pulsar distribution approximately matches the observed one, we have ignored the possibility of a pulsar at a distance r_{lim} from the core interacting with stars in that region. We therefore admit it is a strange result that requires further understanding.

6.1.2 A possible triple system with two pulsars

There is a remarkable coincidence between the celestial coordinates of 47 Tuc G, an isolated pulsar, and 47 Tuc I, a binary pulsar (see Table 6.1). The projected angular distance between these two pulsars is only 120 mas.

To estimate the chance probability of finding two pulsars in such close proximity, suppose that pulsars are randomly distributed in a disk of radius $18''$ (the projected angular distance of these two pulsars from the centre of the cluster). For a given pulsar, the probability of finding a second one at a projected distance of $0\rlap{.}''12$ or less is proportional to the area of a disk of radius $0\rlap{.}''12$ divided by the area of a disk of radius $18''$ or $\sim 4 \times 10^{-5}$. The probability of being at a distance larger than $0\rlap{.}''12$ is then 0.99996. For the five pulsars known within $18''$, we have 10 different possible pairs. The probability of not finding any pulsar within $0\rlap{.}''12$ of any other pulsar is $0.99996^{10} = 0.9996$, i.e., the overall probability of finding one or more pulsars projected within $0\rlap{.}''12$ of any other is 4×10^{-4}, or about one in 2500.

If the pulsars are near to each other but not interacting significantly, then the acceleration caused by the cluster should be similar for both of them. In § 6.3 we see that their values of $\dot{P}/P$ are similar, with a difference of $3 \times 10^{-18}\,\mathrm{s}^{-1}$, in a possible range ~ 20 times larger. Therefore, the combined probability of finding the pulsars with such close projected separation and with such similar accelerations is about one in 50,000.

Given this low formal probability of a chance coincidence, it is possible that these two pulsars are in a hierarchical triple system with a major axis of at least 600 a.u. However, a system with two components 600 a.u. apart is not likely to remain bound for long in the dense environment of a globular cluster. By considering the stellar flux with one-dimensional speeds of $v_z(r)$, a simple estimate for the mean time a binary system can survive in a dense environment (i.e., before it gets hit by another cluster member) is $(n[r]\sigma\sqrt{3}v_z[r])^{-1}$. In this expression, $n(r)$ is the density of stars, $v_z(r)$ is the one-dimensional stellar velocity dispersion near the binary and σ is the cross-sectional area for the interaction of the binary with a star from the cluster. The King model for 47 Tuc predicts $n(r) \sim 4 \times 10^4\,\mathrm{pc}^{-3}$ for this region. With $v_z(r) \sim 10\,\mathrm{km\,s}^{-1}$ we estimate the lifetime to be 10^4–$10^5\,\mathrm{yr}$. This time-scale is comparable to the orbital period of the putative binary system, and 10^{-6}–10^{-5} of the age of the cluster. Thus, despite low formal probability of a chance coincidence, this simple calculation argues against the reality of such an association. Ultimately, the reality or otherwise of this system can be tested by future measurements of second period derivatives for the two pulsars.

6.2   Proper motions

The proper motions listed in Table 5.3 are displayed in Fig. 6.4, together with the value derived for the proper motion of the cluster by Odenkirchen et al. (1997). At the 2-σ confidence level all these proper motions are consistent with each
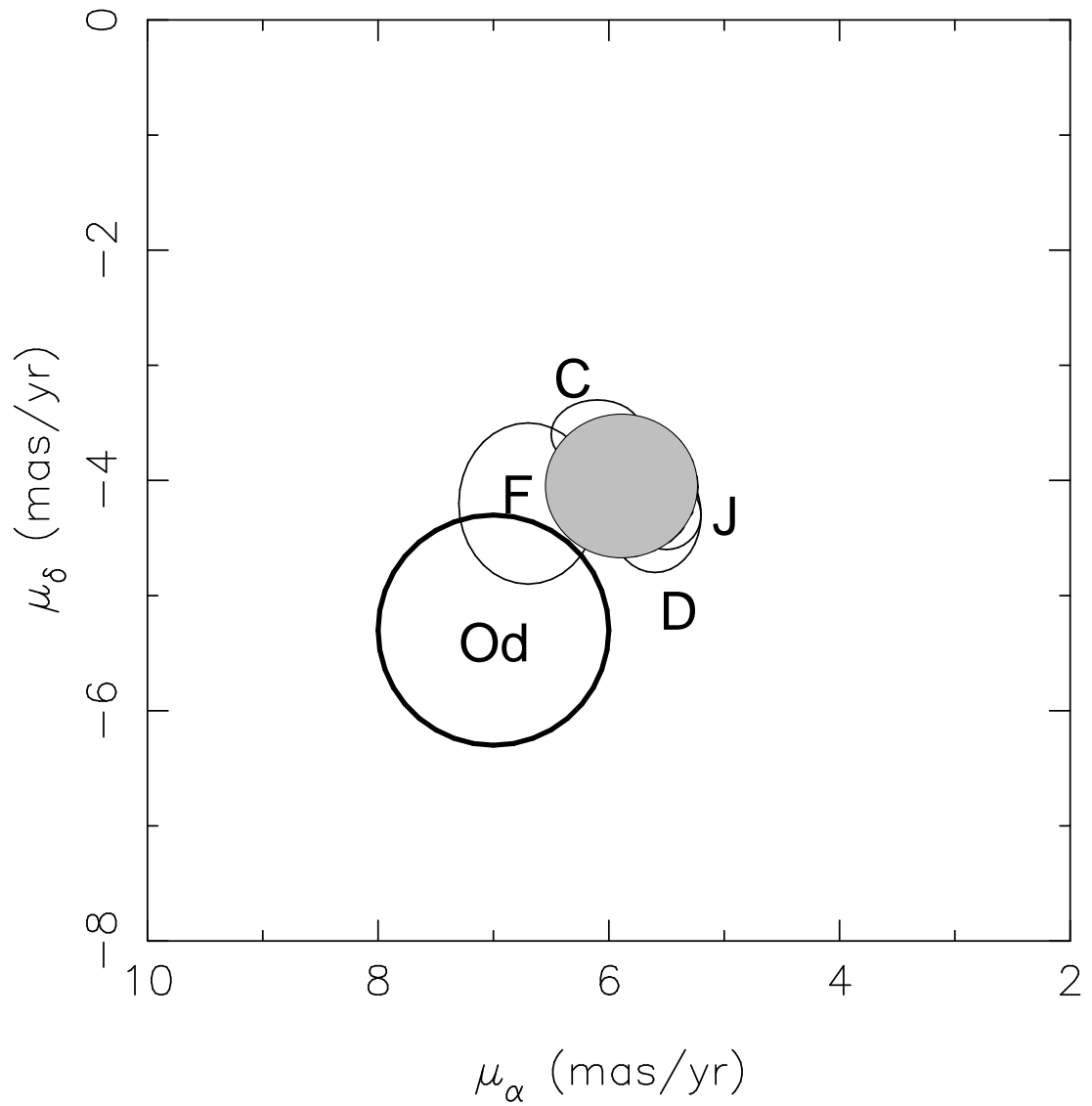
Figure 6.4: Measured proper motions of the pulsars in 47 Tuc. The semi-axes of the ellipses represent the 1-σ errors for the proper motions quoted in Table 5.3. The value for the proper motion of the cluster (Odenkirchen et al. 1997) is indicated by the thick circle. The filled ellipse indicates the motion of the cluster and its error deduced from averaging the measured pulsar proper motions.

other.

If a pulsar is moving with a transverse velocity v_p (km s^{-1}) relative to the centre of the cluster, the difference in proper motions is $\Delta\mu = 0.21 v_p/D \,\text{mas yr}^{-1}$, where D is the distance to the cluster in kpc. The escape velocity of 47 Tuc is about $58 \,\text{km s}^{-1}$ (Table 1.2). Therefore, in order to detect a pulsar in an escape trajectory at the 3-σ level, we would have to measure relative proper motions of about $2.4 \,\text{mas yr}^{-1}$ with a precision better than $0.8 \,\text{mas yr}^{-1}$; for some pulsars we have already achieved such a precision (see Table 5.3), there are no cases of pulsars in escape trajectories. If the pulsars are in thermal equilibrium with the surrounding stars, their relative motions are of the order of the central velocity dispersion or less, i.e., $\sim 12 \,\text{km s}^{-1}$. Thus, detecting their relative motions implies measuring relative proper motions of about $0.5 \,\text{mas yr}^{-1}$ with a precision of $0.15 \,\text{mas yr}^{-1}$.

The assumption of thermal equilibrium for the pulsars implies that, with current timing precision, a measurement of the proper motions of these pulsars is in effect a measurement of the proper motion of the cluster. We can therefore make a weighted average of the four proper motions and determine the motion of the cluster, knowing that the peculiar motions of the pulsars should be smaller than the errors in the individual measurements. The weights chosen are simply the inverse of the uncertainties in each coordinate. For the currently-observed proper motions, we find the weighted average value to be $\mu_\alpha = (5.9 \pm 0.6) \,\text{mas yr}^{-1}$ and $\mu_\delta = (-4.1 \pm 0.6) \,\text{mas yr}^{-1}$. The uncertainties are taken to be the sum in quadrature of the weighted dispersion of the values of proper motion for the pulsars about the average and $0.5 \,\text{mas yr}^{-1}$, which accounts for the expected actual dispersion of proper motions. The proper motion magnitude of the cluster is then $\mu = (7.2 \pm 0.6) \,\text{mas yr}^{-1}$. We use the pulsar-derived value of proper motion of the cluster when determining the final ephemerides of the pulsars (§ 5.3), essentially

because of their superior precision.

6.3 Pulsar accelerations

Nine of the 15 pulsars in Table 5.2 have negative period derivatives ($\dot{P}$). This has
been observed before for some pulsars located in globular clusters (e.g., Wolszczan
et al. 1989). Rather than being due to intrinsic spin-up, negative period derivat-
ives are thought to be caused by the acceleration of the pulsar towards the Earth
in the cluster potential.

In § 6.3.1 we use the observed period derivatives of the pulsars to estimate
lower limits for the surface mass density of the cluster. We then consider the apt-
ness of a King model together with accepted parameters for 47 Tuc in describing
the accelerations experienced by the pulsars as inferred from the period derivat-
ives (§ 6.3.2). We derive limits for the ages and magnetic fields of the pulsars in
§ 6.3.3.

The observed period derivative, $\dot{P}_{\mathrm{obs}}$, is the sum of the pulsar's intrinsic spin-
down, $\dot{P}_{\mathrm{int}}$, and the effect of the acceleration along the line-of-sight, a_l. This sum
may be negative if a negative a_l contribution is not exceeded by a positive $\dot{P}_{\mathrm{int}}$;
i.e., a negative $\dot{P}_{\mathrm{obs}}$ implies $|a_l/c| > \dot{P}/P_{\mathrm{int}}$. It also implies $|a_l/c| > |\dot{P}/P_{\mathrm{obs}}|$.

The acceleration along the line-of-sight has several components, denoted by
a_S, a_G, and a_C in

$$\left(\frac{\dot{P}}{P}\right)_{\mathrm{obs}} = \frac{a_S}{c} + \frac{a_G}{c} + \frac{a_C}{c} + \left(\frac{\dot{P}}{P}\right)_{\mathrm{int}}, \tag{6.8}$$

where the terms represent:

1. The centrifugal acceleration (Shklovskii 1970), given by

$$\frac{a_S}{c} = \frac{\mu^2 D}{c}. \tag{6.9}$$

This term amounts to $a_S/c = (+6.2 \pm 1.7) \times 10^{-19}\,\mathrm{s}^{-1}$.
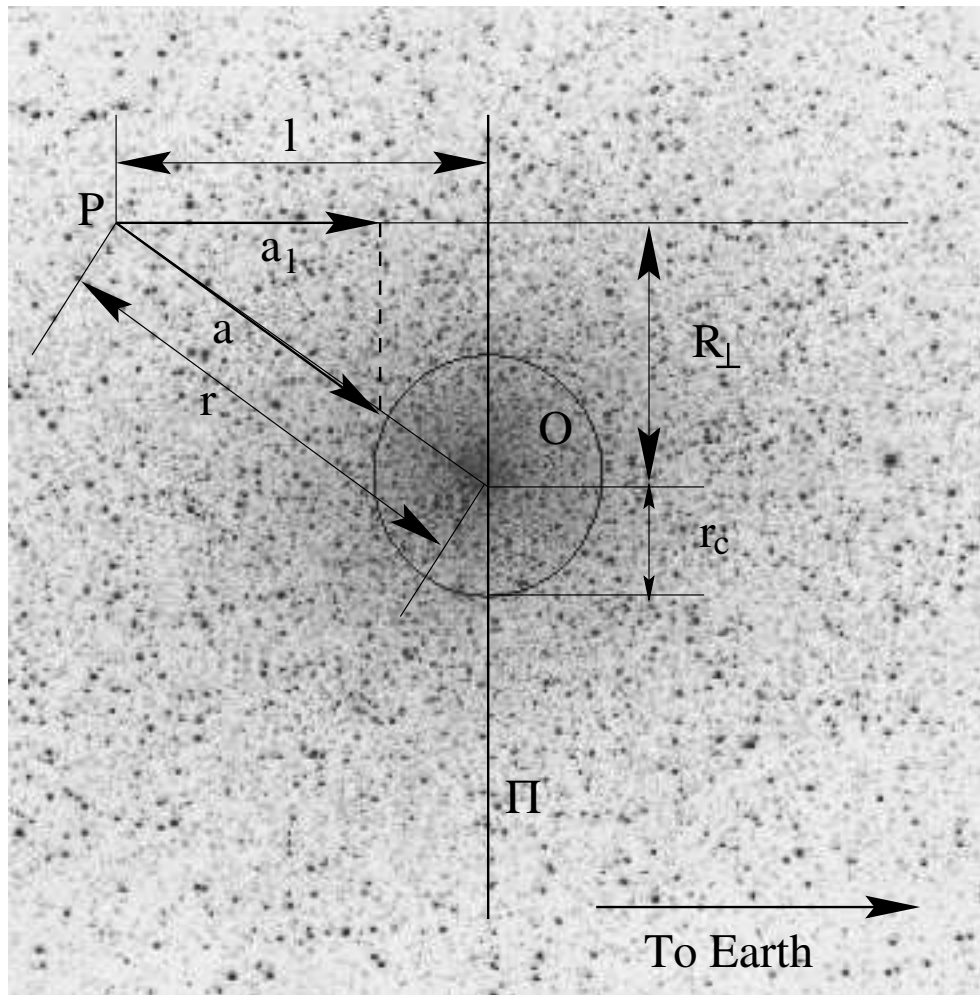
Figure 6.5: Geometrical parameters used in § 6.3: Π is a plane perpendicular to the line-of-sight that passes through the centre of the cluster, at point O, with core radius r_c. For a pulsar at point P, $R_\perp$ is the projected distance to, and a is the acceleration of the pulsar towards, the centre of the cluster. The line-of-sight component of a, a_l, is the only one detectable from the Earth (located in the plane of the figure).

2. The difference in Galactic acceleration along the line-of-sight between a given object and the barycentre of the solar system (a_G). This is a function of the object's Galactic latitude b, longitude l, and distance from the solar system D. For 47 Tuc we have $b = -44.9°$, $l = 305.9°$ and $D = 5.0 \pm 0.4\,\mathrm{kpc}$. Using Paczynski's (1990) model of the gravitational potential of the Galaxy, we obtain $a_G/c = (-4.5 \pm 0.2) \times 10^{-19}\,\mathrm{s}^{-1}$.

3. Accelerations due to the gravitational field of the globular cluster and its individual stars (a_C). This is the interesting contribution from an astrophysical point of view.

Contributions 1 and 2 total $(+1.7 \pm 1.6) \times 10^{-19}\,\mathrm{s}^{-1}$. Henceforth, $(\dot{P}/P)_{\mathrm{obs}}$ indicates the measured value of $\dot{P}/P$ minus these contributions, and a_l refers solely to a_C. All conclusions in this section apply only to the pulsars with known coherent timing solutions.

Before starting this discussion, it will be useful to define some geometrical parameters, which we will use throughout much of the remainder of this section, these are shown in Fig. 6.5. The plane Π passes through the centre of the cluster and is perpendicular to the line-of-sight, and the core radius is given by $r_c = D\theta_c$. A particular observed pulsar has unknown distance to the centre of the cluster, r, and to Π, l — we know only the projected distance of the pulsar to the centre of the cluster, $R_\perp = D\theta_\perp$. The acceleration along the line-of-sight, a_l, is the only component potentially detectable from the Earth.

6.3.1 Surface mass density of 47 Tuc

We now derive constraints for the surface mass density of the cluster in its inner regions. The following equation is valid to within $\sim 10\%$ for all plausible cluster models, and for all $R_\perp$ (Phinney 1993):

$$\frac{a_{l\,\mathrm{max}}(R_\perp)}{c} \simeq 1.1 \frac{GM_{\mathrm{cyl}}(< R_\perp)}{c\pi R_\perp^2} =$$

Table 6.2: Constraints on projected surface mass density for 47 Tuc obtained from nine pulsars with negative $(\dot{P}/P)_{obs}$ (see § 6.3.1). The distance to the cluster is taken to be 5.0 kpc.

Pulsar	$(\dot{P}/P)_{obs}$ $(10^{-17}\,\mathrm{s}^{-1})$	$R_\perp$ (pc)	$\overline{\Sigma}(< R_\perp)$ $(10^3\,\mathrm{M}_\odot\,\mathrm{pc}^{-2})$	$M_{cyl}(< R_\perp)$ $(10^3\,\mathrm{M}_\odot)$
C	−0.88	1.75	> 17	> 170
D	−0.08	0.99	> 1.6	> 4.8
G	−1.06	0.43	> 21	> 12
H	−0.07	1.11	> 1.3	> 5.1
I	−1.33	0.43	> 26	> 15
J	−0.48	1.46	> 9.5	> 63
L	−2.82	0.20	> 55	> 7.2
M	−1.06	1.53	> 21	> 150
N	−0.73	0.72	> 14	> 23

$$5.1 \times 10^{-19} \left(\frac{\overline{\Sigma}(< R_\perp)}{10^3\,\mathrm{M}_\odot\,\mathrm{pc}^{-2}} \right) \mathrm{s}^{-1}, \tag{6.10}$$

where $M_{cyl}(< R_\perp)$ is the mass of all the matter with a projected distance smaller than $R_\perp$, and $\overline{\Sigma}(< R_\perp)$ is the corresponding projected surface mass density. The limit on $\overline{\Sigma}$ does not depend on estimates of the distance to the cluster or core radius. The pulsars with negative observed period derivatives provide a lower bound on $a_{l\,max}(R_\perp)$ and therefore, with equation 6.10, on $\overline{\Sigma}$ and M_{cyl}. These limits are presented in Table 6.2.

6.3.2   Accounting for the pulsar accelerations

We have already introduced in Fig. 6.3 the normalized gravitational potential calculated for 47 Tuc with a King model. This potential, together with some cluster parameters, predicts acceleration as a function of radius. In this section we investigate whether the King model and its input parameters are adequate to explain the observed pulsar period derivatives, which are largely influenced by the cluster acceleration.

Any King model requires three numerical parameters. One of them expresses how centrally condensed the cluster is, and is calculated from the ratio of the

Table 6.3: Comparison of estimates of "observed" pulsar accelerations A_o with predicted average accelerations, $A_a(R_\perp)$, derived using a King model for 47 Tuc with $D = 5.0 \pm 0.4\,\mathrm{kpc}$ and $v_z(0) = 11.6 \pm 1.4\,\mathrm{km\,s}^{-1}$ (see § 6.3.2). The maximum acceleration predicted by the model for each projected pulsar offset from the centre of the cluster, used in Fig. 6.6, is also listed.

Pulsar	$\|A_o/c\|$ $(10^{-17}\,\mathrm{s}^{-1})$	$\|A_a(R_\perp)/c\|$ $(10^{-17}\,\mathrm{s}^{-1})$	$\|a_{l\,\max}(R_\perp)/c\|$ $(10^{-17}\,\mathrm{s}^{-1})$	$\|A_o/A_a(R_\perp)\|$
C	1.38	0.6 ± 0.2	1.0 ± 0.3	2.5 ± 1.0
D	0.57	1.2 ± 0.5	1.8 ± 0.7	0.5 ± 0.2
E	2.28	1.3 ± 0.5	1.9 ± 0.7	1.8 ± 0.7
F	1.95	2.1 ± 0.8	3.6 ± 1.3	0.9 ± 0.4
G	1.55	2.0 ± 0.7	3.2 ± 1.1	0.8 ± 0.3
H	0.57	1.1 ± 0.4	1.6 ± 0.6	0.5 ± 0.2
I	1.84	2.0 ± 0.7	3.2 ± 1.1	0.9 ± 0.4
J	0.99	0.8 ± 0.3	1.2 ± 0.5	1.2 ± 0.5
L	3.33	2.0 ± 0.7	3.8 ± 1.4	1.6 ± 0.7
M	1.56	0.7 ± 0.3	1.2 ± 0.4	2.1 ± 0.9
N	1.23	1.6 ± 0.6	2.4 ± 0.8	0.8 ± 0.3
O	0.63	1.4 ± 0.5	4.0 ± 1.4	0.4 ± 0.2
Q	0.33	0.8 ± 0.3	1.3 ± 0.4	0.4 ± 0.2
T	3.36	1.9 ± 0.7	3.0 ± 1.0	1.7 ± 0.7
U	1.67	0.9 ± 0.3	1.3 ± 0.5	2.0 ± 0.7

tidal and core radii. With the knowledge of this parameter, the general potential in Fig. 6.3 can be derived. The gradient of that potential yields a "normalized acceleration", $a_n(r/r_c)$.

The remaining two parameters are the central dispersion of line-of-sight velocities, $v_z(0)$, and the core radius, $r_c \equiv D\theta_c$. These allow the calculation of actual accelerations,

$$A(r/r_c) = a_n(r/r_c)\frac{v_z^2(0)}{D\theta_c}. \tag{6.11}$$

We do not, of course, know the actual distance of each pulsar from the cluster centre, only its projection $R_\perp$. We will therefore compare the "observed acceleration" of each pulsar to the ensemble average along the relevant lines-of-sight calculated from the King model, taking the pulsar distribution in the cluster to have a density proportional to r^{-2} and a cut-off radius of 4 core radii, as inferred

in § 6.1.1. In order to calculate the contribution to $(\dot{P}/P)_{\text{obs}}$ of the accelera-
tion of a pulsar at a given radius, we multiply $A(r)$ by l/r, so as to obtain the
line-of-sight component of the acceleration. The average acceleration along each
line-of-sight (integrated over only one hemisphere) is thus

$$A_a(R_\perp) = \frac{1}{N} \int_{l=0}^{l=\sqrt{r_{\text{lim}}^2 - R_\perp^2}} \frac{\lambda^{-1}}{r^2} A(r/r_c) \frac{l}{r} dl, \qquad (6.12)$$

where λ is a constant of integration related to the total number of pulsars along
the line-of-sight, N.

How do these "average" theoretical accelerations along each line-of-sight com-
pare with the observed accelerations? The observed acceleration, A_o, can be
obtained for each pulsar by subtracting the intrinsic $\dot{P}/P$ from $(\dot{P}/P)_{\text{obs}}$. Un-
fortunately, the intrinsic period derivative is not known. Here we assume that
each pulsar has a characteristic age of $3\,\text{Gyr}$ and subtract the corresponding
$\dot{P}/P = +0.5 \times 10^{-17}\,\text{s}^{-1}$[1] from each observed value (listed in Table 6.4) to obtain
estimates for A_o, these are presented in Table 6.3.

We are now in a position to compare the "observed" and average predicted
accelerations. We do this for each pulsar in the last column in Table 6.3. This
value is significantly biased for some individual pulsars by the subtraction of
a fixed $\dot{P}/P = 0.5 \times 10^{-17}\,\text{s}^{-1}$, our first-order attempt at accounting for the
intrinsic period derivatives. However, the average of all values in the last column
of the table should be approximately unity, if the modeling described above is to
be consistent with the actual accelerations experienced by the pulsars — which
indeed it is, despite considerable uncertainty: $\overline{|A_o/A_a(R_\perp)|} = 1.2 \pm 0.7$.

As an additional consistency check on the King model of the cluster potential
we performed a Monte Carlo simulation of the pulsar population of 47 Tuc. The
aim of this simulation is to see, given reasonable input assumptions, whether we

---

[1]This value of $\dot{P}/P$ coincides with a weighted average of the observed $\dot{P}/P$, for which the
weights are $1/a_n(r/r_c)$ if the pulsar has a positive $\dot{P}$ and $6/[9a_n(r/r_c)]$ if the pulsar has a
negative $\dot{P}$
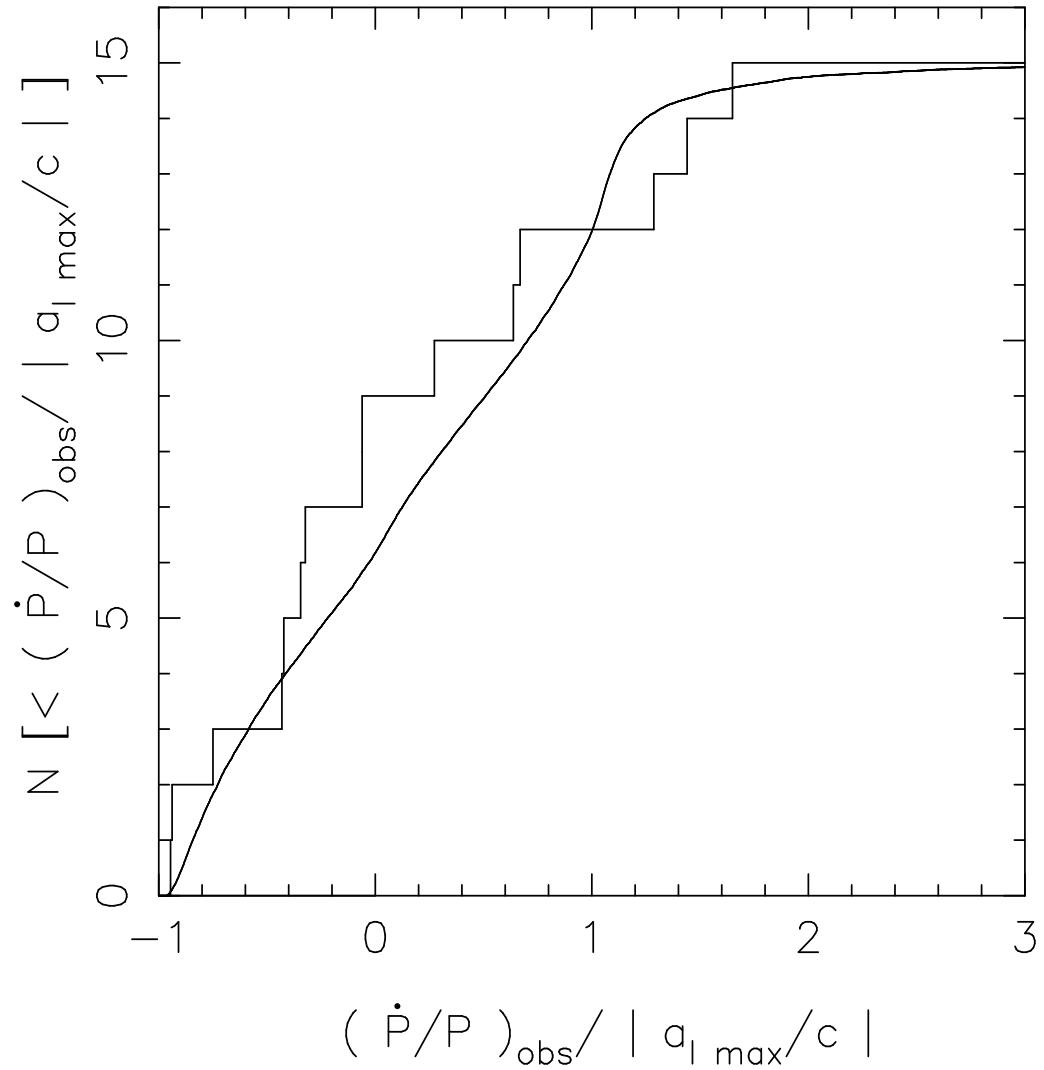
Figure 6.6: Cumulative distributions of $(\dot{P}/P)_{\mathrm{obs}}/|a_{l\,\mathrm{max}}/c|$ for 15 observed pulsars, and for a simulated population (smooth curve), normalized by the observed distribution (see § 6.3.2).

can reproduce the *distribution* of $(\dot{P}/P)_{\mathrm{obs}}$.

In the simulation, we generate a spherically symmetric population of 10^6 pulsars with an isothermal radial distribution with a cutoff of 4 core radii. Each of the pulsars was randomly assigned an age from a flat distribution ranging between $500\,\mathrm{Myr}$ and $10\,\mathrm{Gyr}$ — the mean $\dot{P}/P = 0.5 \times 10^{-17}\,\mathrm{s}^{-1}$ corresponding to what was assumed before. These assigned ages correspond to the intrinsic $\dot{P}/P$ of each of the model pulsars. Finally, given the position of each of the model pulsars relative to the cluster centre, we calculate the contribution to $\dot{P}/P$ from the acceleration in the cluster determined from the King model with $D = 5.0\,\mathrm{kpc}$ and $v_z(0) = 11.6\,\mathrm{km\,s}^{-1}$. By adding this contribution to the intrinsic $\dot{P}/P$ we have, for each pulsar, a model observed $\dot{P}/P$ which can then be directly compared to the sample of 15 pulsars for which we have coherent timing solutions.

The results of this simulation are shown in Fig. 6.6, where we present a cumulative plot of $(\dot{P}/P)_{\mathrm{obs}}/|a_{l\,\mathrm{max}}(R_\perp)/c|$ for the real and simulated samples. Given the relatively small size of the observed distribution, and the straightforward simulation that we have performed, the agreement between the model and observed samples is good.

Our overall conclusion is therefore that a King model for 47 Tuc, with $D = 5.0\pm0.4\,\mathrm{kpc}$, $v_z(0) = 11.6\pm1.4\,\mathrm{km\,s}^{-1}$, and a small contribution from the intrinsic $\dot{P}/P$s of the pulsars, provides a good description of the observed $\dot{P}/P$s.

6.3.3   Limits on pulsar ages and magnetic fields

We now obtain one-sided limits for the characteristic age and the inferred surface dipole magnetic field strength of the pulsars, by calculating the maximum intrinsic period derivative for each pulsar, $\dot{P}_{\mathrm{int\,max}}$. First, suppose we have a reliable estimate for the maximum acceleration for each pulsar's line-of-sight, $a_{l\,\mathrm{max}}(R_\perp)$. Next, assume that each pulsar actually experiences such a maximum
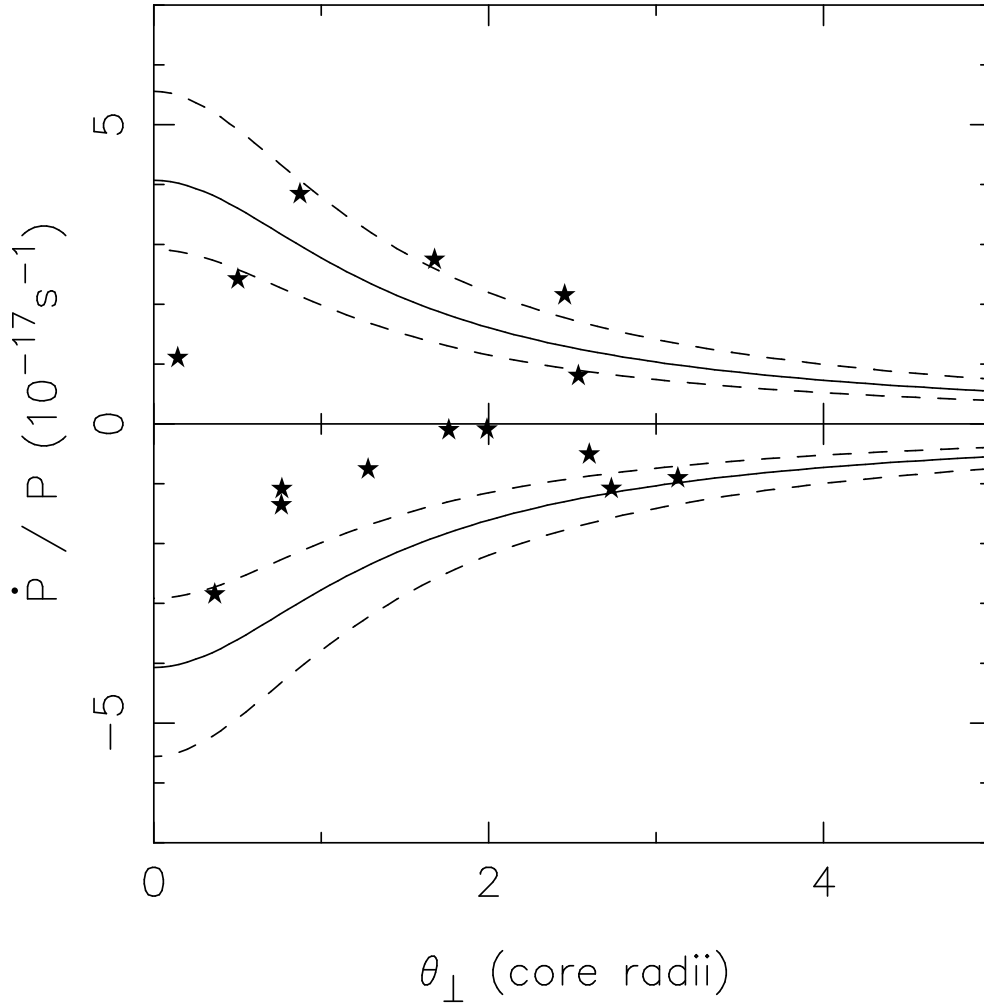
Figure 6.7: The values for $(\dot{P}/P)_{\mathrm{obs}}$ (Table 6.4) are plotted versus $\theta_\perp$ for the 15 pulsars with coherent timing solutions (stars). We also plot the maximum acceleration along each line-of-sight calculated from a King model with the nominal distance and central velocity dispersion (solid line), and accounting for the uncertainties in those quantities (dashed lines). See Table 1.2 for cluster parameters.

(negative) acceleration. Under such conditions, an observed $|\dot{P}/P|$ that is smaller than $|a_{l\,\max}(R_\perp)/c|$ is caused by a finite (positive) intrinsic $\dot{P}/P$. Hence, $(\dot{P}/P)_{\rm int} < |a_{l\,\max}(R_\perp)/c| + (\dot{P}/P)_{\rm obs}$.

After determining $\dot{P}_{\rm int\,max}$ we derive a minimum characteristic age of the pulsar using equation 1.2 and an upper limit for the magnetic field using equation 1.3.

Only a reliable upper limit for the acceleration along each line-of-sight remains to be calculated. Phinney (1993) calculated the maximum acceleration expected near the centre of a globular cluster,

$$a_{l\,\max}(R_\perp) = \frac{3}{2}\frac{v_z^2(R_\perp)}{\sqrt{r_c^2 + R_\perp^2}}. \tag{6.13}$$

This expression is valid to within $\sim 10\%$ for $R_\perp \leq 2r_c$, provided that the function $v_z(R_\perp)$ is accurately known.

The values of $\dot{P}/P$ observed for the pulsars (reflecting in part the gravitational potential of the cluster) do not appear to decrease greatly with $R_\perp$ (Fig. 6.7), so we first assume conservatively that $a_{l\,\max}(R_\perp)$ does not decrease with $R_\perp$. Therefore, the absolute upper limit for $a_{l\,\max}(R_\perp)$ is $a_{l\,\max}(0)$. Within the constraints imposed by the parameters and uncertainties in Table 1.2, the maximum possible value for $a_{l\,\max}$ at the centre of the cluster is obtained with $D = 4.6\,{\rm kpc}$ and $v_z(0) = 13.0\,{\rm km\,s^{-1}}$: $a_{l\,\max}/c = 5.3 \times 10^{-17}\,{\rm s^{-1}}$.

The limits for the pulsar parameters obtained with this constant maximum acceleration are presented in Table 6.4. All characteristic ages are larger than $170\,{\rm Myr}$ and all pulsars have magnetic fields lower than $2.3 \times 10^9\,{\rm Gauss}$. These values are consistent with those measured for Galactic millisecond pulsars (e.g., Camilo, Thorsett & Kulkarni 1994). Note that these limits are extremely conservative, and are independent of any detailed modeling of the cluster. It is nevertheless clear that even with such a crudely over-estimated $a_{l\,\max}(R_\perp)$ we can derive useful limits for the parameters of the pulsars.

By modeling the cluster and obtaining better constraints for $a_{l\,\max}(R_\perp)$, more

Table 6.4: Limits on characteristic age and magnetic field for the pulsars in 47 Tuc. The $(\dot{P}/P)_{\mathrm{obs}}$ have been corrected for the acceleration terms a_S and a_G. The values indicated with subscript "1" were obtained using $D = 4.6\,\mathrm{kpc}$, $v_z(0) = 13.0\,\mathrm{km\,s^{-1}}$ and $a_{l\max}(R_\perp)/c = a_{l\max}(0)/c = 5.32 \times 10^{-17}\,\mathrm{s^{-1}}$. The values indicated with "2" were derived from the maximum accelerations (also indicated) calculated with an isotropic single-mass King model for 47 Tuc with the same values of cluster parameters (see § 6.3.3).

Pulsar	$(\dot{P}/P)_{\mathrm{obs}}$ $(10^{-17}\,\mathrm{s^{-1}})$	$\tau_{\mathrm{c}1}$ $(10^8\,\mathrm{yr})$	B_1 $(10^5\,\mathrm{T})$	$\lvert a_{l\max}/c \rvert$ $(10^{-17}\,\mathrm{s^{-1}})$	$\tau_{\mathrm{c}2}$ $(10^8\,\mathrm{yr})$		B_2 $(10^5\,\mathrm{T})$	
C	-0.88	> 3.6	< 1.2	1.33	> 36	...	< 0.4	...
D	-0.08	> 3.0	< 1.2	2.48	> 6.6	...	< 0.8	...
E	2.77	> 2.0	< 1.0	2.60	> 3.0	< 92	< 0.8	> 0.15
F	2.44	> 2.0	< 0.7	4.89	> 2.2	...	< 0.7	...
G	-1.06	> 3.7	< 0.8	4.30	> 4.9	...	< 0.7	...
H	-0.07	> 3.0	< 0.7	2.21	> 7.4	...	< 0.5	...
I	-1.33	> 4.0	< 0.7	4.31	> 5.3	...	< 0.6	...
J	-0.48	> 3.3	< 0.5	1.66	> 13	...	< 0.2	...
L	-2.82	> 6.5	< 0.7	5.15	> 6.8	...	< 0.7	...
M	-1.06	> 3.7	< 0.8	1.57	> 31	...	< 0.3	...
N	-0.73	> 3.5	< 0.7	3.23	> 6.3	...	< 0.5	...
O	1.13	> 2.5	< 0.7	5.42	> 2.4	...	< 0.7	...
Q	0.83	> 2.6	< 1.0	1.71	> 6.2	...	< 0.7	...
T	3.86	> 1.7	< 2.3	4.06	> 2.0	...	< 2.2	...
U	2.18	> 2.1	< 1.2	1.78	> 4.0	< 40	< 0.9	> 0.3

stringent limits can be derived. For this reason, we now compare the observed pulsar $\dot{P}/P$ with the maximum accelerations along each line-of-sight calculated from the King model (see Fig. 6.7). The limits for the pulsar parameters derived from this cluster model are also presented in Table 6.4. As expected, these are more constraining than those derived before. In particular, the characteristic ages for 47 Tuc C and M exceed $3\,\mathrm{Gyr}$, and a simple average of the lower limits on age for all pulsars yields $\overline{\tau_c} > 0.9\,\mathrm{Gyr}$, while the magnetic field strengths of 47 Tuc J and M are less than $3 \times 10^8\,\mathrm{Gauss}$, very close to the lowest values observed among Galactic disk pulsars. These values depend, of course, on the particular cluster model used in calculating the accelerations.

Limits for the characteristic ages and magnetic fields of the pulsars in M15 have been derived by Anderson (1992), using a mass model for the cluster based on the surface luminosity density and assuming a constant mass-to-light ratio. The majority of pulsars in that cluster have characteristic ages $\sim 10^{10}\,\mathrm{yr}$ (Anderson 1992), but there are signs of a relatively recent burst in pulsar formation. At least two pulsars have maximum characteristic ages $\sim 10^8\,\mathrm{yr}$ and magnetic fields of about $(10\text{–}20) \times 10^9\,\mathrm{Gauss}$. This is attributed to the ongoing core collapse in M15, leading to much increased recycling of pulsars. In 47 Tuc, on the other hand, there are no visible signs of such a recent burst in pulsar formation: all the known pulsars for which a timing solution has been obtained have characteristic ages (probably much) greater than $170\,\mathrm{Myr}$, weak magnetic fields, and very short rotational periods.

6.4   Relation of DM with period derivative

The observations made with the $2 \times 512 \times 0.5\,\mathrm{MHz}$ filterbank since August 1999 have allowed a three-fold improvement in time resolution. This provides for better pulse profiles and timing, but it also improved the precision of the dispersion

measures of the pulsars in 47 Tuc compared to the values presented in Camilo et al. (2000) and Freire et al. (2000b). These new estimates of DM are presented in Table 5.2.

With these new estimates of DM, we can already say that the pulsars with negative $\dot{P}$ have generally higher DMs than the pulsars with positive $\dot{P}$. In Figure 6.8, we can see this relation between DM and $(\dot{P}/P)_{\mathrm{obs}}$ more clearly. The pulsars with positive $(\dot{P}/P)_{\mathrm{obs}}$ have DMs between 24.2 and 24.4 cm^{-3} pc, but a group of 7 pulsars on the distant side of the cluster (47 Tuc C, D, G, I, J, M, N) have significantly higher DMs.

A similar group of globular cluster pulsars with known positions and DMs was known before, in the globular cluster M15. The differences in DM among the seven pulsars near the core of that cluster (i.e., not taking into account M15 C, which lies considerably further from the centre), have been attributed to a gradient in the galactic electron column density (Anderson 1992), in the case of M15 this can explain the observed differences in the DMs of the inner pulsars. If such a gradient in galactic column density exists in the direction of 47 Tuc, then it should be apparent in the distribution of DM and offsets from the centre. To the observed distribution, we fitted a function of the type

$$DM(x,y) = a + u_x.x + u_y.y \qquad (6.14)$$

where x and y are the east-west and north-south offsets of the pulsars relative to the centre of the cluster, measured in arcminutes. The result of such a fit is

a = (24.42 ± 0.04) cm^{-3} pc,

u_x = (-0.07 ± 0.07) cm^{-3} pc arcmin^{-1},

u_y = (0.08 ± 0.08) cm^{-3} pc arcmin^{-1}.

The large relative errors in the measurement of the gradient coefficients indicate that no such gradient is clearly detectable.

Figure 6.8: DM as a function of $(\dot{P}/P)_{\mathrm{obs}}$. Notice that the pulsars with positive $\dot{P}$ have consistently lower DMs. The pulsars near the core of the cluster are indicated with a circle.

We note that the pulsars in 47 Tuc are spread over a relatively large area in the sky compared to those in M15, which, with the exception of M15 C, are all closer than $17''$ from the centre of the cluster. M15 C itself is at about one arcminute from the centre of the cluster. At the distance of M15 from the Solar System, this represents a projected distance of 2.8 pc. In spite of its large distance from the centre of the cluster, this pulsar has a DM which is very similar to all the remaining pulsars; the difference is significantly smaller than what might be expected from a naive extrapolation of the DM gradient observed for the inner pulsars. From this, Anderson (1992) concluded that the fluctuations in column density that apparently cause the differences in the DMs of the pulsars in M15 do not extend to spatial scales of the order of one parsec. Therefore, we should not expect the presence of a gradient with a scale of 1 pc for 47 Tuc as well.

This lack of coherence in the column density of plasma at spatial scales of about one parsec should therefore imply an essentially random DM value for the pulsars in 47 Tuc around the average DM of the cluster. Assuming this is indeed the case, we can calculate the probability of a random occurrence of the observed relation between $\dot{P}$ and DM: the total number of distinct sets of seven pulsars among the fifteen with a know timing solution is $15!/(8! \times 7!) = 6435$. In principle, any of these sets could be the one with the seven higher DMs. The number of sets of seven pulsars among the nine pulsars with negative period derivatives is 36. Therefore the chance probability of all pulsars among the top seven having negative period derivatives is $36/6435 = 0.0056$, or about one in 180.

At this stage, we can still argue that, although such a chance coincidence is unlikely, it is definitely not impossible. However, there is another characteristic of the observed DM/projected offset distribution which we have not mentioned so far. If the DMs are a random function of position in the sky, the dispersion in

DM values for the pulsars in the core should be the same as for the other pulsars.

In Fig. 6.8, we circled the pulsars that are projected within the core of the cluster, and these have, instead, a smaller dispersion in DM, in fact, these five pulsars are among the six closest to DM = 24.4. These pulsars are also seen to have the largest dispersion in $\dot{P}/P$, as expected. Therefore, the DMs of the pulsars don't appear to be a random function of their position.

If there is a gradient in the galactic electron column density, the dispersion of DMs of the pulsars in the core will be smaller because these pulsars have a small dispersion in projected distances to the centre; if, on the other hand, there is a plasma cloud in the cluster, the dispersion of DMs of the pulsars in the core will also be smaller because these pulsars have, on average, a smaller dispersion in distances along the line-of-sight. We have seen, however, that no large-scale gradient in the electron column density is observed or should be expected, or can even explain why the pulsars with negative $\dot{P}$ have higher DMs. Therefore, the best explanation for the differences in the observed DMs is the presence of a plasma cloud in 47 Tuc.

If we accept this idea, then we can use the argument in reverse and conclude that the pulsars with negative $\dot{P}$ are more distant than those with a positive period derivative, because there is extra plasma between them and the solar system compared to the remaining pulsars. This agrees with the idea that these pulsars are on the distant side of the cluster and have negative line-of-sight accelerations caused by its gravity. Therefore, the possibility that the negative period derivative is caused by some sort of accretion onto the pulsar is definitely excluded.

We notice as well that the plasma cloud in the cluster cannot totally explain all the DMs observed. For instance, 47 Tuc L has the largest negative $\dot{P}$, and it is therefore on the distant side of the cluster. On the other hand, 47 Tuc T

has the largest positive $\dot{P}$, and it is in the near side of the cluster. Contrary to expectations, the DM of 47 Tuc L is smaller than that of 47 Tuc T. If 47 Tuc L was further from the centre of the cluster compared to 47 Tuc T, we could explain its DM by assuming that the plasma density decreases from the centre of the cluster outwards (this could explain, in principle, the low DM of 47 Tuc H). However, 47 Tuc L is closer to the centre of the cluster than 47 Tuc T. These small differences in DM (of less than 0.05 cm^{-3} pc) could in principle be explained by the aforementioned random variations in the galactic plasma density, superposed to the main effect of the plasma cloud in the cluster. We notice, however, that these pulsars (47 Tuc H, L and T, together with 47 Tuc I, M and Q) are among those for which the precision of the measurement of DM is still relatively low. Continued observations of 47 Tuc with high time resolution will eventually detect these scintillating pulsars with a high (S/N) on several occasions; these detections will allow better estimates for the DMs of these pulsars.

Looking at Figure 6.8 we conclude that the total column density of electrons in the cluster is of the order of 0.5 cm^{-3} pc. The region occupied by the pulsars is about 3 pc wide, therefore, the average density should be about 0.15 electrons cm^{-3}. We can easily compare this with the average electron density between the solar system and 47 Tuc. Dividing 24.4 cm^{-3} pc by the distance to 47 Tuc (5 kpc), we obtain an average density along the way of the order of 0.005 electrons cm^{-3}. Therefore, the average electron density in the cluster is about thirty times larger than in the space between it and the solar system.

This result is at odds with the conclusion of Spergel (1991), which finds that 47 Tuc and other globular clusters should be devoid of any plasma, owing to the kinetic effects of strong winds from the pulsars. It is therefore difficult to explain the origin of the observed plasma cloud; this is clearly a subject that deserves further investigation. We are presently modelling the plasma cloud, which will

allow us to derive more reliable values for its parameters and also to derive three-dimensional positions for the pulsars. The results of this detailed analysis will be published elsewhere.

Chapter 7

Binary systems

In chapter 2 we note that the binary systems in 47 Tuc are divided into two main groups, segregated by companion mass. The first is composed of binaries with very short periods (1.5–5.5 hr) and companion masses $\sim 0.03\,\mathrm{M}_\odot$. We have timing solutions for three of these binaries (47 Tuc I, J and O). 47 Tuc J displays eclipses at 660 MHz, 47 Tuc O is eclipsed at 1400 MHz, and it is very faint at 660 MHz. There is no evidence for eclipses in 47 Tuc I. The properties of the 47 Tuc J system are described in more detail in § 7.4. The second group of binaries has binary periods in the range 0.4–2.3 d, and companion masses $\sim 0.2\,\mathrm{M}_\odot$; we refer to this group as "normal" binaries. Of these, 47 Tuc E, H, Q, T and U have a timing solution at the moment. The mass function f and P_B are plotted in Figure 7.1 for all the binaries in globular clusters listed in Table 1.1 and for the Galactic binaries listed in Camilo (1995a) and Lyne et al. (1998).

In this chapter we will address several questions concerning these binaries. In § 7.1, we will discuss in some detail the origin and evolution of the 47 Tuc binary pulsar systems. This analysis has been published in Rasio (2000), we refer the reader to Rasio, Pfahl & Rappaport (2000) for a more detailed account of the history of the binary pulsars in 47 Tuc. That work is based on the observational results published in Camilo et al (2000) and Freire et al. (2000a).
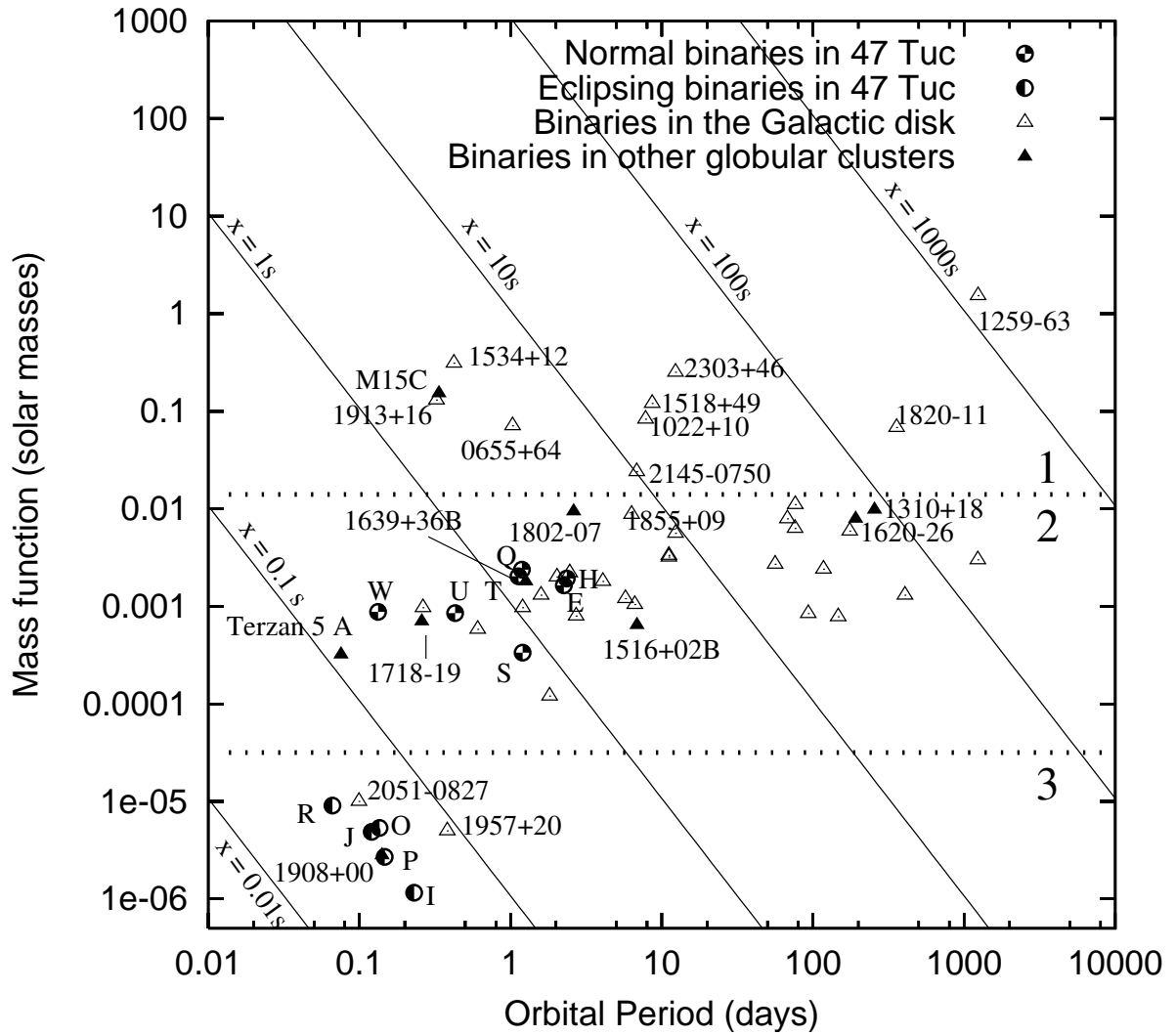
Figure 7.1: Variation of mass function with P_B for globular cluster and galactic binaries. We can divide the binaries in three main groups, their difference is essentially the mass of the companion objects. Those in region **1** have either heavy white dwarf, neutron star or main-sequence companions. Binaries in region **2** have companions in the range 0.07 to 0.5 $M_\odot$. Binaries in region **3** have companions with masses of 0.01–0.03 $M_\odot$, and most of them display eclipses. This plot suggests that Terzan 5 A, 47 Tuc W and the remaining "normal" neutron star - white dwarf binaries in region **2** have a similar formation mechanism; but this is still open to debate. The inclined lines indicate a constant x. It is interesting to note that the three binaries with the lowest mass function (PSR B1908+00, 47 Tuc I and 47 Tuc P) do not display eclipses, suggesting that these systems have higher inclinations and a companion mass which is similar to the remaining eclipsing systems.

In § 7.2, we discuss how the binaries obtained their present eccentricities, which are generally higher than for similar systems in the disk of the Galaxy. The high eccentricity of the 47 Tuc H binary system permits the measurement of the rate of advance of periastron for this system, and therefore the measurement of its mass. This section was previously published as section 6 of Freire et al. (2000b).

Finally, in § 7.4, we study in detail one eclipsing system, 47 Tuc J. We show how its DM changes with orbital period, and draw some conclusions about the mass-loss rates and the ablation process. This section will eventually be part of a paper now being prepared (Freire et al. 2000d) which will make a detailed description of the eclipsing binary pulsars in 47 Tuc.

7.1 Origin and evolution of the 47 Tuc binaries

It has been realized over the last ten years that there are significant amounts of primordial binaries in globular clusters (Hut et al. 1992). This means that old neutron stars, not detectable as pulsars, can acquire main-sequence binary companions through exchange interactions (a fact mentioned in § 1.3.1). Exchange interactions with hard primordial binaries (with semi-major axis of $0.1 - 1$ AU) can naturally form the wide binary millisecond pulsars seen in some low-density globular clusters. An example is PSR B1310+18, which is a member of a 255-day binary system in M53 (see Table 1.1). M53 has the lowest central density for any globular cluster with known pulsars (10^3 $M_\odot$ pc^{-3}, Kulkarni & Anderson 1996). When the newly acquired main-sequence companion, with a mass up to about 1 $M_\odot$, evolves into a giant, the orbit circularizes and a period of *stable* mass transfer begins, during which the neutron star is recycled (Rappaport et al. 1995). The resulting neutron star-white dwarf binaries have orbital periods in the range $P_B \sim 1 - 10^3$ d. However, this scenario does not explain the formation of binary

systems with periods shorter than ~ 1 day. To obtain such short periods, the initial primordial binary must be extremely tight, with d less than about 0.01 AU, but the recoil velocity of the system following the exchange interaction would then almost certainly exceed the escape velocity of 47 Tuc (~ 60 km s^{-1}, see Table 1.2).

One can get around this problem by considering more carefully the *stability* of mass transfer in neutron-star/main sequence binaries formed through exchange interactions. While all main-sequence stars in the globular cluster today have masses below 1 M$_\odot$, the rate of exchange interactions may well have peaked at a time when significantly more massive MS stars were still present.

If that is the case, these massive stars will concentrate on the core of the cluster in a timescale of the order of 10^9 years, which is comparable to the lifetime of a main-sequence stars with 2–3 M$_\odot$. The same sort of mass segregation also applies to neutron stars, thus increasing their probabilities of interacting with the massive binaries, eventually producing the so-called Intermediate Mass X-ray Binaries (IMXB).

The evolution of such a binary is drastically different from the evolution of a LMXB. When the main-sequence star evolves and fills its Roche Lobe, the mass transfer becomes dynamically unstable and leads to a common-envelope (CE) phase. The emerging binary will have a low-mass white dwarf in a short-period circular orbit around the neutron star.

This idea is at the basis of the dynamical scenario developed by Rasio, Pfahl and Rappaport (2000). They find that a significant fraction of neutron star-white dwarf binaries emerging from the CE phase undergo further evolution during a period of stable mass transfer driven by gravitational radiation and tidal heating of the companion. For an arbitrary number of 5×10^6 primordial binaries, this model produces three main groups of binaries:

Group A (~ 1000 members) corresponds to companion masses well below 0.1 $M_\odot$ and orbital periods from 15 minutes to ~ 6 hours. It is formed by objects that decayed through gravitational radiation to very short orbital periods, of the order of a few minutes, the orbital period eventually increased due essentially to mass transfer. This is the group to which 47 Tuc I, J, O, P and R belong. Our failure to detect 15-minute binary systems, if they exist, is probably due to the selection effects discussed at length in § 2.5.

Group B binaries (~ 2400 members) have relatively massive ($0.3 - 1$ $M_\odot$) white dwarf companions that had insufficient time to evolve, through gravitational wave emission, to decay to Roche-lobe contact, their origin is similar to that of group A (IMXB). A third group (C, ~ 3500 members) represents stable mass flow from a relatively low-mass sub-giant star to a neutron star (LMXB). The binaries in 47 Tuc that don't belong to group A (47 Tuc E, H, Q, S, T, U and W) lie somewhat between these two groups, so their origin is not yet well established.

There is another important difference between the simulated and detected binaries: in the simulated systems, a sizable fraction of the binaries in Groups B and C have orbital periods from a few days to one month, while the longest known orbital period for a binary pulsar in 47 Tuc is 2.35 days (47 Tuc H). There are no selection effects against the detection of such binaries; thus the lack of binary pulsars with longer orbital periods is probably a genuine feature of the pulsar population of 47 Tuc.

This result is quite important, although it was not explicitly mentioned as such by Rasio, Pfahl and Rappaport (2000). If indeed a large number of binaries with periods between a few days and one month formed, the present distribution of orbital periods tells us that binaries with longer periods were either tightened by interactions with other stars or disrupted by the high stellar density near the centre of the cluster. High stellar densities near the core are a characteristic

feature of clusters undergoing core collapse, and binary tightening is a known source of kinetic energy to the remaining stars in the cluster during a phase of pre-core collapse (the cluster is said to be "burning its binaries"), thus suggesting that 47 Tuc had a high-density core in the last few billion years, and that such a core has been sustained from further collapse by energy provided by the binaries (Hut et al. 1992). If the cluster had just reached the present core density, we should still see binaries with relatively long orbital periods of about one month.

7.2   Eccentricities

Coherent timing solutions give extremely detailed orbital information, and often allow the measurement of very small eccentricities. Most millisecond pulsar–white dwarf systems in the Galactic disk have very low, but measurably significant eccentricities (e.g., Camilo 1999)**?**. These are thought to result from tidal interactions between the neutron star and convective cells in the envelope of its companion during the giant phase of its evolution, and a relationship between orbital period and eccentricity can be derived for such systems (**?**). The millisecond pulsar–white dwarf systems in globular clusters have, more often, larger eccentricities than those in the disk of the Galaxy (**?**). These are thought to result from interactions with other stars in the cluster: the denser the environment, the more likely one is to find a relatively large degree of eccentricity in the system.

The five eccentricities measured for binary pulsars in 47 Tuc (for the normal binaries 47 Tuc E, H, Q, T and U; see Table 5.4) are all much larger than one would expect for similar systems in the Galactic disk, and are therefore, presumably, a fossil remnant of gravitational interactions between the binary systems and other cluster stars. Rasio & Heggie (1995) calculate the expected value of this eccentricity for a system with a particular binary period that has interacted with other stars in a region of known density for a certain length of time. Unfortunately

we do not know the relevant densities or interaction time scales for the pulsars observed in 47 Tuc with any degree of certainty, possibly not even to an order of magnitude. Nevertheless, taking plausible estimates for density and time scales, we derived some "predicted" eccentricities. Those for 47 Tuc E, Q, and T are within an order of magnitude of the observed values, which is as close to agreement as we can expect to attain given the uncertainties in input parameters. The computed eccentricity for 47 Tuc U is two orders of magnitude below the observed value, while that for 47 Tuc H is under-predicted by a factor of 1000.

One possible explanation for the unexpectedly large eccentricity of 47 Tuc U, and possibly that of 47 Tuc H, is that they have in the past spent a considerable amount of time in a region with a much higher stellar density than they are found in at present. For instance, if 47 Tuc L (an isolated pulsar) had spent 10^{10} yr in its present location while part of a 2.35-day binary, its computed eccentricity would be 0.5. These large expected eccentricities near the centre of the cluster suggest why no "normal" binaries are observed in the core (see Rasio 2000). Therefore, some of the pulsars we observe relatively far from the centre of the cluster may have non-circular orbits in the cluster potential which take them through higher-density regions periodically, generating some of the large eccentricities measured.

Alternatively, the high eccentricity of the 47 Tuc H binary system, by far the largest in the cluster, could indicate that it obtained its present companion as an already-formed white dwarf through an exchange interaction. However, such exchanges tend to produce even higher eccentricities (**?**).

The large eccentricity of 47 Tuc H has permitted a measurement of its rate of advance of periastron: $\dot{\omega} = (0.073 \pm 0.005)^\circ \, \mathrm{yr}^{-1}$ (Table 5.4). Assuming that this advance is entirely due to general relativity, and not to any tidal effects (which is likely, since both stars are presumably degenerate and have negligible dimensions compared to the orbital separation), the total mass of the binary system can be
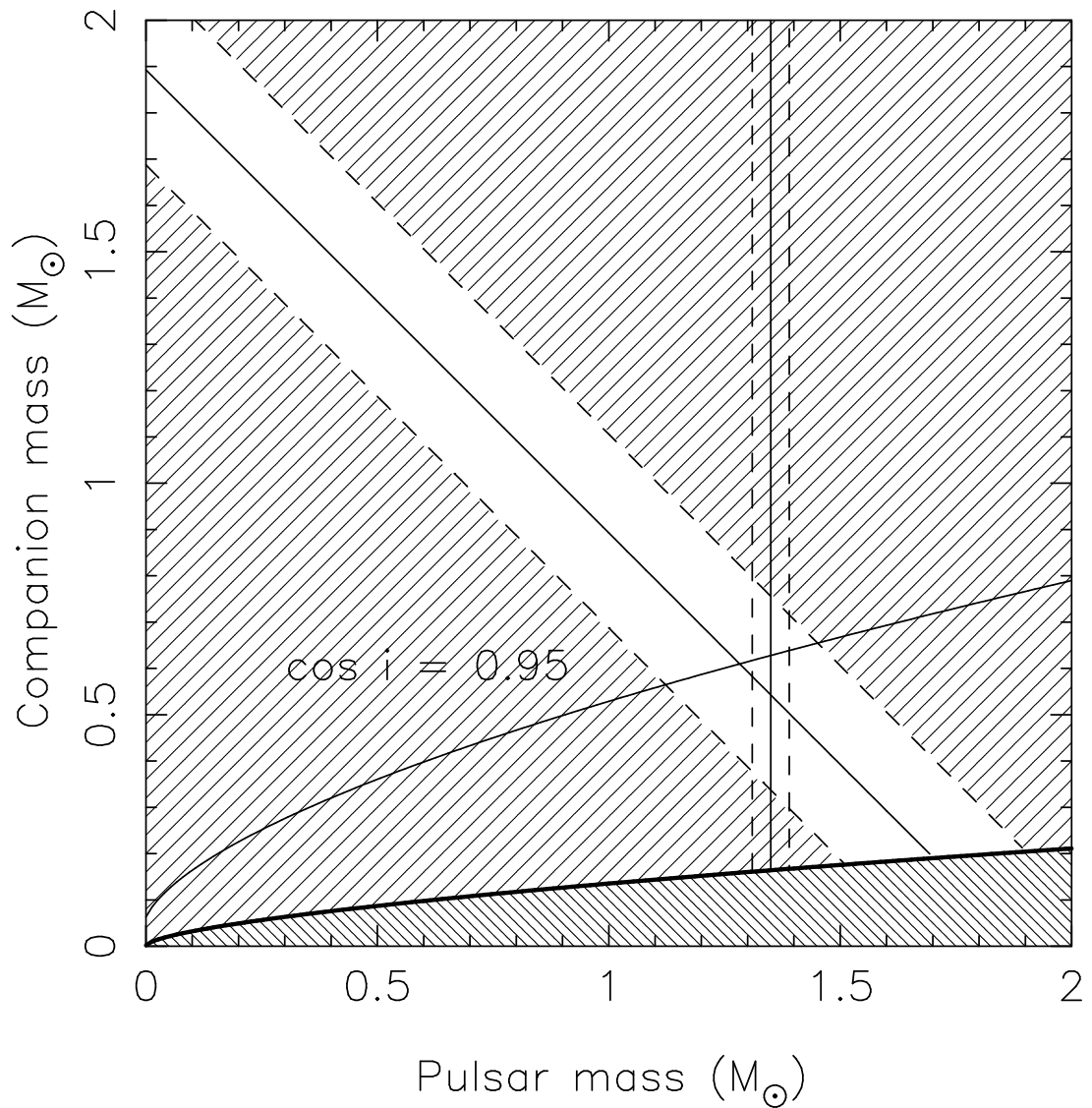
Figure 7.2: Mass–mass diagram for the 47 Tuc H system. The allowed range of total mass (sloping straight line surrounded by dashed lines) is derived from the measured rate of advance of periastron and its 2-σ uncertainty. The area below the thick curving line is excluded by the measured mass function and the requirement that $\cos i \geq 0$. There is a 95% a priori probability that the system lies at $\cos i \leq 0.95$. The vertical lines indicate the average measured mass for neutron stars in the radio pulsar population, $1.35 \pm 0.04 \, \mathrm{M_\odot}$ (Thorsett & Chakrabarty 1999).

obtained from equation 5.16: $1.9 \pm 0.2 \, M_\odot$ (all uncertainties here are given at the 2-σ confidence level). A mass-mass diagram is shown in Fig. 7.2, from which limits on the individual masses can be derived: $m_p < 1.9 \, M_\odot$ and $m_c > 0.15 \, M_\odot$. It is also improbable that $m_p < 1.1 \, M_\odot$ or $m_c > 0.65 \, M_\odot$, because this would require $\cos i > 0.95$.

7.3 A brief history of eclipsing binary pulsars

In the Galactic disk there are two known eclipsing binary pulsars, PSRs B1957+20 and J2051−0827. Both are millisecond pulsars in very circular orbits with $\sim$ $0.03 \, M_\odot$ companions, with orbital periods of a few hours. These pulsars are both eclipsed by their companions, apparently bloated to fill their Roche lobes. PSR B1957+20 was discovered in 1988 (Fruchter, Stinebring & Taylor 1988). It is a 1.6 ms pulsar in an 8-hour binary system with a companion of mass ~ 0.02 $M_\odot$. The lack of emission at superior conjunction was immediately apparent, the inferred radius of the companion object is 1.5 $R_\odot$, clearly too big for such a light white dwarf.

It was then proposed that relativistic winds from the pulsar were ablating its companion (Phinney et al. 1988), creating a large plasma cloud around it. An average extra column density of plasma was subsequently measured and published in Ryba & Taylor (1991). This and later timing studies found a derivative in orbital period (Arzoumanian et al. 1994) which changes sign over time (Arzoumanian 1995); the sort-term variations in orbital period are now thought to be stochastic.

This binary system was soon found at optical wavelengths (van Paradijs et al. 1988, Fruchter, Gunn, Lauer & Dressler 1988) and orbital light curves for it have been improving since (Callanan et al. 1989, Callanan et al. 1995, Fruchter et al. 1995); the light comes mainly from the side of the companion facing the

pulsar, indicating that emission from the pulsar is heating the companion. The pulsar has also been detected in X-rays (Kulkarni et al. 1992, Fruchter et al. 1992).

The second eclipsing binary pulsar in the Galactic disk, PSR J2051−0827, was discovered in 1996 (Stappers et al. 1996). It is a 4.5 ms pulsar in a 2.37-hour binary system. Its eclipse phenomenology is different; while PSR B1957+20 always displays eclipses for $\sim 20\%$ of its orbit, at all frequencies, PSR J2051−0827 is eclipsed at low radio frequencies, but is visible at all orbital phases at 20 cm. In the latter instance, however, the radio pulses suffer extra time delays as they propagate in a dispersive medium. The differences observed in these systems are likely due to a combination of different masses and chemical compositions of the companions, and possibly evolutionary states; the energy that is deposited at the companion by the relativistic pulsar wind, which in turn depends on the pulsar spin parameters, beaming geometry, and orbital separation; and geometrical effects. Orbital period derivatives have been measured for this pulsar as well (Stappers et al. 1998), and optical emission from the side of the companion object facing the pulsar has also been detected, its variation with orbital phase is now well documented (Stappers et al. 1999, Stappers et al. 2000).

Two eclipsing binary pulsars are known in globular clusters other than 47 Tuc, and both are rather different from the two galactic eclipsing binary pulsars. The first to be discovered and timed was PSR 1744−24A, an 11-ms pulsar in Terzan 5 (Lyne et al. 1990, Nice & Thorsett 1992). This system displays irregular eclipses that never last less than one third of the whole orbit and has a very short orbital period (1.8 hr) and a companion mass of about 0.1 $M_\odot$, i.e., about three times heavier that the companions found in the two galactic eclipsing systems. The second system, PSR B1718−19 is located in the globular cluster NGC 6342, and contains a strange 1004 millisecond pulsar (Lyne et al. 1993), which has the shortest characteristic age of any pulsar associated with a globular cluster. The

companion star has recently been detected in optical wavelengths (van Kerkwijk et al. 2000).

In 47 Tuc, one eclipsing pulsar was known before this work, 47 Tuc J. Robinson (1994) and Robinson et al. (1995) show that, at 70 and 50 cm, 47 Tuc J is eclipsed by its companion for about a quarter of its orbit.

The searches described in this work (see chapter 2) have increased the number of eclipsing pulsar binaries in 47 Tuc to a minimum of four. 47 Tuc O, a pulsar system in many respects similar to 47 Tuc J, is always eclipsed for about 10–15% of its orbit at 20 cm, and has not been clearly detected at lower frequencies. 47 Tuc R has an orbital period of 96 minutes only, and it was eclipsed for $\sim 25\%$ of its orbit, centered with the pulsar at superior conjunction (Fig. 2.3). It has been detected on two different observations. These three eclipsing binary pulsars have orbital periods of less than 6 h and $\sim 0.03\,\mathrm{M_\odot}$ companions.

The remaining two systems are different, with heavier companion objects. 47 Tuc V also displays apparent eclipses, but we cannot yet characterize the system or its eclipses, which may be irregular (§ 2.3.2); 47 Tuc W, with $m_c \sim 0.15\,\mathrm{M_\odot}$, was eclipsed for $\sim 30\%$ of its orbit on the only occasion it was detected (Fig. 2.3). While based on orbital parameters (§ 2.3.2) we suggest that the system may be somewhat similar to the eclipsing pulsar B1744−24A , we cannot yet be sure.

There are other short-period binary pulsars in globular clusters (PSR B1908+00, 47 Tuc I and 47 Tuc P) wich have very low-mass companions and do not display eclipses, these systems have the three lowest mass functions measured for all binary pulsars. This suggests these short-period systems have companion masses centered at around ~ 0.02 M$_\odot$, but in the cases of 47 Tuc I, P and PSR B1908+00 the binaries are seen with higher inclinations, hence their lack of eclipses and their lower mass functions. Thus it appears that these short-period

binary systems have a narrow range of companions masses, this is the only way the correlation between lack of eclipses and low mass function can be understood. If indeed there is a narrow mass distribution for the companion objects, then binary systems discovered in the future with very small apparent companion masses and small orbital periods will not display eclipses, for they will present large inclinations to the line-of-sight.

7.4 PSR J0023−7203J

We find that at 20 cm, contrary to what happens at lower frequencies, 47 Tuc J is always visible at all orbital phases. This binary system is therefore superficially similar to PSR J2051−0827. We also find, from the 50 cm observations made in January 1998, that the previously reported 660-MHz eclipse feature is not persistent. For instance, an eclipse apparently did occur in the orbit observed on the 11th of January 1998, the strength of the signal diminished greatly during superior conjunction but the pulse remained detectable (this effect could also be due to scintillation), but no eclipse was detectable in the orbits observed on the 12th and 13th January. These findings seem to suggest that the configuration of the system changes significantly from one day to the next. However, the extra delay of the 660-MHz TOAs near superior conjunction presented a stable configuration. We will now discuss this feature in more detail.

7.4.1 Variation of DM with orbital phase

47 Tuc J is the brightest pulsar in the cluster, and also the one having the shortest known rotational period. This combination makes DM measurements for this pulsar remarkably precise. In Table 7.1, we can see how the DM of the pulsar changes with orbital phase: it peaks at superior conjunction (orbital phase

of 90°). Notice too that the variations in DM are very small (less than 0.01 cm^{-3} pc).

We determined this variation by creating TOAs every 8.5 minutes at four different sub-bands across the 20 cm bandwidth. This integration time is about 1/20th of the orbital cycle of the pulsar, and we can reasonably assume that there is no large variation in DM during the integration time for each TOA.

We then divide all TOAs into 18 bins of orbital phase, comprising 20 degrees each. For the TOAs in each bin, we used the ephemeris for 47 Tuc J published in Freire et al. (2000b) but did not fit for any parameter, except for epoch of pulse and DM (this was done using a program called PSRTIME). The result of this fitting is an average value of DM for each bin, and it can be seen in Table 7.1.

The first set of DMs was determined using 1998/1999 data, using both the 1400 MHz TOAs (obtained with the $2 \times 96 \times 3$ MHz filterbank until August 1999) and the 660 MHz TOAs obtained in January and February of 1998. In this set, the absolute DMs are not very precise. The reason for this is that it is difficult to precisely align the different standard pulse profiles at different frequencies (see § 5.3). However, this inaccurate alignment does not change with time or orbital phase, therefore small *changes* in DM can be measured more accurately than the DM itself. We also note that at an orbital phase of $\sim 90°$, the eclipse causes a dearth of reliable 660 MHz TOAs, therefore the value of DM for that phase depends mostly on 1400 MHz data, which by itself does not have the accuracy to measure DMs with this level of precision.

The second set of DMs was determined using only the high-resolution timing data obtained since August 1999 with the $2 \times 512 \times 2$ MHz filterbank. The accuracy in the TOAs is high enough to permit the measurement of DM variations using only the 256-MHz bandwidth. The absolute values of DM, in this case, are more accurate, because there are no problems in aligning different pulse profiles at

Orbital phases (degrees)	DM (1998/1999) (cm^{-3} pc)	DM (1999/2000) (cm^{-3} pc)
0 - 20	24.5859(8)	24.5848(19)
20 - 40	24.5878(8)	24.5852(18)
40 - 60	24.5875(8)	24.5874(16)
60 - 80	24.5903(12)	24.5892(17)
80 - 100	24.5960(24)	24.5923(19)
100 - 120	24.5904(12)	24.5908(24)
120 - 140	24.5879(12)	24.5874(15)
140 - 160	24.5871(10)	24.5859(20)
160 - 180	24.5857(8)	24.5869(24)
180 - 200	24.5846(10)	24.5883(21)
200 - 220	24.5841(8)	24.5857(13)
220 - 240	24.5828(8)	24.5866(15)
240 - 260	24.5826(10)	24.5865(13)
260 - 280	24.5864(10)	24.5846(16)
280 - 300	24.5854(8)	24.5853(14)
300 - 320	24.5856(10)	24.5834(16)
320 - 340	24.5849(10)	24.5857(16)
340 - 360	24.5834(10)	24.5849(14)

Table 7.1: Variation of DM as a function of orbital phase for 47 Tuc J.

different frequencies. However, there is apparently less precision in the detection of changes of DM with orbital phase.

The good timing precision of this second set of TOAs was also used to measure the absolute DM for the pulsar, we made a fit (using PSRTIME) for all the data at more than $70°$ from the phase of the eclipse ($90°$), and obtained a value of 24.5855 ± 0.0005 cm^{-3} pc.

The data presented in Table 7.1 is plotted in Figure 7.3, the increase at superior conjunction is clearly visible in both figures. In that Figure, we also present weighted fits of Gaussian functions we made to both sets of data (although there is no particular theoretical argument favouring this function over any other). The parameters fitted are: the base DM, the height of the Gaussian K, and the half-width at half the maximum value of the Gaussian, W. The centre of the Gaussian was assumed to be at $90°$ (there are no strong indications of asymmetry in the shape of the variation of DM with orbital phase). For the first set of DMs, we obtain, to one-sigma

DM = (24.5846 ± 0.0003) cm^{-3} pc; $K = (0.0065 \pm 0.0010)$ cm^{-3} pc; $W = 57° \pm 8°$.

For the second set, we obtain

DM = (24.5856 ± 0.0003) cm^{-3} pc; $K = (0.0064 \pm 0.0010)$ cm^{-3} pc; $W = 34° \pm 6°$.

The amplitude parameter K measures the extra DM introduced by the ionosphere of the companion, this value is remarkably similar in both measurements. The width of the feature, W, is apparently different for both measurements. The reasons for this effect, or even its very existence, are unclear.

There is a curious feature at an orbital phase of $\sim 250°$ in the DMs obtained with the first data set. We don't know if that feature is significant, one of the reasons for that is the fact that such a feature is missing in the second DM set. This could also indicate that the precision in the individual DM measurements for the first data set is not as good as it is indicated by the errorbars. The main dispersive delay is the only feature that is common to both sets of DMs.

It would be interesting to investigate if the variation of DM with orbital phase is similar for all individual orbits, and check if it is always similar to the average DM, or if it presents important deviations with each orbit. The measurements made for PSR J2051−0827 (see 7.3 and references within) indicate that the second possibility is more probable. The variations in the properties of the 660-MHz eclipse suggest this as well, and could account for the different properties of the two sets of DMs presented in Table 7.1 (namely W), however the vast majority of the detections were made at 20 cm, where the extra delay is small compared to the uncertainties in the timing residuals, so any conclusions on this topic are

Figure 7.3: DM as a function of orbital phase for 47 Tuc J. The empty triangles indicate the values for DM obtained from 1998-1999 data, the filled triangles indicate measurements made with 1999-2000 data (see text and Table 7.1); the latter are displayed 0.01 cm^{-3} pc below their measured values for clarity.

premature at the moment. This topic clearly deserves further investigation.

In any case, the knowledge of the average variation of DM with orbital phase is in itself quite useful in improving the ephemeris for the pulsar. We have derived a DM correction for each TOA of 47 Tuc J, and this correction was taken into account by TEMPO when deriving the timing solution that can be seen in § 5.3.

7.4.2   The plasma envelope of the companion

In explaining the very low masses for the companion objects of pulsars like 47 Tuc J, it is commonly postulated that the companion objects undergo mass loss (e.g., Deich et al. 1993). Two mechanisms were put forward for the mass loss in the case of 47 Tuc J. The first is Roche Lobe overflow of a main-sequence star in a highly inclined orbit; the second is ablation of the companion object by the pulsar. Robinson (1994) favoured the second scenario, mainly based on the fact that we observe an eclipse, which renders the high masses (necessary for Roche lobe overflow by a main-sequence star) and the corresponding low inclinations unlikely.

The data we present in the previous section reinforces this conclusion. In fact, the object eclipsing 47 Tuc J has a radius $\gtrsim 0.5 R_\odot$, but it is transparent at frequencies of 1400 MHz and sometimes even at 660 MHz; this effectively rules out Roche lobe overflow by any conceivable bloated main-sequence or sub-giant star. It is instead a diffuse plasma cloud.

We now estimate the average density of this plasma cloud. This can be made using the extra DM at an orbital phase of $90°$, which is 0.0065 cm^{-3} pc, i.e, an extra column density of 2×10^{17} electrons cm^{-2}. Considering that the diameter of the companion object is about 1 $R_\odot$, this implies an average electron density along the line-of-sight of $\sim 10^6$ cm^{-3}.

The occasional eclipses at a frequency of 660 MHz that can last for about 25%

of the orbit imply that at some point along the line-of-sight the plasma frequency has reached 660 MHz. According to equation 2.2, this means that at that point the electron density is $\sim 5 \times 10^9$ cm^{-3}, a value that is thousands of times larger than the average density of plasma around the companion. This suggests that the plasma cloud is clumpy.

It is interesting to speculate on the nature of this clumpiness. The maximum density over the whole envelope seems to change coherently over time, because sometimes we detect the pulsar at 660 MHz through superior conjunction, and sometimes we do not. The clumpiness could be due to a shock front, where the plasma emanating from the companion meets the pulsar wind. If, for some reason, there is a variation in the wind pressure at this shock front, its thickness and density will vary, the latter increasing sometimes to the point at which it produces an eclipse. This would not have a strong effect on the total number of electrons, which is consistent with what was observed in January 1998. The fact that the whole object is transparent at a frequency of 1400 MHz indicates, according to equation 2.2, that nowhere along the line-of-sight has the electron density reached 2.4×10^{10} cm^{-3}.

The mass loss of these binary systems is associated with long-term evolution of their orbital periods. We have not yet conclusively detected such an evolution for any of the binaries, so we won't discuss this important subject here.

We finish making a preliminary estimate of the visual magnitudes of these systems in 47 Tuc. As remarked in § 7.3, the optical emission originates in the face of the companion that is exposed to the pulsar, therefore the optical light-curve is modulated according to the orientation of this face as seen from the Solar System; the period of this modulation is, off course, the orbital period of the binary. The estimated maximum red magnitudes for PSR B1957+20 and PSR J2051−0827 are respectively 19.5 and 22.3 (Callanan et al. 1995, Stappers,

Bessell & Bailes 1996). Since the distances to these pulsars are 1.6 kpc and 1.3 kpc respectively (see previous references), their absolute red magnitudes are 8.4 and 11.7. At the distance of 47 Tuc, these magnitudes will be increased by the distance modulus, 13.5 (Reid 1998), therefore if placed in 47 Tuc these binaries would have apparent magnitudes of 21.9 and 25.2. The binary systems 47 Tuc I, J, O, P, R and possibly W probably have rather similar visual magnitudes, which means that in principle some of these binary systems should be detectable on the extensive and deep observations of 47 Tuc that have been made by the HST in the last few years. This detection should now be made much easier with the precise positions we have obtained in this work for 47 Tuc I, J and O. We are presently part of a collaboration that is investigating this possibility.

Chapter 8

Conclusion

8.1 Overview of results presented in this work

The results in this work represent a vast improvement of our knowledge of the pulsar population in 47 Tuc. Before, eleven millisecond pulsars were known, the searches described in this work added nine binary millisecond pulsars and detected all the previous pulsars.

Before, only three orbital solutions were known, now we know 12. We find the binaries divide into two main groups, with companions masses of ~ 0.03 and ~ 0.1–0.2 M$_\odot$. One of the pulsars with a low-mass companion (47 Tuc R) has the shortest orbital period measured for any radio pulsar (1.6 hours).

Although all these pulsars have rotational periods below 8 ms, we determined that their pulsewidth distribution is similar to that of the pulsars in the disk of the galaxy, we have also determined that the pulsar luminosity distribution is similar to that observed for the pulsars observed in the galactic disk and in M15.

Some of the newly discovered pulsars are extremely faint and have orbital periods of about one day. They are detected only occasionally (i.e., every few hundred days), when interstellar scintillation amplifies their emission. This made

the determination of their orbital parameters an apparently insurmountable problem. We describe a new technique that allows us to determine orbital parameters without the need to know the number of orbits between detections; this procedure needs only the accelerations and periods provided by the accelerated pulsar searches. With the estimates of orbital parameters provided by this procedure, we describe methods that allow us to remove orbital period ambiguities even with extremely sparse data sets and to obtain very precise estimates of the orbital period.

Before, we knew of one eclipsing binary (47 Tuc J), now we know of at least four in 47 Tuc (47 Tuc J, O, R, W and possibly V), there are at least as many known eclipsing binary pulsars in 47 Tuc as in the rest of the Universe.

Before, we knew only two timing solutions, now 15. This latest piece of information allowed us to determine accurate positions, periods, period derivatives and DMs for all 15 pulsars and extremely precise orbital parameters for 8 of the binaries. We find that all pulsars in the cluster lie within $1\overset{\prime}{.}2$ from the centre of the cluster, and that their distribution inside that region is consistent with an isothermal ($\rho(r) \propto 1/r^2$) distribution similar to that found for the blue straggler stars. This sort of distribution is unlike that found for the pulsars in M15. We have determined the proper motions for four pulsars, and reached the conclusion that these motions are mainly caused by the motion of the cluster. All the individual pulsar motions, and in particular their average, are consistent with the values of proper motion determined for 47 Tuc using data from the Hipparcos satellite.

We have used the negative period derivatives of some pulsars to place constraints on the projected surface mass density of the cluster, and have seen that the accelerations are compatible with those predicted by a single-mass King model. We could also derive limits for the ages and magnetic fields of the pulsars,

these are consistent with the galactic millisecond pulsar population. No pulsar is younger than 170 Myr and none has a magnetic field stronger than 2.3×10^5 T; which again does not happen in M15, which seems to be undergoing a burst of pulsar formation. The difference is probably due to the fact that the globular cluster M15 is presently undergoing core collapse, which leads to a much increased rate of LMXB and MSP formation; the core of 47 Tuc is comparatively more relaxed. This fundamental difference probably explains the different pulsar radial distributions as well. We have also used the newly determined, precise values of the DMs and period derivatives to infer the presence of a cloud of plasma in 47 Tuc; which is perhaps the most surprising result.

We have reviewed some of the current thinking about the formation and evolution of the millisecond pulsars in globular clusters in general and in 47 Tuc in particular. The binary pulsars with light companions seem to have had IMXBs as progenitors and undergone a later episode of orbit decay and mass transfer, while the remaining binaries will have both IMXBs and LMXBs as progenitors. The cluster lacks binary pulsars with periods longer than ~ 2 days, this suggests that the core of the cluster has been rather dense for a few billion years, with the tightening of the binaries providing the energy necessary to sustain the core of the cluster against gravitational collapse. If the cluster had just reached its present central density, then we should expect the presence of a few binary systems with longer orbital periods. This result probably explains the very high incidence of pulsars (and also blue stragglers) in 47 Tuc compared to other clusters with similar (or higher) masses and central densities; it is plausible that a long episode of pre-core collapse will lead to increased formation rates for these objects.

The large number of binaries now known has allowed us to notice for the first time an apparent correlation, among short-period binaries, of lack or eclipses with very low mass functions. This result, if confirmed by new discoveries, can only

be understood if these eclipsing short-period, low-mass binaries have a narrow distribution of companion masses.

We discussed the origins of the eccentricities of the 47 Tuc binaries and used one of these eccentricities to measure the total mass of the 47 Tuc H binary system, one of the most precise determinations so far of the mass of a neutron star-white dwarf binary. We have also measured the variations of the DM of 47 Tuc J as a function of orbital phase, thus probing the plasma emanating from the companion object. The eclipsing object is transparent at frequencies of 1400 MHz, and it has an average density of $\sim 10^6$ electrons cm^{-3} along the line-of-sight.

8.2 Future observations

A continuing timing programme will certainly lead to vast improvements in the measurements of the proper motions of the pulsars. The typical precision for the positions of the weakest pulsars is around $5\,\text{mas}$. In order to obtain a precision of $0.15\,\text{mas}\,\text{yr}^{-1}$ required to measure their intrinsic motions in the cluster with a 3-σ confidence level, we would need to measure the positions of these pulsars again in ~ 50 years' time. However, for the brightest pulsars, with positional accuracies of about $0.5\,\text{mas}$, it will be enough to make another measurement in about 5 years, using current data-acquisition systems. These times can be cut by $\sqrt{N}$ if precise positions measurements are made in N years, i.e., for the weakest pulsars measuring positions 16 years in a row with the recently acquired timing precision would give a precision in proper motion of 2×5 mas $/ 16$ years $/ \sqrt{16} = 0.16$ mas yr^{-1}. The brightest pulsars would have their proper motions determined with ten times this accuracy. The measurement of such precise proper motions would add two dimensions to dynamical studies of the cluster using pulsar data, and significant constraints to the mass model of the cluster.

Continued timing will also allow a better determination of the orbital parameters of 47 Tuc H, and will test whether 47 Tuc G and I are physically associated by determining limits for their $\dddot{P}$. Additional solutions for known pulsars may also be determined. For instance, 47 Tuc P, R and W might have their timing solutions determined soon. For these pulsars, with well known P, P_B, x and DM, a search for the pulsar in each observation will soon be made. For each observation, the only parameter being searched is the time of ascending node T_{asc}, for this is the only unknown parameter that is necessary for the proper folding of the whole observation. The value of this parameter is not precisely known because at this stage the value for P_B is not precise enough to predict exactly the orbital phase many days before or after the available detections of these pulsars. We will be sure of a detection of the pulsar if its known pulse profile emerges from the folding of an observation. A set of T_{asc} can then be used to refine the orbital period by using the procedures described in § 4.3, or the program "ORBITFIT". A coherent timing solution for 47 Tuc S might be determined even sooner, because for this pulsar the orbital ephemeris is now so precise that we can search for the signal in new observations just by folding new data.

A pulsar like 47 Tuc V must have its orbit determined in the first place. The signal from this pulsar seems to be rather strong, but it is, apparently, eclipsed most of the time, as if the pulsar was shrouded in the gas envelope of the companion object. Perhaps observations at higher frequencies might increase the number of detections of this and other eclipsing pulsars, and even uncover new pulsars. It is clear that new pulsars will be found just by continuing observations of 47 Tuc at 1400 MHz. Continued radio monitoring of this cluster is therefore likely to remain a worthy enterprise.

Also, searches for the pulsars and their companions should be made in optical and X-ray wavelengths, using HST, Chandra and XMM data and the precise

pulsar positions presented in this work. According to the estimate made in § 7.4.2, some HST data sets should be deep enough to detect some of the pulsar companions. On the other hand, Chandra has a powerful combination of sensitivity and spatial resolution that should allow the detection of at least some of the pulsars in X-Rays.

Appendix A

The orbital fitting programs

A.1 CIRCORBIT

Fitting an ellipse to set of points can be quite cumbersome, at least from a computational point of view. However, eqns. (4.8) and (4.9) can be combined to derive a simple expression, which is linear in the unknown parameters and hence easy to fit. By squaring each of the equations, multiplying one of the squares by an appropriate constant and summing them, we obtain the simple equation of a parabola, given in the form

$$A^2 = a_2 P^2 + a_1 P + a_0, \tag{A.1}$$

where A and P represent the accelerations and periods. It is straightforward to model the set of squares of the accelerations and the corresponding periods, (A_k^2, P_k) by applying a linear least squares fitting algorithm. We use the Singular Value Decomposition method, as for instance described by Press et al. (1992), to determine the coefficients a_0, a_1 and a_2. [1] The period and the orbital parameters are then given by

---

[1] We note as a technical detail, that instead of using the original periods, P_k, we use in fact a scaled version of those during the fit to avoid numerical problems, i.e. we use an expression $C \cdot (P_k - \bar{P})$, where C is a constant and $\bar{P}$ the mean of all measured P_k's.
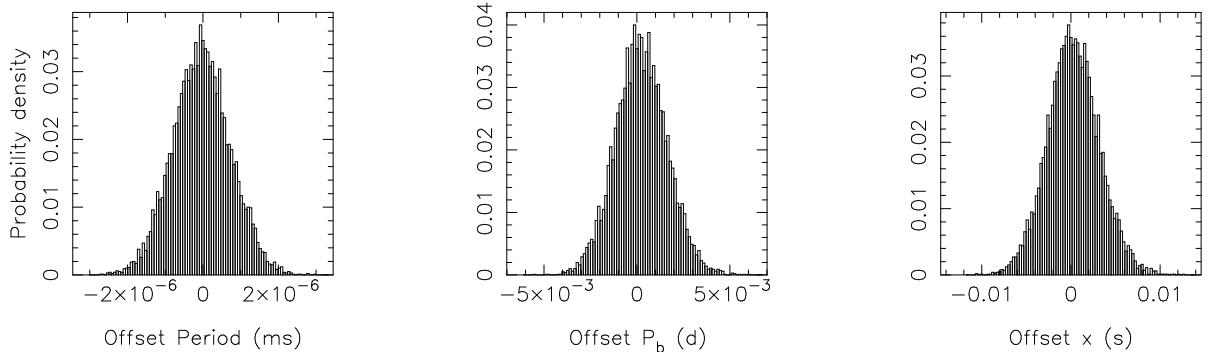
Figure A.1: Distributions of the parameters obtained by fitting 10000 synthetic data sets generated in the Monte Carlo simulation in the case of 47 Tuc W. The values for the orbital parameters so determined are accurate to within 1%. Each distribution shows the offset from the best fit value.

$$P_0 = -\frac{a_1}{2a_2} \tag{A.2}$$

$$P_B = \frac{2\pi c}{P_0\sqrt{-a_2}} \tag{A.3}$$

$$x = \frac{P_B}{2\pi P_0}\sqrt{P_0^2 - \frac{a_0}{a_2}} \tag{A.4}$$

Despite the simplicity of the problem, there are large covariances among the fitted parameters a_0, a_1 and a_2, making it difficult to obtain reliable error estimates for the derived parameters. For this reason, we employed a Monte-Carlo method in our fitting algorithm, which provides not only precise values of the orbital parameters but also reliable and realistic estimates of their uncertainties. To achieve this, we generate a total of 10000 synthetic data sets, each having the same number of observations as the original set of real observations. For a given synthetic data set, the generated random periods and accelerations are Gaussian distributed while centred on the real observed data points, with dispersions given by the observational uncertainties.

We perform the described fit algorithm for each synthetic data set and obtain

probability distributions for the orbital parameters as shown in Figure A.1 for the case of 47 Tuc W. We choose the median of each probability distribution as our best fit value of a given orbital parameter and calculate its uncertainty from the spread in its distribution. The reliability of this method is demonstrated in Table 4.1 where we compare the parameters obtained using this method (columns 2 to 4) with the parameters as determined in the subsequent timing analysis (columns 5 to 8). The comparison clearly demonstrates that our new procedure provides accurate values and calculates reasonable error estimates. The program with the implementation of the algorithm described above is called "CIRCORBIT", because it applies only to low-eccentricity orbits.

The Monte-Carlo method is also used in estimating the orbital phases for each period/acceleration point and the T_{asc} of each orbit according to equations 4.12 and 4.13. These estimates are necessary for next step of the refinement of the orbit, which is made using the program described next.

A.2 ORBITFIT

We have developed two independent methods to perform the task of refining the estimate of the orbital period of the pulsar, as explained in §4.3, which are more accurate than the periodogram method explained in that section, and have been implemented in a program called "ORBITFIT". In the first method, we essentially treat each $T_{\mathrm{asc,k}}$ derived from Eqn. (4.13) as a TOA. For each observation, k, we compute a "residual"

$$R_k = \frac{T_{\mathrm{asc,k}} - T_{\mathrm{asc,1}}}{P_B} - \lfloor \frac{T_{\mathrm{asc,k}} - T_{\mathrm{asc,1}}}{P_B} \rfloor \qquad (\mathrm{A.5})$$

(where $\lfloor a \rfloor$ is the largest integer smaller than a) and plot it against each $T_{\mathrm{asc,k}}$. If the previous estimate of P_B used in eq. A.5 is correct, then all R_k should be randomly distributed around zero. An error in P_B results in a slope in the data

points. Hence, we model this by performing a least squares fit of a straight line and repeat this procedure for a set of trial P_Bs. We start with our previous best estimate and search a range of P_Bs, such that the total phase difference over the whole time span, $T_{\mathrm{asc,n}} - T_{\mathrm{asc,1}}$ does not exceed unity (as we can assume that our previous guess was sufficiently close to the correct value). We note that for each trial P_B, we re-calculate the $T_{\mathrm{asc,k}}$'s using the phases, ϕ_k, from Eqns. (4.12) and (4.13). The results of the straight line fit are then used to correct the previous estimates for T_{asc} and P_B. If the fitted P_B and T_{asc} are at some point coincident with those of the binary, we should expect to see a sharp decrease in the residuals given by eq. A.5.

In the second method, we make direct use of the phase information, ϕ_k, by fitting the function

$$\phi = \frac{T - T_{\mathrm{asc}}}{P_B} - \lfloor \frac{T - T_{\mathrm{asc}}}{P_B} \rfloor \qquad (A.6)$$

to our data set of observing epochs and derived phase information (T_k, ϕ_k). We perform a least squares minimization, where due to the non-linear nature of Eqn. A.6 we employ a robust Downhill-Simplex algorithm (Press et al. 1992) to obtain T_{asc} and P_B. We start the simplex routines for various starting points using $T_{\mathrm{asc,1}}$ and a variation of P_B as in the first method. In order to obtain reliable error estimates, we again use a Monte-Carlo simulation as described before, generating a synthetic data set from the real (T_k, ϕ_k)'s and the error estimates for the phase as derived from the first Monte-Carlo application.

Our experience shows that both methods yield very similar results, usually agreeing within the errors. However, depending on the spread of the data points, length of total time covered and uncertainties, one or the other method may yield superior results. While the orbital solution for 47 Tuc T was refined using the first method, the second method provided better results in the case of 47 Tuc S. Applying both methods at the same time serves in fact as a good indicator whether

the obtained solution is unique.

A.3   FITORBIT

The "classical" pulsar period analysis is made at Jodrell Bank using the program FITORBIT, which was written originally by A. Brinklow and A. Lyne. This program acts in three main steps:

1) Reads in the parameters describing the rotation, binary motion and position of the pulsar (i.e., the pulsar ephemeris) from file (pulsar name).eph.

2) Reads in the observed rotational periods of the pulsar at the barycentre ($P_{b,i}$), and the corresponding barycentric epochs (t_i) from file (pulsar name).per.

3) Minimizes the sum of the squares of the differences of the $P_{b,i}$ and the rotational periods of the pulsar at the barycentre predicted by the pulsar ephemeris, $p_{b,i}$ for the same epochs t_i by varying a group of ephemeris parameters selected by the user. This is accomplished using the Levenberg-Marquardt Method (also called "LMM", see Press et al. 1992).

In this program, the predicted periods p_i depend on 10 parameters: two of them are rotational (the intrinsic rotational period at T_0, P_0 and the period derivative, $\dot{P}$), two of them describe the position of the pulsar in the celestial sphere (α and δ), five are the Keplerian parameters for the orbit (Time of passage through periastron T_0, binary period P_B, the projected semi-major axis of the orbit in light seconds, x, the longitude of periastron, ω, and the eccentricity, e). The last parameter is the particular time of each observation, t_i, in the barycentre of the solar system. To simplify the problem, this time is assumed to be the same in the reference frame of the pulsar and in the reference frame of the centre of mass of the binary (henceforth "CM"). This is not a problem because, even in a fast binary, significant changes in the observed rotational period occur in timescales of at least a few minutes.
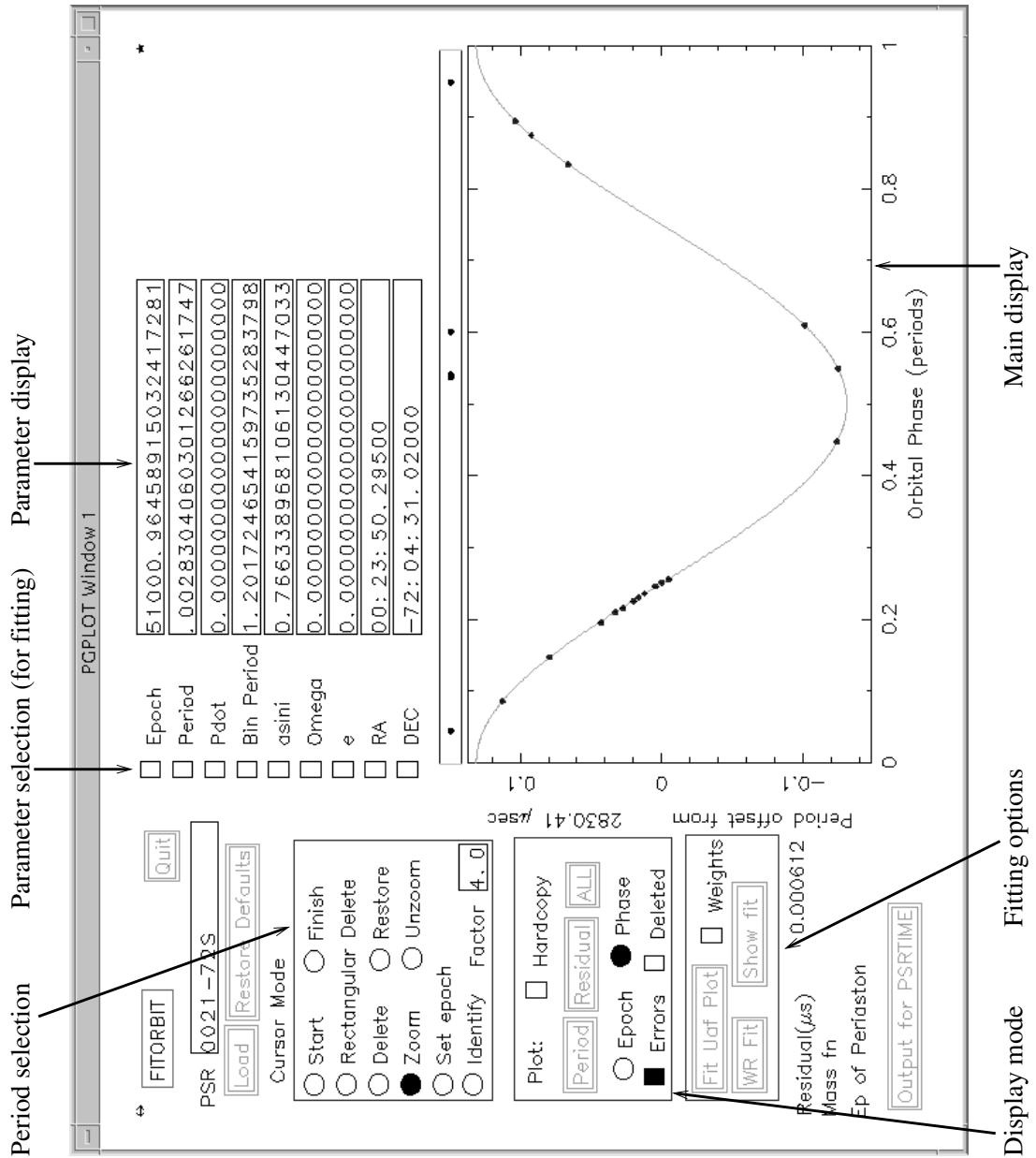
Figure A.2: The FITORBIT interface. In the main display, the sinusoidal line represents the orbital model's prediction of the barycentric rotational period of the pulsar being displayed, the dots represent the observed barycentric rotational periods of that pulsar.

The predicted period $p_{b,i}$ is calculated in two steps. In the first step, we calculate the intrinsic rotational period of the pulsar, P, using the following equation:

$$P = P_0 + \dot{P}(t_i - T_0) \tag{A.7}$$

In the second step, we calculate an eccentric anomaly $E(T)$ from the value of the mean anomaly $M(T) = n_B(T - T_0)$ by solving Kepler's equation (eq. 4.15, for an easy reference on the iterative methods to solve this equation see e.g. Roy 1988). From the value for the eccentric anomaly, we calculate the true anomaly f using equation 4.14. From this true anomaly, we calculate a velocity along the line-of-sight v_l using equation 4.5. From this velocity, we calculate a Doppler-shifted period p using equation 4.6, with no second or higher order terms:

$$p_{b,i} = P\left(1 + \frac{v_l(t_i)}{c}\right) \tag{A.8}$$

This is the rotational period predicted in the barycentre of the solar system. If the orbital parameters are right, the $p_{b,i}$ should be very similar to the observed $P_{b,i}$, provided that these $P_{b,i}$ were properly calculated from the rotational periods for the pulsar measured at the telescope (the "topocentric periods", or $P_{t,i}$). This calculation subtracts the effect on the rotational period of the pulsar pulsar caused by the component of the velocity of the radio telescope relative to SSB ($\mathbf{v}_\oplus$) along the assumed direction of the pulsar, $\mathbf{n}'$.

$$P_{b,i} = P_{t,i} - \frac{\mathbf{v}_\oplus(t_i)}{c}.\mathbf{n}' \tag{A.9}$$

the quantity $\mathbf{v}_\oplus.\mathbf{n}'$ is calculated using a solar system ephemeris. However, if this direction is in error by an amount $d\alpha$ in right ascension and $d\delta$ in declination, the velocity of the Earth is being projected in the wrong axis, and therefore the calculated $P_{b,i}$ is in error by an amount $\Delta P_{b,i}/P_{b,i} = \Delta V(t)/c$, where $\Delta V(t)$ is given by

$$\Delta V(t) = \mathbf{v}_\oplus(t).(\mathbf{n} - \mathbf{n}') \tag{A.10}$$

where $\mathbf{n}$ is the true direction to the pulsar. This error displays itself as an apparent yearly variation in the rotational period of the pulsar. The positional parameters α and δ can be fitted so that ΔV vanishes, i.e., $\mathbf{n}' = \mathbf{n}$, the resulting α and δ should then be the true position of the pulsar in the sky.

The previous effect on the rotational period of the pulsar, although very small compared to the velocity contributions normally caused by binary systems, is sometimes noticeable. The average orbital velocity of the Earth is about $29\,\mathrm{km\,s^{-1}}$. For a direction to a pulsar perpendicular to the motion of the Earth, an error in position of one arcminute represents an error in velocity $\Delta V = 8.4\,\mathrm{m\,s^{-1}}$. This is detectable if the relative error in the measurement of the period is of the order or smaller than $\Delta V/c$, in the previous case this is $\sim 3 \times 10^{-8}$. For some isolated pulsars, rotational periods with much better precisions can be measured over several intervals of the order of a week to a month. These periods can be converted to SSB, if the assumed position for the pulsar was incorrect, then a yearly modulation appears in the calculated SSB periods (due to an incorrect subtraction of the motion of the Earth). In that case, minimizing the ΔVs in equation A.10 will lead to a position for the pulsar in the sky which can in some cases be accurate to a few arcseconds; such a procedure can in some cases ease considerably the determination of a phase-coherent timing solution.

FITORBIT has a user-friendly interface, which is depicted in figure A.2.

Appendix B

The ELL1 orbital model

Details of the implementation of the orbital model ELL1, by Norbert Wex, in 1998, have never been published, although they have been presented by himself in a workshop in Aspen, in 1998.

This appendix is to be presented in a study of PSR J1012+5307, by Lange et al. (2000)**?**, which has recently been submitted to *MNRAS*. The author of this thesis does not claim to have had any contribution to the implementation of this orbital model; nor in writing what follows in this Appendix, but presents it here for the sake of completeness; there are, so far, no published or easily available references on the subject.

B.1   A timing model for small-eccentricity binary pulsars

The Roemer delay due to the motion of a pulsar in a binary system is given in Blandford & Teukolsky (1976), or D'Amour and Deruelle (1986) by equation 5.9. Neglecting terms of order e^2, the 3-D position of a pulsar $\mathbf{X}(T) = R(T) \times$

$(\sin\phi, \cos\phi, 0)$ is given by (Roy 1988)

$$R = a_P(1 - e\cos M) \tag{B.1}$$

$$\phi = M + 2e\sin M \tag{B.2}$$

As before, $M = n_B(T - T_0)$ represents the mean anomaly and n_B the mean angular velocity of the binary. The position $M = \phi = 0$ corresponds to the location of periastron. To first order approximation in the small eccentricity e the Roemer delay can be written as

$$\triangle_R = x\left(\sin\Phi + \frac{\kappa}{2}\sin 2\Phi - \frac{\eta}{2}\cos 2\Phi\right) \tag{B.3}$$

where

$$\Phi = n_B(T - T_{\mathrm{asc}}) \tag{B.4}$$

and

$$\eta = e\sin\omega \tag{B.5}$$

$$\kappa = e\cos\omega \tag{B.6}$$

are the Laplace-Lagrange parameters. The actual time when the pulsar passes through the ascending node is given by $T_{\mathrm{asc}} + \eta P_B/\pi$. The time of superior conjunction is given by $T_{\mathrm{asc}} + P_B/4 - 2\kappa P_B/\pi$.

Equation B.3 accounts only for first-order corrections in e. Therefore, the difference between the exact expression given by equation 5.9 and B.3 can grow up to e^2. For most of the low-eccentricity binary pulsars the error in the TOA measurements is much larger than xe^2, so the model linear in e is sufficient.

Secular changes in the parameters n_B, x, e and ω are accounted for in the new timing model by using

$$\Phi = n'_B(T - T_{\mathrm{asc}}) + \frac{1}{2}\dot{n}_B(T - T_{\mathrm{asc}}) \tag{B.7}$$

and

$$x = x_0 + \dot{x}(T - T_{\text{asc}}), \tag{B.8}$$

$$\eta = \eta_0 + \dot{\eta}(T - T_{\text{asc}}), \tag{B.9}$$

$$\kappa = \kappa_0 + \dot{\kappa}(T - T_{\text{asc}}). \tag{B.10}$$

in equation B.3. The terms used in the last equations are defined by

$$n_B' = n_B + \dot{\omega} - \dot{n}_B(T_0 - T_{\text{asc}}) \tag{B.11}$$

$$T_{\text{asc}} = T_0 - \frac{\omega_0}{n_B + \dot{\omega}} \tag{B.12}$$

$$\dot{\eta} = \dot{e}\sin\omega + e\cos\omega\dot{\omega} \tag{B.13}$$

$$\dot{\kappa} = \dot{e}\cos\omega - e\sin\omega\dot{\omega}. \tag{B.14}$$

B.2 Small-eccentricity orbits and Shapiro delay

For small-eccentricity binary pulsars the Shapiro delay can be written as

$$\triangle_S = -2r\ln(1 - s\sin\Phi) \tag{B.15}$$

where $r = Gm_c/c^3$ and $s = \sin i$. As a Fourier series, equation B.15 takes the form

$$\triangle_S = 2r(a_0 + b_1\sin\Phi - a_2\cos 2\Phi + ...) \tag{B.16}$$

where

$$a_0 = -\ln\left(\frac{1 + \sqrt{1 - s^2}}{2}\right), \tag{B.17}$$

$$b_1 = 2\frac{1 - \sqrt{1 - s^2}}{s}, \tag{B.18}$$

$$a_2 = 2\frac{1 - \sqrt{1 - s^2}}{s^2} - 1. \tag{B.19}$$

Only for orbits where $\sqrt{1 - s^2} << 1$ (nearly edge-on) higher harmonics become significant. Otherwise, the Shapiro delay cannot be separated from the

Roemer delay. Consequently, the observed values for x and η differ from their intrinsic values by

$$x^{\mathrm{obs}} \quad = \quad x + 2rb_1, \tag{B.20}$$

$$\eta^{\mathrm{obs}} \quad = \quad \eta + 4ra_2/x \tag{B.21}$$

as can be seen from a comparison of equations B.16 with equation B.3. This means that the observed values of eccentricity e and longitude of periastron ω are different from the intrinsic values of these parameters.

Therefore, a small but significant η does not necessarily imply the detection of a small eccentricity, but a non-zero κ cannot be explained otherwise.

Bibliography

Alpar, M. A., Cheng, A. F., Ruderman, M. A. & Shaham, J. (1982), 'A new class of radio pulsars', *Nature* **300**, 728–730.

Anderson, S. B. (1992), A study of recycled pulsars in globular clusters, PhD thesis, California Institute of Technology.

Anderson, S. B., Gorham, P. W., Kulkarni, S. R. & Prince, T. A. (1990), 'Discovery of two radio pulsars in the globular cluster M15', *Nature* **346**, 42–44.

Anderson, S. B., Wolszczan, A., Kulkarni, S. R. & Prince, T. A. (1997), 'Observations of two millisecond pulsars in the globular cluster NGC 5904', *ApJ* **482**, 870–873.

Arzoumanian, Z. (1995), Radio Observations of Binary Pulsars: Clues to Binary Evolution and Tests of General Relativity, PhD thesis, Princeton University.

Arzoumanian, Z., Fruchter, A. S. & Taylor, J. H. (1994), 'Orbital variability in the eclipsing pulsar binary PSR B1957+20', *ApJ* **426**, L85–L88.

Arzoumanian, Z., Joshi, K., Rasio, F. & Thorsett, S. E. (1996), Orbital parameters of the PSR B1620−26 triple system, *in* Johnston et al. (1996), pp. 525–530.

Baade, W. & Zwicky, F. (1934), 'On super-novae', *Proc. Nat. Acad. Sci.* **20**, 254–259.

Backer, D. C. (1993), A pulsar timing tutorial and NRAO Green Bank observations of PSR 1257+12, *in* J. A. Phillips, S. E. Thorsett & S. R. Kulkarni, eds, 'Planets around Pulsars', Astron. Soc. Pac. Conf. Ser. Vol. 36, pp. 11–18.

Backer, D. C., Foster, R. F. & Sallmen, S. (1993), 'A second companion of the millisecond pulsar 1620−26', *Nature* **365**, 817–819.

Backer, D. C., Kulkarni, S. R., Heiles, C., Davis, M. M. & Goss, W. M. (1982), 'A millisecond pulsar', *Nature* **300**, 615–618.

Backer, D. C. & Thorsett, S. E. (1995), PSR 1620−26 - A Triple System, *in* A. Fruchter, M. Tavani & D. Backer, eds, 'ASP Conf. Ser. 72: Millisecond Pulsars. A Decade of Surprises', pp. 387–390.

Bailyn, C. D. & Grindlay, J. E. (1990), 'Neutron stars and millisecond pulsars from accretion–induced collapse in globular clusters', *ApJ* **353**, 159–167.

Bhattacharya, D. (1991), The formation of neutron stars in the galaxy, *in* J. Ventura & D. Pines, eds, 'Neutron Stars: Theory and Observation', Kluwer, Dordrecht, pp. 103–123.

Bhattacharya, D. (1998), Detection of radio emission from pulsars: a pulsar observation primer, *in* Bucheri & van Paradijs M. A. Alpar (1998), pp. 103–128.

Biggs, J. D., Bailes, M., Lyne, A. G., Goss, W. M. & Fruchter, A. S. (1994), 'Two radio pulsars in the globular cluster NGC 6624', *MNRAS* **267**, 125–128.

Biggs, J. D. and Lyne, A. G. and Manchester, R. N. and Ashworth, M., 1990. IAU Circ. No. 4988.

Bionta, R. M., Blewitt, G., Bratton, C. B., Casper, D., Ciocio, A., Claus, R., Cortez, B., Crouch, M., Dye, S. T., Erreded, S., Foster, G. W., Gajewski, W., Ganezer, K. S., Goldhaber, M., Haines, T. J., Jones, T. W., Kielczewaska,

D., Kropp, W. R., Learned, J. G., LoSecco, J. M., Matthews, J., Miller, R., Mudan, M. S., Park, H. S., Price, L. R., Reines, F., Schultz, J., Seidel, S., Shumard, E., Sinclair, D., Sobel, H. W., Stone, J. L., Sulak, L. R., Svoboda, R., Thornton, G., van der Velde, J. C. & Wuest, C. (1987), 'Observation of a neutrino burst in coincidence with supernova 1987A in the Large Magellanic Cloud', *Phys. Rev. Lett.* **58**, 1494–1496.

Blandford, R. & Teukolsky, S. A. (1976), 'Arrival-time analysis for a pulsar in a binary system', *ApJ* **205**, 580–591.

Bucheri, R. & van Paradijs M. A. Alpar, J., eds (1998), *The Many Faces of Neutron Stars (NATO ASI Series)*, Kluwer, Dordrecht, Boston, London.

Callanan, P. J., Charles, P. A. & van Paradijs, J. (1989), 'The optical light curve of PSR 1957+20', *MNRAS* **240**, 31P–34P.

Callanan, P. J., van Paradijs, J. & Regelink, R. (1995), 'The orbital light curve of PSR 1957+20', *ApJ* **439**, 928–932.

Camilo, F. (1995*a*), A Search for Millisecond Pulsars, PhD thesis, Princeton University.

Camilo, F. (1995*b*), Millisecond pulsar searches, *in* A. Alpar, Ü. Kiziloğlu & J. van Paradis, eds, 'The Lives of the Neutron Stars (NATO ASI Series)', Kluwer, Dordrecht, pp. 243–257.

Camilo, F., Lorimer, D. R., Freire, P., Lyne, A. G. & Manchester, R. N. (2000), 'Observations of 20 millisecond pulsars in 47 Tucanae at 20 cm', *ApJ* **535**, 975–990.

Camilo, F., Nice, D. J. & Taylor, J. H. (1996), 'A search for millisecond pulsars at galactic latitudes $-50° ltblt - 20°$', *ApJ* **461**, 812–819.

Camilo, F., Thorsett, S. E. & Kulkarni, S. R. (1994), 'The magnetic fields, ages and original spin periods of millisecond pulsars', *ApJ* **421**, L15–L18.

Carreta, E., Gratton, R. G., Clementini, G. & Fusi Pecci, F. (2000), 'Distances, ages, and epoch of formation of globular clusters', *ApJ* **533**, 215–235.

Chandrasekhar, S. (1931), 'The Maximum Mass of Ideal White Dwarfs', *ApJ* **74**, 81–82.

Chen, K. & Ruderman, M. (1993), 'Origin and radio pulse properties of millisecond pulsars', *ApJ* **408**, 179–185.

Colgate, S. A. & White, R. H. (1966), 'The hydrodynamic behavior of supernovae explosions', *ApJ* **143**, 626–681.

Cordes, J. M. & Chernoff, D. F. (1997), 'Neutron Star Population Dynamics. I. Millisecond Pulsars', *ApJ* **482**, 971–992.

Da Costa, G. S. (1979), 'The structure and stellar content of globular clusters. i - surface-brightness profiles for four southern clusters', *Astron. J.* **84**, 505–514.

D'Amico, N., Bailes, M., Lyne, A. G., Manchester, R. N., Johnston, S., Fruchter, A. S. & Goss, W. M. (1993), 'PSR B1802-07: A globular cluster pulsar in an eccentric binary system', *MNRAS* **260**, L7–L10.

D'Amico, N. and Lyne, A. G. and Bailes, M. and Johnston, S. and Manchester, R. N. and Staveley–Smith, L. and Lim, J. and Fruchter, A. S. and Goss, W. M., 1990. IAU Circ. No. 5013.

Damour, T. & Deruelle, N. (1986), 'General relativistic celestial mechanics of binary systems. II. The post-Newtonian timing formula', *Ann. Inst. H. Poincaré (Physique Théorique)* **44**, 263–292.

Damour, T. & Taylor, J. H. (1991), 'On the orbital period change of the binary pulsar PSR 1913+16', *ApJ* **366**, 501–511.

De Marchi, G., Paresce, F., Stratta, M. G., Gilliland, R. L. & Bohlin, R. C. (1996), 'The density profile of 47 Tucanae', *ApJ* **468**, L51–L54.

Deeter, J. E., Pravdo, S. H. & Boynton, P. E. (1981), 'Pulse-timing observations of Hercules X-1', *ApJ* **247**, 1003–1012.

Deich, W. T. S., Middleditch, J., Anderson, S. B., Kulkarni, S. R., Prince, T. A. & Wolszczan, A. (1993), 'The binary pulsar PSR 1908+00 in NGC 6760', *ApJ* **410**, L95–L98.

Dewey, R., Stokes, G., Segelstein, D., Taylor, J. & Weisberg, J. (1984), The period distribution of pulsars, *in* S. Reynolds & D. Stinebring, eds, 'Millisecond Pulsars', NRAO : Green Bank, pp. 234–240.

Djorgovski, S. G. (1993), Physical parameters of galactic globular clusters, *in* Djorgovski, S. G. and Meylan, G. (1993), pp. 373–382.

Djorgovski, S. G. and Meylan, G., ed. (1993), *ASP Conf. Ser. 50: Structure and Dynamics of Globular Clusters*, Astronomical Society of the Pacific, San Francisco.

Djorgovski, S. & Meylan, G. (1993), The Galactic Globular Cluster Systems - a List of the Known Clusters and Their Positions, *in* Djorgovski, S. G. and Meylan, G. (1993), pp. 325–336.

Edmonds, P. D., Gilliland, R. L., Guhathakurta, P., Petro, L. D., Saha, A. & Shara, M. M. (1996), 'Stellar Variability in the Central Populations of 47 Tucanae from WF/PC Observations with the Hubble Space Telescope. II. Binary Systems', *ApJ* **468**, 241–260.

Ferguson, C., Lei, F., Dean, A. J., Bird, A. J. & Lockley, J. J. (1999), 'New observational constraints on hard X-/gamma -ray millisecond pulsar emission from 47 Tucanae', *A&A* **350**, 847–851.

Foster, R. S., Backer, D. C., Taylor, J. H. & Goss, W. M. (1988), 'Period derivative of the millisecond pulsar in globular cluster M28', *ApJ* **326**, L13–L15.

Fruchter, A. S., Bookbinder, J. & Bailyn, C. (1995), 'HST images of the eclipsing pulsar PSR B1957+20', *ApJ* **443**, L21–L24.

Fruchter, A. S., Bookbinder, J., Garcia, M. R. & Bailyn, C. D. (1992), 'X-rays from the eclipsing pulsar 1957+20', *Nature* **359**, 303–304.

Fruchter, A. S. & Goss, W. M. (2000), 'Deep Radio Imaging of Globular Clusters and the Cluster Pulsar Population', *ApJ* **536**, 865–874.

Fruchter, A. S., Gunn, J. E., Lauer, T. R. & Dressler, A. (1988), 'Optical detection and characterization of the eclipsing pulsar's companion', *Nature* **334**, 686–689.

Fruchter, A. S., Stinebring, D. R. & Taylor, J. H. (1988), 'A millisecond pulsar in an eclipsing binary', *Nature* **333**, 237–239.

Giaconni, R., Gursky, H., Paolini, F. R. & Rossi, B. (1962), 'Evidence for X-rays from sources outside the solar system', *Phys. Rev. Lett.* **9**, 439–443.

Gilliland, R. L., Bono, G., Edmonds, P. D., Caputo, F., Cassisi, S., Petro, L. D., Saha, A. & Shara, M. M. (1998), 'Oscillating Blue Stragglers in the Core of 47 Tucanae', *ApJ* **507**, 818–845.

Glendenning, N. K. (1992), 'Limiting rotational period of neutron stars', *Phys. Rev. D* **46**, 4161–4168.

Gold, T. (1969), 'Rotating neutron stars and the nature of pulsars', *Nature* **221**, 25–27.

Goldreich, P. & Julian, W. H. (1969), 'Pulsar electrodynamics', *ApJ* **157**, 869–880.

Gratton, R. G., Fusi Pecci, F., Carretta, E., Clementini, G., Corsi, C. E. & Lattanzi, M. (1997), 'Ages of Globular Clusters from Hipparcos Parallaxes of Local Subdwarfs', *ApJ* **491**, 749–771.

Guhathakurta, P., Yanny, B., Schneider, D. P. & Bahcall, J. N. (1992), 'Globular cluster photometry with the Hubble Space Telescope. I. Description of the method and analysis of the core of 47 Tuc', *Astron. J.* **104**, 1790–1817.

Hamilton, T. T., Helfand, D. J. & Becker, R. H. (1985), 'A search for millisecond pulsars in globular clusters', *Astron. J.* **90**, 606–608.

Hasinger, G., Johnston, H. M. & Verbunt, F. (1994), 'Discovery of multiple X-ray sources in 47 Tucanae', *A&A* **288**, 466–471.

Hewish, A., Bell, S. J., Pilkington, J. D. H., Scott, P. F. & Collins, R. A. (1968), 'Observation of a rapidly pulsating radio source', *Nature* **217**, 709–713.

Hirata, K., Kajita, T., Koshiba, M., Nakahata, M., Oyama, Y., Sato, N., Suzuki, A., Takita, M., Totsuka, Y., Kifune, T., Suda, T., Takahashi, K., Tanimori, T., Miyano, K., Yamada, M., Beier, E. W., Feldsher, L. R., Kim, S. B., Mann, A. K., Newcomer, F. M., Van Berg, R., Zhang, W. & G., C. B. (1987), 'Observation of a neutrino burst from the supernova 1987A', *Phys. Rev. Lett.* **58**, 1490–1493.

Howell, J. H., Guhathakurta, P. & Gilliland, R. L. (2000), 'Resolving the Controversy Over the Core Radius of 47 Tucanae', *PASP* **112**, 1200–1211.

Hulse, R. A. & Taylor, J. H. (1974), 'A high sensitivity pulsar survey', *ApJ* **191**, L59–L61.

Hut, P., McMillan, S., Goodman, J., Mateo, M., Phinney, E. S., Pryor, C., Richer, H. B., Verbunt, F. & Weinberg, M. (1992), 'Binaries in globular clusters', *PASP* **104**, 981–1034.

Hut, P., Murphy, B. W. & Verbunt, F. (1991), 'The formation rate of low mass X–ray binaries in globular clusters', *A&A* **241**, 137–141.

Jayawardhana, R. & Grindlay, J. E. (1996), Pulse profiles of millisecond pulsars, *in* Johnston et al. (1996), pp. 231–232.

Johnston, H. M. & Kulkarni, S. R. (1991), 'On the detectability of pulsars in close binary systems', *ApJ* **368**, 504–514.

Johnston, H. & Verbunt, F. (1995), 'The globular cluster population of low-luminosity x-ray sources', *A&A* **312**, 80–87.

Johnston, S., Walker, M. A. & Bailes, M., eds (1996), *Pulsars: Problems and Progress, IAU Colloquium 160*, Astronomical Society of the Pacific, San Francisco.

Joshi, K. J. & Rasio, F. A. (1997), 'Distant Companions and Planets around Millisecond Pulsars', *ApJ* **479**, 948–959.

Joss, P. C., Rappaport, S. & Lewis, W. (1987), 'The core mass-radius relation for giants - A new test of stellar evolution theory', *ApJ* **319**, 180–187.

Kaspi, V. M., Taylor, J. H. & Ryba, M. (1994), 'High-precision timing of millisecond pulsars. III. Long-term monitoring of PSRs B1855+09 and B1937+21', *ApJ* **428**, 713–728.

King, I. (1966), 'The structure of star clusters. III. Some simple dynamical models', *Astron. J.* **71**, 64–75.

Kramer, M., Lange, C., Lorimer, D. R., Backer, D. C., Xilouris, K. M., Jessner, A. & Wielebinski, R. (1999), 'The characteristics of millisecond pulsar emission: III. From low to high frequencies', *ApJ* **526**, 957–975.

Kramer, M., Wex, N. & Wielebinski, R., eds (2000), *Pulsar Astronomy - 2000 and Beyond, IAU Colloquium 177*, Astronomical Society of the Pacific, San Francisco.

Kramer, M., Xilouris, K. M., Lorimer, D. R., Doroshenko, O., Jessner, A., Wielebinski, R., Wolszczan, A. & Camilo, F. (1998), 'The characteristics of millisecond pulsar emission: I. Spectra, pulse shapes and the beaming fraction', *ApJ* **501**, 270–285.

Kulkarni, S. R. & Anderson, S. B. (1996), Pulsars in globular clusters, *in* P. Hut & J. Makino, eds, 'Dynamical Evolution of Star Clusters - Confrontation of Theory and Observations', Kluwer, Dordrecht, pp. 181–201.

Kulkarni, S. R., Anderson, S. B., Prince, T. A. & Wolszczan, A. (1991), 'Old pulsars in the low–density globular clusters M13 and M53', *Nature* **349**, 47–49.

Kulkarni, S. R., Phinney, E. S., Evans, C. R. & Hasinger, G. (1992), 'X-ray detection of the eclipsing millisecond pulsar PSR 1957+20', *Nature* **359**, 300–302.

Landau, L. D. (1938), 'Origin of stellar energy', *Nature* **141**, 333–334.

Lewin, W. H. G. & Joss, P. C. (1983), X–ray bursters and the X-ray sources of the

Galactic bulge, *in* W. H. G. Lewin & E. P. J. van den Heuvel, eds, 'Accretion Driven Stellar X-Ray Sources', Cambridge University Press, Cambridge, p. 41.

Lorimer, D. R., Bailes, M., Dewey, R. J. & Harrison, P. A. (1993), 'Pulsar statistics: The birthrate and initial spin periods of radio pulsars', *MNRAS* **263**, 403–415.

Lorimer, D. R., Yates, J. A., Lyne, A. G. & Gould, D. M. (1995), 'Multifrequency flux density measurements of 280 pulsars', *MNRAS* **273**, 411–421.

Lundgren, S. C., Foster, R. S. & Camilo, F. (1996), Hubble space telescope observations of millisecond pulsar companions: Constraints on evolution, *in* Johnston et al. (1996), pp. 497–500.

Lyne, A. G., Biggs, J. D., Brinklow, A., Ashworth, M. & McKenna, J. (1988), 'Discovery of a binary millisecond pulsar in the globular cluster M4', *Nature* **332**, 45–47.

Lyne, A. G., Biggs, J. D., Harrison, P. A. & Bailes, M. (1993), 'A long-period globular-cluster pulsar in an eclipsing binary system', *Nature* **361**, 47–49.

Lyne, A. G., Brinklow, A., Middleditch, J., Kulkarni, S. R., Backer, D. C. & Clifton, T. R. (1987), 'The discovery of a millisecond pulsar in the globular cluster M28', *Nature* **328**, 399–401.

Lyne, A. G., Camilo, F., Manchester, R. N., Bell, J. F., Kaspi, V. M., D'Amico, N., McKay, N. P. F., Crawford, F., Morris, D. J., Sheppard, D. C. & Stairs, I. H. (2000), 'The Parkes multibeam pulsar survey: PSR J1811−1736 – a pulsar in a highly eccentric binary system', *MNRAS* **312**, 698–702.

Lyne, A. G. and Johnston, S. and Manchester, R. N. and Staveley–Smith, L. and

D'Amico, N. and Lim, J. and Fruchter, A. S. and Goss, W. M., 1990. IAU Circ. No. 4974.

Lyne, A. G., Manchester, R. N. & D'Amico, N. (1996), 'PSR B1745-20 and young pulsars in globular clusters', *ApJ* **460**, L41–L44.

Lyne, A. G., Manchester, R. N., D'Amico, N., Staveley-Smith, L., Johnston, S., Lim, J., Fruchter, A. S., Goss, W. M. & Frail, D. (1990), 'An eclipsing millisecond pulsar in the globular cluster Terzan 5', *Nature* **347**, 650–652.

Lyne, A. G., Manchester, R. N., Lorimer, D. R., Bailes, M., D'Amico, N., Tauris, T. M., Johnston, S., Bell, J. F. & Nicastro, L. (1998), 'The Parkes Southern Pulsar Survey – II. Final Results and Population Analysis', *MNRAS* **295**, 743–755.

Lyne, A. G., Manchester, R. N. & Taylor, J. H. (1985), 'The Galactic population of pulsars', *MNRAS* **213**, 613–639.

Lyne, A. G., Mankelow, S. H., Bell, J. F. & Manchester, R. N. (2000), 'Radio pulsars in Terzan 5', *MNRAS* **316**, 491–493.

Manchester, R. N. (1992), 'The pulsar phenomenon', *Philos. Trans. Roy. Soc. London A* **341**, 3–15.

Manchester, R. N., Lyne, A. G., D'Amico, N., Bailes, M., Johnston, S., Lorimer, D. R., Harrison, P. A., Nicastro, L. & Bell, J. F. (1996), 'The Parkes Southern Pulsar Survey I. Observing and data analysis systems and initial results', *MNRAS* **279**, 1235–1250.

Manchester, R. N., Lyne, A. G., D'Amico, N., Johnston, S., Lim, J. & Kniffen, D. A. (1990), 'A millisecond pulsar in 47 Tucanae', *Nature* **345**, 598–600.

Manchester, R. N. and Lyne, A. G. and Johnston, S. and D'Amico, N. and Lim, J. and Kniffen, D. A., 1989. IAU Circ. No. 4892.

Manchester, R. N., Lyne, A. G., Robinson, C., D'Amico, N., Bailes, M. & Lim, J. (1991), 'Discovery of ten millisecond pulsars in the globular cluster 47 Tucanae', *Nature* **352**, 219–221.

Manchester, R. N. & Peterson, B. A. (1996), 'A search for optical pulsations in SN 1987A', *ApJ* **456**, L107–L109.

McConnell, D. & Ables, J. G. (2000), 'Radio sources near the core of the globular cluster 47 Tucanae', *MNRAS* **311**, 841–845.

McKenna, J. & Lyne, A. G. (1988), 'Timing measurements of the binary millisecond pulsar in the globular cluster M4', *Nature* **336**, 226–227. Erratum ibid., 336, 698.

Meylan, G. (1989), 'Studies of dynamical properties of globular clusters. V - Implications of the observed flat MS mass function in 47 Tucanae', *A&A* **214**, 106–112.

Meylan, G. & Mayor, M. (1986), 'Studies of dynamical properties of globular clusters. II - The rotation, velocity dispersion and mass of Omega Centauri and 47 Tucanae', *A&A* **166**, 122–142.

Michel, F. C. (1987), 'Origin of millisecond pulsars', *Nature* **329**, 310–312.

Middleditch, J. & Kristian, J. (1984), 'A search for young, luminous optical pulsars in extragalactic supernova remnants', *ApJ* **279**, 157–161.

Middleditch, J. & Priedhorsky, W. C. (1986), 'Discovery of rapid quasi-periodic oscillations in Scorpius X-1', *ApJ* **306**, 230–237.

Nice, D. J. & Thorsett, S. E. (1992), 'Pulsar PSR 1744−24A: Timing, eclipses, and the evolution of neutron star binaries', *ApJ* **397**, 249–259.

Odenkirchen, M., Brosche, P., Geffert, M. & Tucholke, H. J. (1997), 'Globular cluster orbits based on Hipparcos proper motions', *New Astronomy* **2**, 477–499.

Oppenheimer, J. R. & Volkoff, G. (1939), 'On massive neutron cores', *Phys. Rev.* **55**, 374–381.

Pacini, F. (1967), 'Energy emission from a neutron star', *Nature* **216**, 567–568.

Pacini, F. (1998), The History of Neutron Stars: from Early Speculations to Current Problems, *in* Bucheri & van Paradijs M. A. Alpar (1998), pp. 3–12.

Paczyński, B. (1990), 'A test of the Galactic origin of gamma-ray bursts', *ApJ* **348**, 485–494.

Phinney, E. S. (1993), Pulsars as probes of globular cluster dynamics, *in* S. G. Djorgovski & G. Meylan, eds, 'Structure and Dynamics of Globular Clusters', Astronomical Society of the Pacific Conference Series, pp. 141–169.

Phinney, E. S., Evans, C. R., Blandford, R. D. & Kulkarni, S. R. (1988), 'Ablating dwarf model for eclipsing millisecond pulsar PSR 1957+20', *Nature* **333**, 832–834.

Phinney, E. S. & Sigurdsson, S. (1991), 'Ejection of pulsars and binaries to the outskirts of globular clusters', *Nature* **349**, 220–223.

Press, W. H., Teukolsky, S. A., Vetterling, W. T. & Flannery, B. P. (1992), *Numerical Recipes: The Art of Scientific Computing, 2nd edition*, Cambridge University Press, Cambridge.

Prince, T. A., Anderson, S. B., Kulkarni, S. R. & Wolszczan, W. (1991), 'Timing observations of the 8 hour binary pulsar 2127+11C in the globular cluster M15', *ApJ* **374**, L41–L44.

Pryor, C. & Meylan, G. (1993), Velocity dispersions for galactic globular clusters, *in* S. Djorgovski & G. Meylan, eds, 'ASP Conf. Ser. 50: Structure and Dynamics of Globular Clusters', pp. 357–371.

Rappaport, S., Podsiadlowski, P., Joss, P. C., DiStefano, R. & Han, Z. (1995), 'The relation between white dwarfs mass and orbital period in wide binary radio pulsars', *MNRAS* **273**, 731–741.

Rasio, F. A. (1994), 'Is there a planet in the PSR 1620–26 triple system', *ApJ* **427**, L107–L110.

Rasio, F. A. (2000), Theoretical Implications of the 47 Tuc Pulsars, *in* Kramer et al. (2000), p. 589.

Rasio, F. A., Pfahl, E. D. & Rappaport, S. (2000), 'Formation of short-period binary pulsars in globular clusters', *ApJ* **532**, L47–L50.

Rasio, F. R. & Heggie, D. C. (1995), 'The orbital eccentricities of binary millisecond pulsars in globular clusters', *ApJ* **445**, L133–L135.

Refsdal, S. & Weigert, A. (1971), 'On the Production of White Dwarfs in Binary Systems of Small Mass', *A&A* **13**, 367–373.

Reid, N. (1998), 'Hipparcos subdwarf parallaxes - metal-rich clusters and the thick disk', *Astron. J.* **115**, 204–228.

Rickett, B. J. (1977), 'Interstellar scattering and scintillation of radio waves', *ARAA* **15**, 479–504.

Robinson, C. (1994), Searches for radio pulsars in 47 Tucanae and other globular clusters, PhD thesis, The University of Manchester.

Robinson, C. R., Lyne, A. G., Manchester, A. G., Bailes, M., D'Amico, N. & Johnston, S. (1995), 'Millisecond pulsars in the globular cluster 47 Tucanae', *MNRAS* **274**, 547–554.

Romani, R. W. (1990), 'A unified model of neutron–star magnetic fields', *Nature* **347**, 741.

Roy, A. E. (1988), *Orbital Motion*, Institute of Physics Publishing, Bristol and Philadelphia.

Ryba, M. F. & Taylor, J. H. (1991), 'High-precision timing of millisecond pulsars. II - Astrometry, orb ital evolution, and eclipses of PSR 1957+20', *ApJ* **380**, 557–563.

Shklovskii, I. S. (1970), 'Possible causes of the secular increase in pulsar periods', *Sov. Astron.* **13**, 562–565.

Sigurdsson, S. (1995), 'Assessing the Environmental Impact on PSR B1620-26 in M4', *ApJ* **452**, 323–331.

Sigurdsson, S. & Phinney, E. S. (1993), 'Binary–single star interactions in globular clusters', *ApJ* **415**, 631–651.

Spergel, D. N. (1991), 'Evacuation of gas from globular clusters by winds from millisecond pulsars', *Nature* **352**, 221–222.

Spitzer, L. (1987), *Dynamical Evolution of Globular Clusters*, Princeton University Press, Princeton.

Staelin, D. H. & Reifenstein, III, E. C. (1968), 'Pulsating radio sources near the Crab Nebula', *Science* **162**, 1481–1483.

Stairs, I. H., Thorsett, S. E. & Camilo, F. (1999), 'Coherently-dedispersed polar-imetry of millisecond pulsars', *ApJS* **123**, 627–638.

Stappers, B. W., Bailes, M., Lyne, A. G., Manchester, R. N., D'Amico, N., Tauris, T. M., Lorimer, D. R., Johnston, S. & Sandhu, J. S. (1996), 'Probing the eclipse region of a binary millisecond pulsar', *ApJ* **465**, L119–L122.

Stappers, B. W., Bailes, M., Manchester, R. N., Sandhu, J. S. & Toscano, M. (1998), 'The Orbital Evolution and Proper Motion of PSR J2051-0827', *ApJ* **499**, L183–L186.

Stappers, B. W., Bessell, M. S. & Bailes, M. (1996), 'Detection of an irradiated pulsar companion', *ApJ* **473**, L119–L121.

Stappers, B. W., van Kerkwijk, M. & Bell, J. F. (2000), HST Observations of PSR J2051−0827: Asymmetry, Variability and Modelling, *in* Kramer et al. (2000), pp. 627–630.

Stappers, B. W., van Kerkwijk, M. H., Lane, B. & Kulkarni, S. R. (1999), 'The Light Curve of the Companion to PSR J2051-0827', *ApJ* **510**, L45–L48.

Staveley-Smith, L., Wilson, W. E., Bird, T. S., Disney, M. J., Ekers, R. D., Freeman, K. C., Haynes, R. F., Sinclair, M. W., Vaile, R. A., Webster, R. L. & Wright, A. E. (1996), 'The Parkes 21 cm multibeam receiver', *Proc. Astr. Soc. Aust.* **13**, 243–248.

Stella, L., Priedhorsky, W. & White, N. E. (1987), 'The discovery of a 685 second orbital period from the X-ray source 4U 1820–30 in the globular cluster NGC 6624', *ApJ* **312**, L17–L21.

Taylor, J. H. (1992), 'Pulsar timing and relativistic gravity', *Philos. Trans. Roy. Soc. London A* **341**, 117–134.

Taylor, J. H. & Weisberg, J. M. (1989), 'Further experimental tests of relativistic gravity using the binary pulsar PSR 1913+16', *ApJ* **345**, 434–450.

Thorsett, S. E., Arzoumanian, Z., Camilo, F. & Lyne, A. G. (1999), 'The Triple Pulsar System PSR B1620−26 in M4', *ApJ* **523**, 763–770.

Thorsett, S. E., Arzoumanian, Z., McKinnon, M. M. & Taylor, J. H. (1993), 'The masses of two binary neutron star systems', *ApJ* **405**, L29–L32.

Thorsett, S. E., Arzoumanian, Z. & Taylor, J. H. (1993), 'PSR B1620−26: A binary radio pulsar with a planetary companion?', *ApJ* **412**, L33–L36.

Thorsett, S. E. & Chakrabarty, D. (1999), 'Neutron star mass measurements. I. Radio pulsars', *ApJ* **512**, 288–299.

van den Bergh, S. (1993), Globular Clusters - a Provocative Introduction, *in* S. Djorgovski & G. Meylan, eds, 'ASP Conf. Ser. 50: Structure and Dynamics of Globular Clusters', pp. 1–11.

van Kerkwijk, M. H., Kaspi, V. M., Klemola, A. R., Kulkarni, S. R., Lyne, A. G. & Van Buren, D. (2000), 'Optical Observations of the Binary Pulsar System PSR B1718-19: Implications for Tidal Circularization', *ApJ* **529**, 428–434.

van Paradijs, J., Allington-mith, J., Callanan, P., Hassall, B. J. M. & Charles, P. A. (1988), 'Optical observations of the eclipsing binary radio pulsar PSR1957 + 20', *Nature* **334**, 684–686.

Verbunt, F. (1987), 'The formation of ultra–short period binaries in globular clusters', *ApJ* **312**, L23–L25.

Verbunt, F. (1993), 'Origin and evolution of X-ray binaries and binary radio pulsars', *ARAA* **31**, 93.

Verbunt, F. & Hasinger, G. (1998), 'Nine X-ray sources in the globular cluster 47 Tucanae', *A&A* **336**, 895–901.

Webbink, R. F. (1985), Structure parameters of Galactic globular clusters, *in* J. Goodman & P. Hut, eds, 'Dynamics of Star Clusters, IAU Symposium No. 113', Reidel, Dordrecht, pp. 541–577.

Wilsing, J. (1893), 'Ueber die Bestimmung von Bahnelementen enger Doppelsterne aus spectroskopischen Messungen der Geschwindigkeits-Componenten.', *Astronomische Nachrichten* **134**(3198), 90–92.

Wolszczan, A. and Anderson, S. and Kulkarni, S. and Prince, T., 1989. IAU Circ. No. 4880.

Wolszczan, A., Kulkarni, S. R., Middleditch, J., Backer, D. C., Fruchter, A. S. & Dewey, R. J. (1989), 'A 110-ms pulsar, with negative period derivative, in the globular cluster M15', *Nature* **337**, 531–533.

Zahn, J.-P. (1977), 'Tidal friction in close binary stars', *A&A* **57**, 383–394.